January 2015

Empirical Investigation Of The Laminar Thermal Entrance Region And Turbulent Flow Heat Transfer For Non-Newtonian Silica Nanofluid In Hexagonal Tubes

Emeke Kevin Opute

Follow this and additional works at: https://commons.und.edu/theses

EMPIRICAL INVESTIGATION OF THE LAMINAR THERMAL ENTRANCE
REGION AND TURBULENT FLOW HEAT TRANSFER FOR NON-NEWTONIAN
SILICA NANOFLUID IN HEXAGONAL TUBES

by

Emeke K. Opute

Bachelor of Engineering, Nnamdi Azikiwe University, 2008

A Thesis

Submitted to the Graduate Faculty

of the

University of North Dakota

In partial fulfilment of the requirements

for the degree of
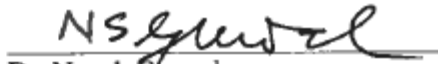
Master of Science

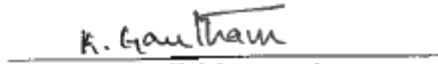Grand Forks, North Dakota, USA
August
2015

This Thesis, submitted by Emeke K. Opute in partial fulfilment of the requirements for the degree of Master of Science in Mechanical Engineering from the University of North Dakota, has been read and approved by the Faculty Advisory Committee under whom the work has be performed and is hereby approved.

_____
Dr. Clement Tang

_____
Dr. Nanak Grewal

_____
Dr. Gautham Krishnamorthy

This thesis is being submitted by the appointed advisory committee as having met all of the requirements of the School of Graduate Studies at the University of North Dakota and is hereby approved

_____
Wayne E. Swisher, Ph.D.
Dean of Graduate School

_____
July 30, 0015
Date

PERMISSION

Title	Empirical Investigation of the Laminar Thermal Entrance Region and Turbulent Flow Heat Transfer for Non-Newtonian Silica Nanofluid in Hexagonal Tubes
Department	Mechanical Engineering
Degree	Master of Science

Emeke K Opute
August 07, 2015

TABLE OF CONTENTS

LIST OF FIGURES

viii

ix

LIST OF TABLES

NOMENCLATURE

English Letter Symbols

A_s	Test section flow surface area [m2]
Br	Ratio of nanolayer to thickness to original particle radius
C^*	Experimentally determined constant
C_f	Equivalent Fanning Friction factor or coefficient
C_{nf}	Specific heat of nanofluid [J/kg K]
C_{np}	Specific heat of nanoparticle [J/kg K]
C_{bf}	Specific heat of basefluid [J/kg K]
D	Hydraulic diameter of test section [m]
D_B	Brownian diffusion coefficient [m2/s]
d_p	Nanoparticle diameter [m]
du/dr	Strain on fluid by wall [1/s]
D_T	Thermal diffusion coefficient [m2/s]
f	Darcy friction factor
F	Parallel force to liquid column [N]

f''	Second derivative of dimensionless velocity
g_c	Conversion factor [ft lb/s2 lbf]
$J_{np,B}$	nanoparticle mass flux due to Brownian diffusion [kg/m2 s]
$J_{np,T}$	nanoparticle mass flux to thermophoresis [kg/m2 s]
K'	Apparent viscosity [Pa.s]
k_2	Thermal conductivity of particle [W/m K]
k_B	Boltzmannn constant [J/K]
k_{bf}	Thermal conductivity of basefluid [W/m K]
k_{eff}	Effective thermal conductivity [W/m K]
k_l	Thermal conductivity of liqid [W/m K]
k_{nf}	Thermal conductivity of nanofluid [W/m K]
k_{np}	Nanoparticle thermal conductivity [W/m K]
k_{pe}	Equivalent thermal conductivity of equivalent particles [W/m K]
L	Length of test section [m]
$\dot{m}$	Average bulk fluid mass flow rate [kg/s]
n'	Degree to which fluid is non-Newtonian
N_{Re}	Reynolds number based on Reed, Metzner (1955)
Nu	Nusselt Number

Nu_D	Nusselt Number based on hydraulic diameter
Nu_x	Average Nusselt number at axial location x
P	Pressure [Pa]
Pe	Peclet number
Pr	Prandtl number
q_s	Heat flux through tube wall [W/m2]
r	Equals D/2 [m]
R	Equals (D/2 + t) [m]
Re	Reynolds number
Re_D	Reynolds number based on hydraulic diameter
T	Nanofluid temperature [K]
t	Test section/tube thickness [m]
T_{bx}	Fluid bulk temperature at x location [K]
T_e	Fluid test section's exit temperature [K]
T_i	Fluid test section's inlet temperature [K]
T_m	Fluid mean temperature
T_{wi}	Inner wall temperature of test section [K]
T_{wo}	Outer wall temperature of test section [K]

u	Velocity of plate [m/s]
V	Velocity of fluid flowing through test section [m/s]
V_{nf}	Volume of nanofluid [m3]
V_T	Thermophoretic velocity [m/s]
x	Axial location along test section or tube [m]
x^+	Dimensionless axial location
y	Boundary layer thickness [m]

Greek Symbols

β	Thermophoretic coefficient
$\partial u/\partial y$	Velocity gradient [1/s]
ΔP	Pressure drop between inlet and exit of test section [Pa]
θ''	Second derivative of dimensionless temperature
μ	Viscosity [Pa.s]
μ_l	Viscosity of liquid [Pa.s]
μ_s	Viscosity of solid (spehere) particles [Pa.s]
ρ	Nanofluid density [kg/m3]
ρ_{np}	Nanoparticle density [kg/m3]
τ	Shear stress [Pa]

τ_w	Shear stress at the wall of test section due to fluid flow [Pa]
ϕ	Volume fraction of solid spheres or nanoparticles
φ_{np}	Mass fraction of nanoparticles

Subscript

B	Brownian motion
b	Bulk
bf	Base fluid
D	Hydraulic diameter
e	Exit
i	Inlet
l	Liquid
nf	Nanofluid
np	Nanoparticle
r	Ratio
s	Surface
T	Thermal or Thermophoretic
w	Wall
wi	Inner wall

| *wo* | Outer wall |
| *x* | Axial location |

Superscript

| $''$ | Second derivative |
| $+$ | Dimensionless |

ACKNOWLEDGEMENTS

ABSTRACT

This research seeks to determine for the flow of stable dispersion of 9.58% silicon-oxide (SiO_2) nanoparticles by volume in water through three hexagonal tubes of hydraulic diameters 1.67 mm, 2.42 mm and 3.26 mm, the pressure drops across the length of the tubes with and without the application of constant heat flux to the test section. Constant heat flux was applied on the wall of each test section (by electric resistance method). The operating temperature range of 15-63°C was maintained for the experiments. Data were analyzed using conventional hydrodynamic and thermal correlations. The test sections were selected and set up (or instrumented) in a manner enabling the measurements of lengthwise local surface temperatures of test sections and the drop in pressure of fluid flow across the axial length of the test sections. Viscosity and thermal conductivity measurements for the nanofluid of interest were acquired by Sharif (2015), and were used in this study.

The 9.58% volume concentration SiO_2-water nanofluid friction coefficients were found to follow the same trend obtained by classical correlations for Newtonian fluids. Results show no significant difference between the friction coefficients of nanofluid and water if the nanofluid is modeled as a power law fluid. The nanofluid, however, sustained laminar flow longer than water over the range of Reynolds number tested when no heat had been applied, the effect is even more pronounced for decreased hydraulic diameter of test section.

For the thermally developing flow, convective heat transfer values for the nanofluid were significantly enhanced compared to water, nearing 20% in the laminar flow regime. The measured local Nusselt numbers for the nanofluid lie within ±30% of the Lienhard and Lienhard (2013) model for laminar thermally developing flow, and about 30% or less of the Gnielinski (1976) correlation for turbulent flow. Pressure drops for the nanofluid flows exceed those of water by over 100%.

CHAPTER I

INTRODUCTION

The past few decades have seen heat transfer systems and applications come under intense scrutinizing, in the wake of alarmingly aggressive depletion and inefficient harnessing of non-renewable energy resources amidst growing environmental concerns. These developments have changed the perspectives with which the suitability of heat transfer concepts are perused. Due to rising cost and scarcity of resources, high energy efficiency and performance of processes and systems have quickly become the primary concern for the modern manufacturer. As it is, what used to be ingenious conventional methods may in effect be inadequate to say the least in this new era of energy utilization. In many conventional applications, increasing heat exchange area, for instance the use of extended surfaces like fins or micro-channels is common practice where higher heat dissipations are required. Well, it turns out that these kinds of solutions usually result in the development of bulky heat exchange systems in the end, many of which have lagged behind and unable to adequately meet new industry challenges.

The apparent rapid miniaturization of technology is accompanied by a dire need for high density cooling. The capabilities of the more common cooling systems in terms of performance are already far outstretched and they no longer appear to be the right choices for the level of performance required by these emerging technologies. One way to achieve more effective cooling is to develop better performing heat exchange fluids which have high area to volume ratios in which high heat flux can be established.

1

Nanoparticle colloids, a fairly recent class of engineered fluid in which very fine particles of highly conductive materials are suspended in a relatively poor conducting liquid have been making waves in the broader topic of heat transfer because they possess extraordinary high surface to volume ratios. According to Wang et al (1999b), addition of only a small volume percent of conductive nano-sized particles to a liquid can dramatically improve the thermal conductivity of the resulting mixture, and this type of enhancement has been achieved with nanofluids. Thus nanofluids are thought of as being potentially capable of providing solutions to the long engineering problem of improving heat transfer in systems without significant increases in heat transfer areas or overall size of facilities suitable for micro-tech applications, for instance as well as for other high efficiency compact cooling applications like micro electromechanical device systems (MEMS) nuclear reactors. Not only could size of heat transfer surfaces or systems be effectively smaller using nanofluids, less fluids would be required for their operation.

The optimisms shared by Eastman and Choi (1995) and many other researchers following the introduction of "nano-fluids", referring a new "class of engineered heat transfer fluids" which contain nano-sized metal or metal oxide particles (herein after referred to as nanoparticles) of an average particle size of about 10 nanometers, however, seem to have declined. A few scientists who had also conducted studies on these fluids seem to think the other way, they have expressed reservations per the adoption of these so-called nanofluids as the preferred choice of heat transfer fluids for compact cooling. One of their reasons being the high pressure drops have observed for nanofluids micro/mini channel flows, especially during the transitioning from laminar flow to turbulent flow regardless of the tube geometry Li and Wu (2010). In fact, some researchers have argued

against any optimisms that might be held for nanofluids by releasing findings and predictions suggesting that the application of nanofluids in heat transfer may after all not be any better than using other conventional heat transfer fluids like water.

Nanofluids, like many other liquid-solid mediums, may be more difficult to transfer than single phase liquids. They are affected by settling, clogging and abrasion, all of which become more prominent with increasing particle concentrations. The stability of the colloid could also be a significant contributor to its performance, and so is vital to the pursuit of their successful utilization. In this thesis, careful observation over extended periods led to the conclusion that the nanofluid being investigated is stable for the purpose of the research. Regardless of the negative opinions about the use of nanofluids, research of them continue to thrive because of their high conductivity and convective heat transfer capabilities.

While considerable amount of research work to explain nanofluid thermo-physical behavior for fully developed flows exist, only few attempt to investigate their entrance region behavior, of which the number quickly drops for flows through geometries other than the circular cross-section. Non-circular cross sectional flow conduits present relatively complex internal and external forced convection problems (which have to be solved anyway) since nowadays more heat transfer applications are constrained the need to use flow channels of complex geometric configurations.

Hexagonal tube heat exchanger can serve to optimize heat exchanger designs with the possibility of multi-faceted heat transfer applications. Hexagonal cross-sectional nanofluid flows can also provide much desired insight into flow and heat transfer for other flow configurations as well, at the same time allowing a basis for analytical comparisons with other common geometries alike.

A scantiness of studies on the entrance region behavior for a nanofluid tube flows is apparent in the literature of nanofluid flow behavior. Because a complete flow solution should include the entrance region solution as well as the fully developed flow solution, this thesis proposes to characterize developing nanofluid flow and heat transfer for hexagonal mini-tube flows for the laminar and transitional turbulent flow regimes.

Of course heat transfer characteristics can be extremely sensitive to existing flow conditions, depending on whether flow is laminar or turbulent. The laminar regime is such that the flow profile is characterized by so-called layers of velocities whose magnitudes appear to increase from the wall to the center line, whereas the turbulent regime is dominated by haphazardly distributed self-sustaining velocity scales. The transient regime, is the evasive region between the turbulent and flow regimes. See Figure 1 for the depiction of the concept of boundary layer development. It is important to note that the concept of boundary layer development is essentially the same for the hydrodynamic and thermal considerations for a fluid.
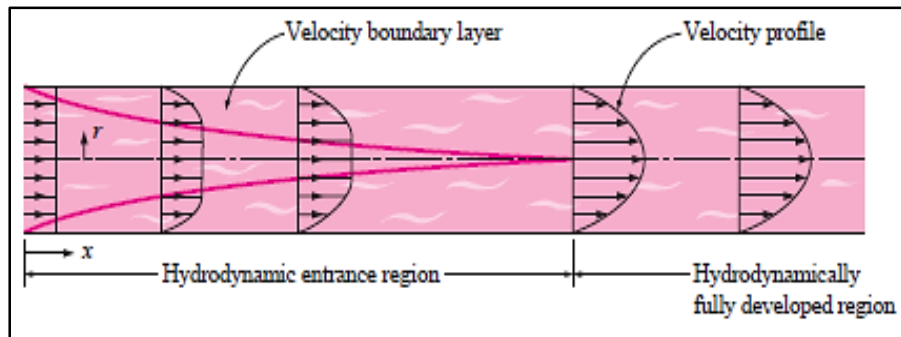
Figure 1. Tube velocity boundary layer development (Çengel and Ghajar, 2011).

Depending on applications and desired system performance, certain flow regime(s) may be preferred to the others. Laminar flow is ultimately desired for compact cooling

4

applications, Lienhard and Lienhard (2013) or laser/water jet and the likes of them. So, statement of specific rheological behaviors of fluid are critical to correctly defining their thermo-physical characteristics.

According to Metzner and Reed (1955), the classification of fluids into commonly known categories could be tantamount to over-simplification since the assignment of arbitrary values to their rheological properties depend extremely on conditions under which the measurements have been carried out. Nonetheless, such classifications are the basis upon which any practical results might be achieved. In this thesis, the nanofluid is classified based on the information provided in the work of Sharif (2015) whose work focused extensively on the physical properties of the nanofluid in view.

The key thermophysical properties of fluids (including nanofluid) are the density, specific heat capacity, thermal conductivity, viscosity and surface tension (Wu and Zhao 2013). In this thesis, the density and the specific heat capacity will be estimated using mixture models. The changes in viscosity, thermal conductivity and or surface tension are complex and it falls outside the scope of this work to determine those changes. Based on the rheological approximation of the nanofluid of interest, the power law model serves the best for the purpose of obtaining the viscosity relationships of the nanofluid in the analysis that will be carried out here.

The thermal entrance region is extremely important for laminar flow because the thermally developing region becomes extremely long for higher Prandtl number (Pr) fluids such as nanofluids (Hussein et al, 2014). In this investigation, local wall temperatures and time-root-mean-square velocities of bulk fluid flows as well as wall heat fluxes have been obtained. Inferences will be drawn from those thermo-data in relations to heat transfer

mechanisms in the thermal entrance region and consequently tested to determine how much they are correlated by existing hypotheses.

1.1 Research objectives

Clarity on the subject matter of using nanofluid for heat transfer purposes, necessitates sound assessment and succinct representation of evidences as they relate to how nanofluids may possess any advantage over traditional heat transfer fluid such as their base fluids. To this end, an effective approach should involve comparing the thermo-physical properties of nanofluid to its base fluid. A thorough investigation of the fluid's viscosity relationships is an absolute necessity if any meaningful result were to be achieved. In essence, an adequate, functional description and documentation of the thermo-physical characteristics of the fluid become absolutely necessary.

The nanofluid (water-based silicon dioxide) being investigated in this thesis, broadly speaking, is non-Newtonian. This marked deviation from the rheology of their base fluid presents several engineering challenges for the use of the fluid. The research entails a systematic review of the literature with emphasis on the viscosity, thermal conductivity and convective heat transfer of nanofluids and of course the results that have been obtained from extensive experimentation on the nanofluid here at the University of North Dakota nanofluid Laboratory. The intent here is to deliver unambiguous and effective data on the nanofluid flow and heat transfer through specific test sections. Rigorous collection of data on the pressure drop and heat transfer for silicon-oxide water-based nanofluid of 9.58% particle concentration by volume is done, thereafter, an empirical analysis are carried out

to ascertain the nanofluids flow and thermal performance relative to the base fluid (distilled water in this case).

This work will shed some light on the suitability of nanofluid for more diverse heat transfer applications. It explores a suitable method of experimentations in view of the low level of confidence surrounding reported data for nanofluids in the literature. Integrity of the experimental setup is insured through painstaking installation, adequate calibration of measuring instruments and exhaustive testing of results collected for the three different test sections using a well know liquid, water.

Overall, the research attempts to verify or disprove claims as surrounding the convective thermal transport of nanofluids as necessary. It explores different means to quantify as well as compare measurements for the nanofluid with a conventional heat transfer fluid.

1.2 Nanofluid Applications

Nanofluids continue to court the attention of engineers as the quest for more efficient heat transfer fluids intensifies with the proliferation of high density energy systems. Overheating in miniature tech systems can result in the oxidation of components and induce early fatigue that could lead to premature failure. Nanofluids can, and in fact have been applied to thermal engineering systems spread across different industries for heat transfer purposes. Developing methods whereby nanofluid systems can be integrated with or used to replace conventional fluid heat transfer systems in existing or new equipment at low costs is also hot in the chase. There are few doubts as to the improved heat transfers recorded with nanofluids, although skepticism still abound the corresponding

viscosity augmentations associated with the fluids. The question then becomes: how can nanofluids then be economically utilized for effective and efficient heat transfer? According to Keblinski et al (2005a), new theoretical descriptions may be needed to account for the unique features of nanofluids should the exciting results on them be confirmed. Some of these unique features include high particle mobility- to which enhanced thermal dispersions have been attributed, and large surface-volume ratios as well.

Both civil and military aviation, land and water vehicle, electronic cooling heat exchange systems, even space and nuclear engineering programs etc. can benefit from the use of nanofluids. Keblinski et al (2005a) attributes the requiring of advanced cooling to advancement in microelectronics and high speed computing, brighter optical devices and higher-power engines which are driving thermal loads among many other factors. Nanofluids have been used in a variety of systems encompassing industrial cooling, CPUs and MEMS, automotive engines and so forth.

1.3 Study Outline

Chapter 1 introduces the fluid of interest and outlines the problems being solved. In Chapter 2, a comprehensive review of literature is presented as a general overview of the subject matter enumerating efforts that have been made to study related nanofluids. A complete report on the experimental setup and analytical methods as adapted for the project follow in Chapter 3. Chapter 4 encompasses review and discussion of results with the work culminating in Chapter 5 as conclusions are drawn, followed by recommendations for future work and then the appendices.

CHAPTER II

LITERATURE REVIEW

This chapter presents an overview of previous research work on the properties and behaviors of nanofluids that will serve as groundwork for the study presented in this report, it takes a comprehensive look at the thermo-physical properties, heat transfer and some other characteristics of nanofluids. The literature review is divided into preparation (or synthesis), viscosity and pressure drop, and heat transfer of nanofluids.

2.1 Synthesis and Characterization of Nanofluids

Synthesis and Stability

The formulation/preparation of every engineering material, for whatever application they may be meant, plays a critical role in their successful utilization. For nanofluids, the stability of the colloid is an important consideration for their use because the aggregation/agglomeration of nanoparticles affect their hydrodynamic and thermal characteristics.

Yu and Xie (2012) outlines two methods for the preparation of nanofluids; the two-step and one-step methods. While the two-step method is more economical than the other, the nanoparticles produced tend to aggregate relatively quickly and as such would require the use of surfactants to insure their stability. This method involves the use of intensive magnetic force agitation, high shear mixing ultrasonic agitation, homogenization and ball milling.

On the other hand, the one-step method simultaneously produces and disperses the nanoparticle in the base fluid unlike the two-step method and uses the vapor condensation method which employs either the vacuum submerged arc nanoparticle synthesis system or phase transfer method. The one-step method, however, is expensive since only small quantities of nanofluids can be synthesized by the method.

Baby and Ramaprabhu (2011) described a method in which nanofluids were prepared using synthesized (by chemical reduction) silver decorated functionalized hydrogen induced exfoliated graphene (Ag/HEG) which were dispersed in deionized water and ethylene glycol by ultrasonic agitation (or simply sonication) achieving stability without resorting to the use of stabilizing surfactants.

According to Fedele et al (2011), the process of dispersion of nanofluids and particle stability are critical points in the development of the fluids. They found that high pressure homogenization coupled with the addition of n-dodecyl sulphate and polyethylene glycol as dispersants to SWCNHs-water and TiO2-water nanofluids produced the more stable colloids.

The use of zeta potential to measure stability of nanofluid is common in the literature. Sahooli et al (2012) studied the effect pH and PVP- polyninylpyrolidone surfactant on the stability on the stability of CuO nano-suspensions in aqueous solution, and suggest that they are closely related to the electro-kinetic properties of the suspension. They determined from nanoparticle surface zeta potential measurements whether or not the electrostatic repulsion between particles suffice to overcome the attraction between them. Where repulsion forces exceeded the attraction forces between particles, the nanofluid was

stable, and if the other way round, unstable. The nanofluid investigated tended to lose stability of scatter with increasing pH values.

Zhu et al (2007) synthesized well dispersed CuO from the transformation of unstable $Cu(OH)_2$ into CuO in water under ultrasonic vibration which was then followed by microwave irradiation. They reported the achievement of higher volume fractions as well as thermal conductivity of the synthesized nanofluid by this method. Apparently, the unstable $Cu(OH)_2$ "precursor" is broken down into small CuO nanoparticles by the ultrasonic vibration aided by the microwave irradiation. The stability of the dispersion or prevention of growth and aggregation of the nanoparticles is made possible by the presence of ammonium citrate.

Characterization and Modeling

The contribution of materials' composition to their heat transfer behaviors cannot be overemphasized. Thus, strategic way to begin an effective description of the systems in view would be to first shed light on the relevant thermo-physical properties of the nanoparticles since, in most of the cases, the characteristics of the basefluid are already well documented in the literature. As far these characteristics are concerned the list is inexhaustible, to keep it precise only those that have been found to be most important are enumerated.

Nanoparticles are materials with distributions in size, shape, compositions (physical and chemical) etc., therefore particle size and geometry quickly come to mind when describing them, but so does their microstructure which is equally significant. Others include the chemical compositions of the particles, dispersion stability, heat capacity and

thermal conductivity of course! The density of the particles as well as their viscosity aren't left out of the list. Next, a brief summary of the functions mentioned above as well as works carried out in this regard are presented.

Especially where laminar flows are desired, insuring stability of the colloid is of great importance. Preparing a stable and durable nanofluid is a prerequisite for optimizing its thermal properties says Ghadimi et al (2011) who reviewed experimental studies and preparation and different stability methods of nanofluids. Jiang et al (2003)(Jiang, Gao et al. 2003) reported a quantitative characterization of stability of colloidal dispersion of carbon nanotubes by UV-VIS spectrophometric measurements. They applied the Zeta potential, auger electron microscopy, and Fourier Transform Infrared Spectroscopy (FTIR) analysis in investigating the adsorption mechanism within the nanofluid and concluded that surfactant containing a single straight-chain hydrophobic segment and a terminal hydrophilic segment can modify the CNTs–suspending medium interface, preventing aggregation over an extended period of time.

Joshi et al (2008) described characterization techniques for nanotechnology applications for textiles, which are by no means different than for other applications. These techniques include the use of particles size analyzer, electron microscopy (SEM—scanning electron microscope, TEM—transmission electron microscopy and electron thermal microscopy and THEM—electron thermal microscopy) to investigate particle size distribution and geometry. Other than limitations such as relatively small viewing fields, the above methods provide detailed results for the dimensions and geometries of nanoparticles. And so for an entire nanofluid sample, multiple viewing windows may have to be used in order to obtain the most accurate result for the whole system where these

methods are used. See Brintlinger et al (2008) for more detailed description of electron thermal microscopy as it applies to nanofluid studies.

Other techniques listed by Joshi, Bhattacharyya et al (2008) are the atomic force microscopy, X-ray diffraction, Raman spectroscopy and X-ray photon spectroscopy. The electron diffraction, ED is another analytical technique with which details of nanoparticles crystallographic structure may be obtained. These methods mostly provide insight into the physical formation/distribution of nanoparticles in the basefluid, it is thus safe to assume they give a lead to how these materials may be chemically composed. The Dynamic light scattering, DLS may also be used to measure the size as well as mobility of nanoparticles in nanofluids. This method is however not effective for high particle concentrations (Keblinski et al, 2005b).

One major concern about the suitability of nanofluid for heat transfer applications is the stability of the particle dispersions. Issues have been raised regarding particle migrations such as settling of nanoparticle during low Re flows. Therefore the stability of the dispersion needs be verified prior to being uses since particle migration in nanofluids may significantly affect their heat transfer.

Buongiorno (2006) in his study of nanofluid heat transfer considered seven slip mechanisms though to be capable of causing relative motion between nanoparticles and the basefluid, they are inertia, Brownian diffusion, thermophoresis, diffusiophoresis, Magnus effect, fluid drainage and gravity. Among these mechanisms, only the Brownian diffusion and thermophoresis are important slip mechanisms in nanofluids boundary layer in the absence of turbulent eddies. Thermophoresis/thermodiffusion, or the Soret effect, or the Ludwig-Soret effect as it may be called, is a phenomenon observed in mixtures of

mobile particles where different particle types exhibit different responses to the force of a temperature gradient.

Buongiorno (2006) outlines the Brownian diffusion coefficient D_B, a measure of Brownian motion as defined by the Einsten-Stoke's equation:

$$D_B = \frac{k_B T}{3\pi\mu d_{np}}$$

(2.1)

A particle mass flux due to Brownian diffusion is $J_{np.B}$ (kg/m^{2}s) is thus given by the following equation:

$$J_{np,B} = \rho p D_B \nabla \phi$$

(2.2)

The following equation is given for thermophoretic velocity V_T:

$$V_T = -\frac{\beta\mu}{\rho} \cdot \frac{\nabla T}{T}$$

(2.3)

where the proportionality factor β is given by (McNab and Meisen 1973).

$$\beta = \frac{0.26k}{2k + k_{np}}$$

(2.4)

Thus, the overall nanoparticle mass flux due to thermophoresis:

$$J_{np,T} = \rho_{np} D_T \frac{\nabla T}{T}$$

(2.5)

D_T is referred to as the thermal diffusion coefficient and is given as:

$$D_T = \frac{\beta\mu}{\rho} \phi$$

(2.6)

Note k here is the thermal conductivity of the nanofluid and k_{np} is the thermal conductivity of the nanoparticles, while k_B is the Boltzmann constant.

A take from Buongiorno (2006) is that a correct modeling of the flow characteristics of the nanofluid as with other types of suspensions/colloids may not be achieved without incorporating the effect of settling and/or mobility of particles. In short, perikinetic flocculation in which particle aggregation is brought about by the random thermal motion of fluid molecule, Howe et al (2012) and its significance cannot be overlooked. Many manufacturing techniques exist to achieve a stable suspension, however, the sonication method is mostly applied for nanofluid development and appears to have greater reliability.

2.2 Nanofluid Viscosity, Pressure Drop and Rheology

Nanofluid hydrodynamic behavior analysis is less complex where the fluid shows Newtonian behaviors than where it behaves as a non-Newtonian fluid. Note: most suspensions tend to be non-Newtonian. Einstein (1906) described the rheological properties of liquid suspensions, he developed an equation to predict the effective viscosity of dilute suspension for rigid, buoyant spheres where there exist only negligible interaction between the spheres. The equation is given as:

$$\mu_s = (1.25\phi + 1)\mu_l \tag{2.7}$$

The above representation of the fluid viscosity has its limitations; it has been shown that the stability of nanofluids depend to some extent on the interaction between the suspended particles.

Duangthongsuk and Wongwises (2010) found the pressure drop of nanofluids to "slightly" loft that of the base fluid (water in this case) at high Reynolds number and

particle concentration. They propose the following correlation to predict the friction factor for their flow. The study had been conducted for Ti-O nanofluid for concentrations ranging between 0.2 and 2.0 vol. %.

$$f = 0.961\phi^{0.052}Re^{-0.375} \qquad (2.8)$$

By their estimate, the equation predicts friction factor for nanofluids with particle volume concentration range same as tested in their experiments to good accuracy level.

Sundar and Singh (2013) carried out a review of literature on some of the correlations for heat transfer and friction factor for different types of nanofluids flowing through tubes for both the laminar and turbulent flow regimes. They are of the opinion that conventional correlations are unsuitable for nanofluid heat transfer and friction factor calculations which has led to the development of more specific relations for these fluids. Table 1 shows a compilation of the friction factor correlations reviewed by them. A compilation of Nusselt number correlations as reviewed are also presented in the next sub-section in Table 2. Not that φ as used here refers to the volume fraction of the nanoparticles in the nanofluid.

Table 1. Friction factor correlations reported in the literature for nanofluid in a tube (Sundar and Singh 2013)

Equation	Nanofluid	φ, (%)	'Re' range
$f = 26.4\,Re^{-0.8737}\,(1+\varphi)^{156.23}$	Al_2O_3–Cu	0.1%	$Re < 2,300$
$f = 0.1648\,Re^{0.97}(1+\varphi)^{107.89}\left(1+\frac{P}{d}\right)^{-4.463}$	CuO	0.3	$2,500 < Re < 6,000$
$f = 0.3491\,Re^{-0.25}\,(1.0+\varphi)^{0.1517}$	Fe_3O_4	0.6	$3,000 < Re < 22,000$
$f = 0.3164\,Re^{-0.25}\left(\frac{\rho_{nf}}{\rho_{bf}}\right)^{0.707}\left(\frac{\mu_{nf}}{\mu_{bf}}\right)^{0.108}$	Al_2O_3, CuO	0.06	$3000 < Re < 16,000$
	SiO_2	0.1	$3,000 < Re < 16,000$

Namburu et al (2007) presented results for an experimental investigation of the rheology of 0-6.12 volume concentration copper oxide nanoparticle in ethylene glycol and water-based nanofluids, for a temperature range (-35-50°C). The nanofluids exhibited Newtonian characteristics for conditions in which they had been observed.

An experimental investigation of the viscosity of nanofluid prepared by dispersing alumina nanoparticles (< 50nm) in commercial car coolant was carried out by (Kole and Dey 2010). The nanofluid which had been prepared with oleic acid surfactant was stable after 80 days. Measuring the viscosity of the nanofluid as a function of both particle concentration and temperature (range: 10-50°C), they observed that the nanofluid, unlike it base-fluid, showed non-Newtonian characteristics, and the viscosity which increased with particle concentration could not be predicted using classical models. Figure 2 is shown for the nanofluid; it behaves as a Bingham plastic.
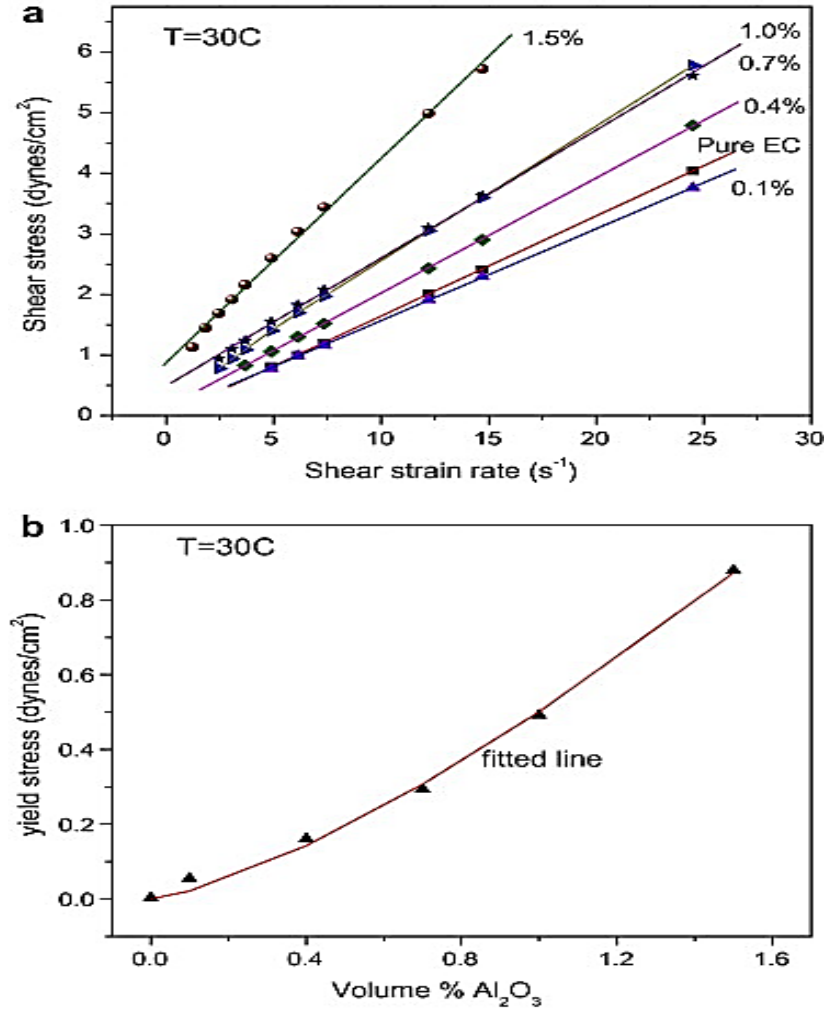
Figure 2. (a) Shear stress vs Shear strain rate for various nanofluids with different volume concentration of Al₂O₃ nanoparticles. (b) Yield stress as a function of vol. % in the nanofluid. Line is the fitted power–law equation: $\tau_y = (0.50063)\phi^{1.3694}$ (Kole and Dey 2010)

Phuoc and Massoudi (2009) reported the effects of the shear rates and particle volume fraction on the shear stress and viscosity of Fe2O3-distilled water nanofluids with polyninylpyrolidone (PVP) or polyethylene oxide, PEO as a dispersant. They found the nanofluids had a yield stress and began to show shear-thinning non-Newtonian fluid behavior after a nanoparticle volume fraction of 0.2% was exceeded. Actually, where PEO dispersant had been used, the fluids began to show shear-thinning non-Newtonian behavior

at particle volume fraction as low as 0.02%. From this and other similar experiments such as Lee et al (2011) and Aladag et al (2012), it can be seen that the type of dispersant used in insuring stability of nanofluids plays an important role in the rheology of the resulting nanofluid suspension. These experiments also found the viscosity of the nanofluids increased with increase in particles concentrations but decreased with increased temperature.

While Dodge and Metzner (1959) showed that a certain amount of drag reduction exists for time independent non-Newtonian fluids compared with Newtonian fluids, they also acknowledge that at the same Reynolds number, drag reduction in the presence of viscoelasticity is much more pronounced. This is a distinction that had not been made by their contemporary (Shaver and Merrill, 1959). The power law or logarithmic relationships are widely used to describe the relationship between friction factor and Reynolds number for non-Newtonian fluids.

2.3 Nanofluid Heat Transfer

Previous works on thermal transport modes are presented for different nanofluids in this section. Three heat transfer modes exists for nanofluids as with all other fluids, they are conduction, convection and radiation. For the purpose of the analyses presented here, radiation has been neglected leaving only conduction and convection to be treated. Discrepancies, inconsistencies are common in the literature of nanofluid heat transfer studies. Whether these are some random inherent anomalous behaviors or error occurrences related to experimentation and/or reporting techniques utilized in the study of the fluids remain to be determined.

2.3.1 Thermal Conductivity

Kakaç and Pramuanjaroenkij (2009) defined thermal conductivity enhancement as the ratio of thermal conductivity of the nanofluid to the thermal conductivity of the base fluid (k_{nf}/k_{bf}). Many thermal conductivity models in the past have been developed based on the Maxwell and Thompson (1892) classical model, whose work encompassed conduction through heterogeneous media. They described the effective thermal conductivity for a two-phase mixture composed of a continuous and non-continuous phases, they developed the following correlation for this effective thermal conductivity as

$$k_{eff} = \frac{[2k_2 + k_1 + \phi(k_2 + k_1)]k_1}{2k_2 + k_1 - 2\phi(k_2 - k_1)} \tag{2.9}$$

where k_1 and k_2 represent the thermal conductivities of liquid and particle respectively, and ϕ the particle volume fraction of particle. This model is often referred to as the effective medium theory.

Thermal conductivity of nanofluids may be affected by a number of factors some of which are nanoparticle size, distribution, volume fraction, interfacial effects, etc. Beck et al (2009) studied the effect of particle size on the thermal conductivity of several alumina water or ethylene glycol based nanofluids whose nanoparticle diameter ranged between 7 nm and 283 nm. They found thermal conductivity to decrease for nanoparticle sizes less than 50 nm and vice-versa, concluding that the observed phenomenon as a as a result of phonon scattering at the solid-liquid interface.

Timofeeva et al (2010) also considered the effect of particle size and interfacial effects on the thermo-physical and heat transfer characteristics of water based α-SiC

nanofluids. They found that for particle sizes varying from 16-90 nm thermal conductivity and viscosity increased with particle size. They also suggest viscosity, independent of thermal conductivity, tends to decrease with pH of the suspension.

Yu and Choi (2003) describes the role of interfacial layers in the enhanced thermal conductivity of nanofluids based on the Maxwell effective medium model. They attempt to explain the connection between a solid-like nano-layer (formed by liquid molecules upon contact with particles suspended in the bulk fluid) and the thermal properties of the suspension. They concluded that the presence of a nano-layer can significantly raise the effective volume fraction, increasing the thermal conductivity of the suspension, and more so where particle diameter is less than 10 nm. Consequently, the addition of particles with diameters less than 10nm would give better results for thermal conductivity enhancement and could significantly boost the optimization of compact technology. Their modified version of the Maxwell equation is for the effective thermal conductivity of the nanofluid k_{eff} given below:

$$k_{eff} = \frac{\left(k_{pe} + 2k_l + 2\left(k_{pe} - k_l\right)(1 + \beta_r)^3\phi\right)k_l}{\left(k_{pe} + 2k_l - \left(k_{pe} - k_l\right)(1 + \beta_r)^3\phi\right)} \tag{2.10}$$

The term k_{pe} is the equivalent thermal conductivity of the equivalent particles calculated, i.e. including the nano-layer as given by Schwartz et al (1995) and k_l denotes the thermal conductivity of the suspension fluid. Where the thermal conductivity of the nanolayer equals that of the particle, on other words there is no nano-layer, the equivalent thermal conductivity becomes the thermal conductivity of the particle. β_r is the ratio of the nanolayer thickness to the original particle radius.

Kabelac and Kuhnke (2006) purports that "colloidal fluidic" systems show very high thermal conductivity on the condition that they stable enough. They however reach diverging results for thermal conductivity of the Nanofluids tested citing the model developed by Wang et al (2003) to explain observed electrochemical interface physics for the system of colloid.

Wang et al (2003) used the effective medium approximation and fractal theory for nanoparticle cluster and radial distribution to develop a modeling method for the effective thermal conductivity of nanofluids. The model thus obtained was tested with data they had obtained from a previous work on dilute suspensions of 50 nm metallic oxide nanoparticles.

In their work Das et al (2003b) investigated the increase of thermal conductivity with temperatures for water based Al_2O_3 and CuO nanofluid systems. Their thermal diffusivity and conductivity measurements, obtained using a temperature oscillation technique, suggest an increase in thermal conductivity of the nanofluids as temperatures increase. They arrived at the conclusion that the observed phenomenon makes nanofluids more appealing to applications which operate at high energy density. They propose, also, the particle size to be a key parameter in the observed nanofluid behavior, further stressing that the usual weighted average type of model for effective thermal conductivity may after all be an unreliable method for predicting high temperature thermal conductivities.

Measurements of thermal conductivity of water and ethylene glycol based nanofluids of metallic oxide particle carried out by (Wang et al, 1999a). Lee et al (1999), Krishnamurthy et al (2006) and Pak and Cho (1998) each having experimented with different types of nanofluids found enhancements in the thermal conductivities of those nanofluids to be in the range of 10% to 30% higher relative to the base fluid.

Sundar and Singh (2013) also reviewed the effect of preparation and stability on the thermal conductivity of various types of nanofluids. The methods of preparation of the nanofluids are the one-step and the two-step methods. They are of the opinion that the agglomeration of nanoparticles due to poor stability, which is a probably a consequence of the preparation method, caused the thermal conductivity of the nanofluid to decrease. As was described by Yu and Xie (2012), their reviews suggest that the two-step method of preparation yielded more stable nanofluids.

Nanoparticles can exist in different shapes and geometries depending on the manufacturing method. The most common forms are nanosphere and nanotubes. They may be modified further into spheres or tubes of multiple layers as well. Carbon nanotubes (CNTs) and carbon multiwall nanotubes (CMWNTs) exhibit greater enhancements in thermal conductivity compared to other forms in which nanoparticles are crafted: thermal conductivity enhancements over 100% have been recorded for CNTs where the nanotubes are modified into multi-walled carbon nanotubes (Assael et al, 2006).

A vast majority of the research publications on this subject of nanofluid thermal conductivity suggest nanofluids have enhanced thermal conductivity compared to conventional heat transfer fluids under different operating conditions, but the reliability of these results as regards using them in real life engineering applications is contestable because of persistent discrepancies in their values. It is evident that there are major discrepancies in the experimental and numerical simulations results on the thermal conductivity of nanofluids and the reasons may not be farfetched. One of those reasons may be differences in the methods of preparation which affects the nature of the

suspension, the other could be the size and distribution of particles and the conditions or parameters under which these tests or simulations are carried out.

2.3.2 Convective Heat Transfer

Convective heat transfer in nanofluids can be complicated as evident in the disparaging results contained in the literature and it causes one to wonder whether the methods of data collection were in the first instance suitable for those types of experiments. Care will be taken in this part of the literature so that it can optimally substantiate those results available out there. Kakaç and Pramuanjaroenkij (2009) described the enhancement of the heat transfer coefficient as a more effective factor than thermal heat conductivity for nanofluids in the design of heat exchangers. In this article, they have reviewed important works carried out to study the enhancement of forced convective heat transfer coefficients for nanofluids. They present results from the experiments performed (for the laminar flow regime, Reynolds number ranging from 650 to 2050) by Heris et al (2006) as shown in the Figure 3.
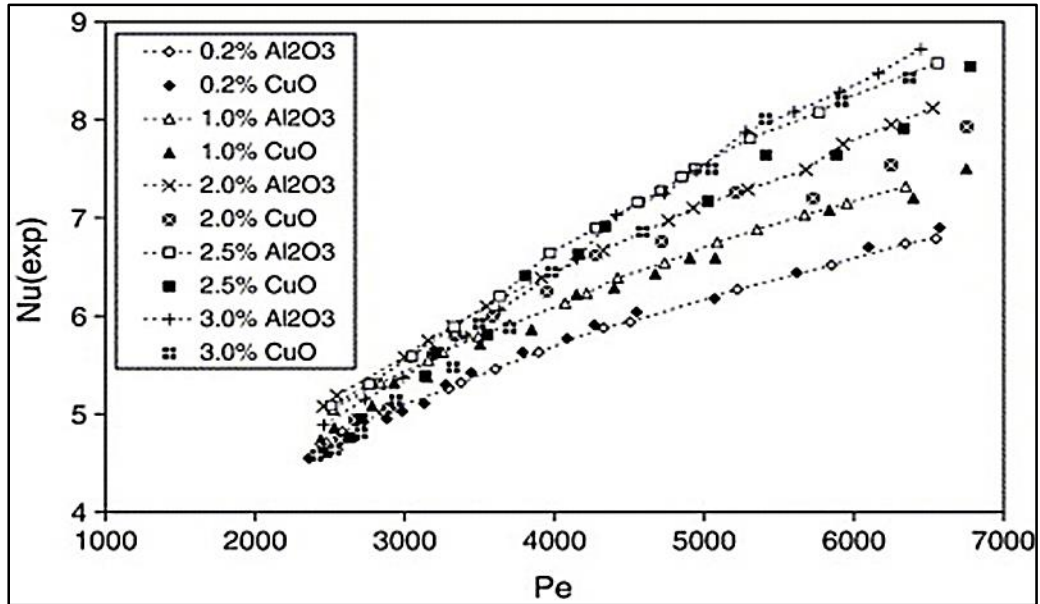
Figure 3. Experimental Nusselt number for Al2O3/water and CuO/water nanofluids (Heris and Etemad et al, 2006)

The Peclet number, *Pe*, represents an effect due to thermal dispersion as caused by micro-convection as well as micro-diffusion of the dispersed nanoparticles. Heris et al (2006) found that Nusselt number, *Nu*, appears to augment for the two nanofluids investigated (Al$_2$O$_3$ and CuO water based nanofluids) as the concentration and/or Peclet number increased. Their final analysis suggest Al$_2$O$_3$ showed superior heat transfer enhancements than CuO water based nanofluids for the same volume concentrations.

Buongiorno (2006) infer that nanofluids have higher thermal conductivity and higher single-phase heat transfer coefficients than their base fluids, stressing, however, that correlations for pure fluids such as the Dittus-Boelter's may not serve to accurately predict their heat transfer coefficients which tend to exceed the mere thermal conductivity effect.

Xuan and Roetzel (2000) questions the authenticity of theories and correlations that have been developed by viewing nanofluids as conventional solid-fluid mixture, claiming nanofluids behave more like single-phase fluid because the discontinuous phase comprises

of ultrafine particles that effectively replaces what would otherwise be a heat transfer interface. They developed a correlation for heat transfer of the nanofluid flowing through a tube as follows:

$$Nu_x = [1 + C^*Pe^n f''(0)]\theta''(0)Re^m]$$ (2.11)

An experimentally determined constant, C^* is obtained for the medium. When $C^* = 0$, it implies there is no dispersion in the medium. The terms f'' and θ'' are the second derivatives of the dimensionless velocity and temperature of fluid, while the exponents 'n' and 'm' depend on the flow pattern.

Maiga et al (2005) numerically investigated the hydrodynamic and thermal characteristics of nanofluid convection flow through a straight heated tube and through the annulus of heated co-axial disk for the laminar flow regime using Ethylene Glycol–γAl_2O_3 and water–γAl_2O_3 nanofluids. They proposed heat transfer enhancement with the increase of nanoparticle concentration and Reynolds number, but also record corresponding drastic negative effect on the wall shear stress.

Duangthongsuk and Wongwises (2010) suggested that the suspension of TiO2 nanoparticles in water use remarkably augmented the heat potential of the base fluid. Working with TiO2-water nanofluids, they had observed that in the flow through a horizontal double counter- flow exchanger for turbulent flow conditions, enhancement in the coefficient of heat transfer reached 26% compared to water, the particle concentrations were been kept at 2% max and 0.2% minimum. They also observed that such enhancements were even more pronounced with increasing Reynolds number. For particle concentrations greater than 2.0 vol. %, however, heat transfer coefficients dropped to as much 14% below

those of the base fluid. The experiments were conducted for Reynolds number ranging between 3000 and 18000. The experimental set up for their experiment is shown in Figure 4.
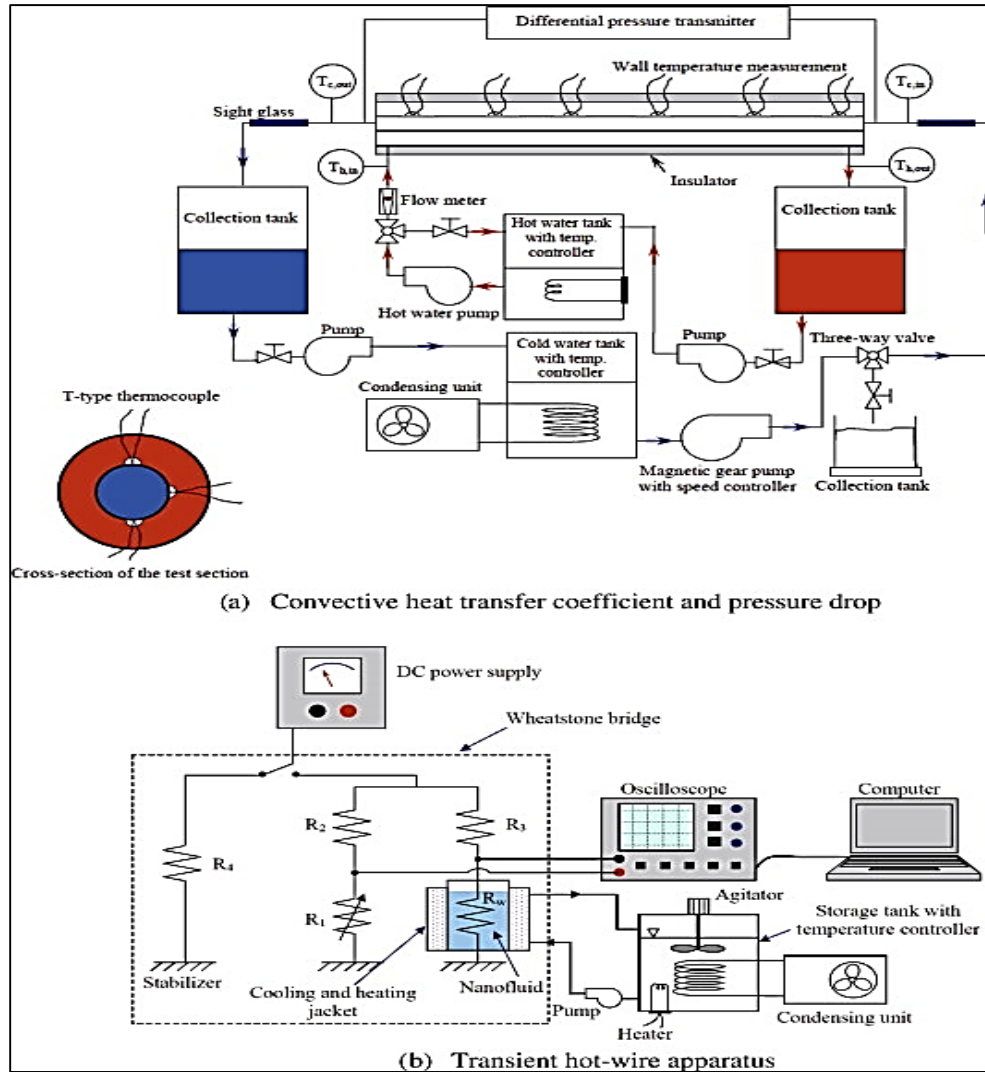
Figure 4. Experimental set ups (a) for measuring pressure drop across test section and (b) apparatus for measuring thermal conductivity of nanofluid. (Duangthongsuk & Wongwises, 2010)

Wen and Ding (2004) also observed enhancement of convective heat transfer in γ-Al_2O_3 nanoparticles and de-ionized water laminar flow through a copper tube, whose wall

was subjected to constant heat flux, in the laminar flow regime. They found that heat transfer was particularly enhanced in the entrance region for the flows. They propose particle migration into the boundary layer and the consequent disturbance of the laminar sub-layer as being partly responsible for the observed enhanced heat transfer. They also observed that classical Shah Equation was unable to predict the observed heat transfer behavior of the nanofluids.

Wu and Zhao (2013) reviewed some of the most recent nanofluid studies on topics including the thermo-physical properties, convective and boiling heat transfer performances as well as critical heat flux (CHF) enhancement. They found that current experimental data of nanofluids neither suffice nor are reliable for engineering applications because there are inconsistencies or contradictions in the measurements or models thus far developed and there appear to be no standard for which experimental results can be compared or ratified. They suggest areas where work needs to be done in order to 'bridge' the gaps in these findings, and these include investigating the stability of nanofluids under flow and non- flow conditions; developing a standard database of thermo-physical properties for nanofluid that would include detailed characterization of nanoparticle sizes, distribution and stabilizers. Other areas where expedient actions need to be taken are the interaction of nanoparticles and boundary layer, surface tension and bubble dynamics of boiling nanofluids as they may provide more insight into nanofluid heat transfer and CHF enhancements.

The following Table 2 shows a number of Nusselt number correlations reviewed for the flow of nanofluid in a tube as reported by (Sundar and Singh, 2013). Note the φ represents the volume concentration of nanoparticles in the nanofluids.

Table 2. Nusselt number correlations reported in the literature for nanofluid in a tube (Sundar and Singh, 2013)

Equation	Nanofluid	φ, (%)	'Re' range
$Nu = 4.36 + \left[a \times x_+^{-b}(1+\varphi^c)exp^{(-dx_+)}\right]\left[1+e\left(\frac{d_p}{d_f}\right)^{-f}\right]$	Al_2O_3	4.0	$500 < Re < 2,000$
$Nu = 0.4328(1 + 11.258\,\varphi^{0.754}Pe_d^{0.218})Re^{0.333}Pr^{0.4}$	Cu	2.0	$800 < Re < 4,000$
$Nu = a\,Re^b Pr^{1/3}\left(\frac{D}{L}\right)^{1/3}\left(\frac{\mu_b}{\mu_s}\right)^{1/3}$	Graphite	2.5	$5 < Re < 120$
	$Al_2O_3\text{-}Cu$	0.1	$Re < 2,300$
$Nu = 1.619\,(x^+)^{1/3},\ x^+ < 0.01,\ x^+ = \frac{2(x/D)}{Re Pr}$ $Nu = 0.021 Re^{0.8}Pr^{0.5}$	Al_2O_3	6.0	$431 < Re < 2,000$
	ZrO_2	3.0	$140 < Re < 362$
	Al_2O_3, TiO_2	3.0	$10^4 < Re < 10^5$
$Nu = 0.0059(1.0 + 7.6286\,\varphi^{0.6886}Pe_d^{0.001})Re^{0.9238}Pr^{0.4}$	Cu	2.0	$10^4 < Re < 2.5 \times 10^4$
$Nu = 0.074\,Re^{0.707}Pr^{0.385}\varphi^{0.074}$	TiO_2	2.0	$3000 < Re < 18,000$
$Nu = 0.086\,Re^{0.55}Pr^{0.5}$ Constant heat flux	Al_2O_3	10.0	$Re \leq 1,000$
$Nu = 0.28\,Re^{0.35}Pr^{0.36}$ Constant wall temperature	Al_2O_3	10.0	$Re \leq 1,000$
$Nu = 0.085\,Re^{0.71}Pr^{0.35}$	Al_2O_3	10.0	$10^4 \leq Re \leq 5 \times 10^5$
$Nu = 0.067\,Re^{0.71}Pr^{0.35} + 0.0005\,Re$	TiO_2	0.25	$5000 < Re < 30,000$
$Nu = 0.02172\,Re^{0.8}Pr^{0.5}(1.0 + \varphi)^{0.5181}$	Fe_3O_4	0.6	$3000 < Re < 22,000$
$Nu = \frac{(f/8)(Re - 1000)Pr}{1 + 0.2\,(f/8)^{1/2}(Pr^{2/3} - 1)}$	Al_2O_3	3.6	$5000 < Re < 65,000$
	ZrO_2	0.9	$5000 < Re < 65,000$
$Nu = 0.0023\,Re^{0.8}Pr^{0.3} + (0.617\varphi - 0.135)Re^{(0.445\varphi - 0.37)}Pr^{(1.081\varphi - 1.305)}$	Silver	0.9	$900 < Re < 12,100$
$Nu = 0.065(Re^{0.65} - 60.22)(1 + 0.0169\varphi^{0.15})Pr^{0.542}$	CuO, SiO_2	0.06	$3,000 < Re < 16,000$
$Nu = 0.065(Re^{0.65} - 60.22)(1 + 0.0169\varphi^{0.15})Pr^{0.542}$	Al_2O_3	0.1	$3,000 < Re < 16,000$
$Nu = 0.00105\,Re^{0.984}Pr^{0.4}(1 + \varphi)^{-80.78}\left(1 + \frac{\xi}{g}\right)^{2.089}$	CuO	0.3	$2,500 < Re < 6,000$

Azizian and Doroodchi et al (2014) in a bold step investigated the effect of external magnetic field strength and uniformity on the convective heat transfer and pressure drop of magnetite nanofluids under laminar flow regime conditions (Re < 830). Their experimental data (which were supported by simulation results) indicated that large enhancements in the local convective heat transfer had occurred with increased magnetic field strength and gradient, and seemed to be more pronounced at higher Reynolds number- with heat transfer coefficients increments reaching four times compared to where there had not been an application of magnetic field.
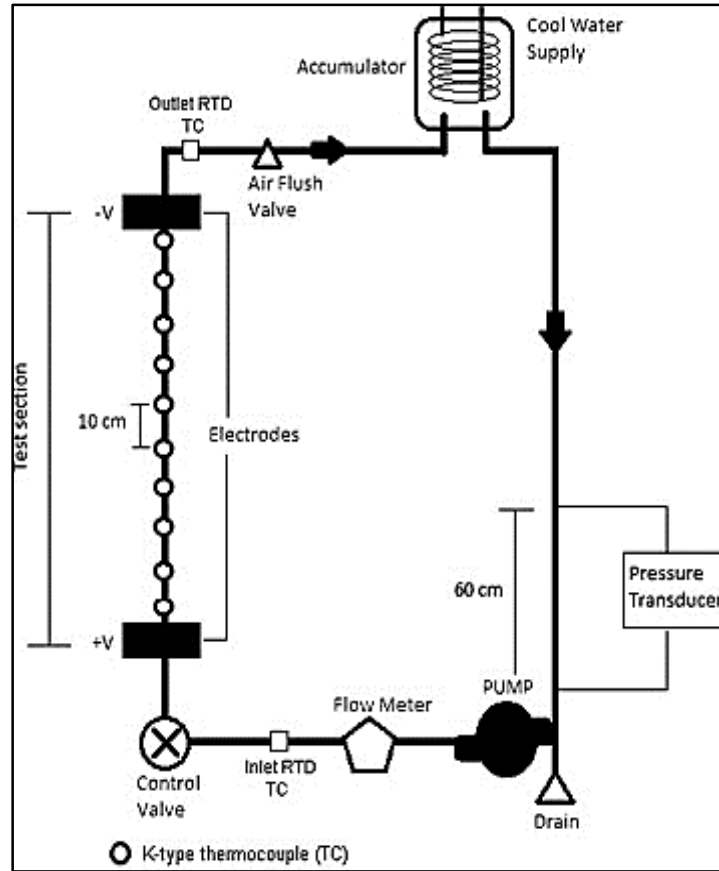
Figure 5. Schematic diagram of the closed loop convective laminar flow system (Azizian, Doroodchi et al, 2014)

Figure 5 is the schematic representation of the experimental setup used by Azizian et al (2014). They observed that the strength of the magnetic field had little influence on the coefficient of heat transfer- magnetic field intensity up to 430 mT and gradients between 8.6-32.5mT caused pressure drop to increase by only 7.5%. They attribute (judging by the results from their simulation of magnetic field and magnetic force distribution) the increments of the heat transfer coefficients to the accumulation of particles near the magnets with the resulting particle aggregates enhancing flow momentum and energy transfer.

The transfer of heat by natural convection will not be discussed here since it can be assumed that due to the short time spent by the fluid in the test section, natural convection will insignificantly affect the heat transfer. It is important, however, to mention that interest in natural convection in nanofluid with regards to MEMS and electronic cooling applications is growing. Other heat transfer phenomena not considered in this work, which may be important for more critical assessments of nanofluids is boiling. Local or pool boiling may adversely affect nanofluid performance in the sense that a phase change could occur which may affect heat transfer surfaces such as channel walls or even the nanoparticles themselves. Das et al (2003a) found that nanoparticles significantly affect boiling and can deteriorate the boiling characteristics of the nanofluid causing excessive surface temperatures and overheating.

CHAPTER III

EXPERIMENTAL APPROACH

In setting up the experimental systems, discrepancies among experimental results in the literature were given carefully considerations bearing in mind the many questions that have been asked about the validity and integrity of methodologies that have been employed in the past to investigate nanofluids

3.1 Description and Preparation of Nanofluid

The nanofluid being investigated in this report is a high concentration silicon (IV) oxide (9.58% in H_20) colloidal dispersion. The dispersed spherical and single walled nanoparticles have an average size of 0.02 micron or 20 nm. The dispersion originally manufactured by Alfa Aesar was diluted from a particle mass concentration of 40% to 20% (or 9.68% concentration by volume). The resulting nanofluid spec was then observed in the laboratory (over 4 weeks) pre and post experiments for settling. The dispersion continued to be stable during these periods of observation with no significant settlements found. Sharif (2015) in his thesis had found that the nanofluid of interest showed non-Newtonian behaviors. The nanofluid was reported as shear thickening between 14 and 55, but did not experience any hysteresis loss in thermal conductivity upon intermittent heating and cooling. Thermal conductivity measurements were obtained for temperatures ranging from 7°C to 50°C. See Appendix A for more details on their work.

Non-Newtonian fluids are defined as materials which do not conform to a direct relationship between shear stress and shear rate while being subjected to steady deformation (Dodge and Metzner, 1959). While numerous rheological relationships exist for non-Newtonian fluids, the fluid considered here has been determined to be time independent, dilatant (shear thickening) and presumed non-viscoelastic.

3.2 Description Test Loop and Test Section

A test flow loop designed to measure pressure loss and convective heat transfer coefficients under fixed wall boundary conditions has been constructed. The flow loop is such that different sizes (i.e. various hydraulic diameters) of test section can be installed. The major components of the flow loop being a reservoir, variable speed gear pump, flow meter, the test section and the pressure transducers. Others are the metering valves (fully open and close control valves) and thermocouples. Data is collected at intervals of 0.1 second with an Agilent data acquisition system. The piping, excluding the tests sections, comprises of quarter inch stainless steel tubes, flexible reinforced unreactive rubber and plastic tubes. Brass ferrules serve to insure smooth entry of flow into test sections and serve as well to seal joints and prevent leaks through them. A gear pump (see specifications in Table 3) circulates nanofluid at steady mass flow rate through loop.
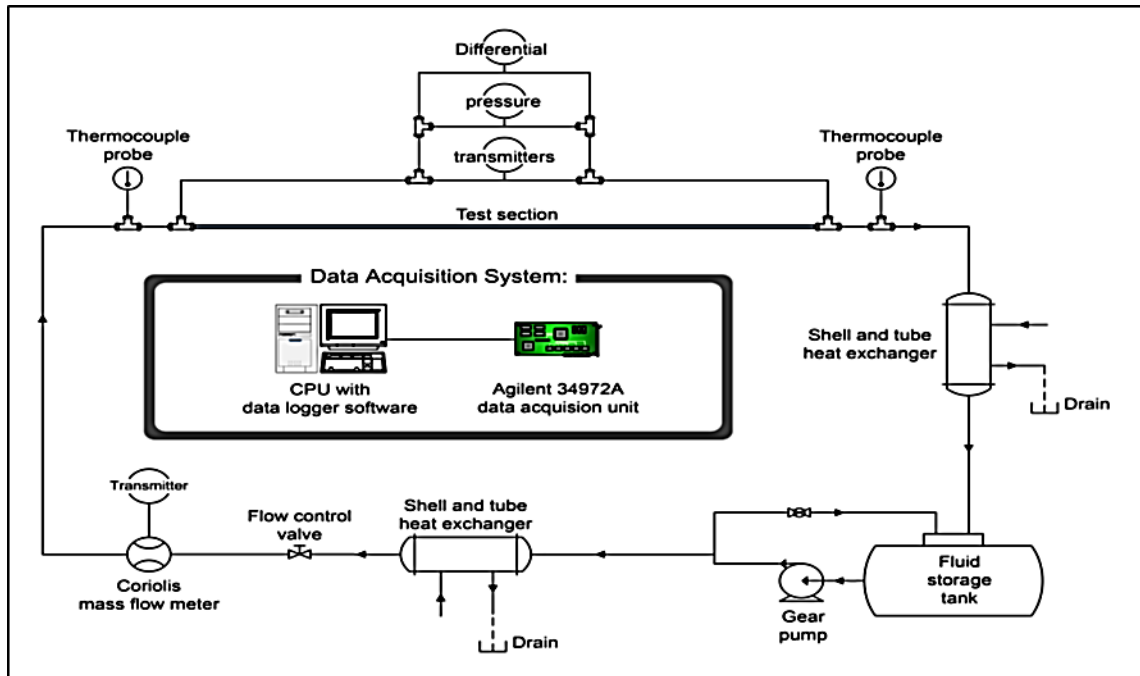
Figure 6. **Schematic of experimental loop or setup (Tiwari, 2012)**

Constant heat is supplied to the test section by delivering direct current through the test section, thus the resistance to the passing currents results in its own heating. The current was delivered through a 2 (32 mm^2), 600 V welding cable that is able to withstand temperatures in the range of -50°C to 105°C. The output current was then routed through a 50 millivolt precision constantan shunt resistor of ±2% accuracy. A section of the flow loop, as shown in the schematic diagram in Figure 6, has been insulated to insure adiabatic boundary conditions enabling constant heat flux through the wall of the test sections to be maintained.

Heat Exchanger: Two counter flow heat exchangers, which may be referred to as the secondary loop, are installed before and after flow through the test section to maintain steady reservoir temperature. The heat exchangers employed in the system formation are

the concentric tube counter flow type, each comprises a 0.5 inch diameter stainless steel

tubing with length of 38 inch. Each of the heat exchangers is fitted in the test loop with the

help of a 0.5 inch tee connection with one bore through fitting from Swagelok on each end.

The bore through fitting has a 0.5 inch thread on one end and a 0.25 inch compression

fitting on the other. The threaded end is connected to the tee while the compression fitting

maintains a seal in between the 0.5 inch tubing and the 0.25 inch tubing.

Figure 7. Pressure tubes-transducer connection

Three pressure transducers were used in the experimental system, each measuring

different maximum pressures. The ranges of pressures measured by the three transducers

are 0 to 9 psi, 0 to 36 psi and 0 to 300 psi respectively. The calibration range of voltage for

the transducers in the order of their measuring capacities starting with the smallest are

1.1263 to 2.4409 Volts, 4.5034 to 9.6039 volts and 37.371 to 74.644 volts. The measured

pressures are differential static pressure between the flow inlet and exit from the test section. The Figure 7 above is a view of a section of the experimental set-up showing how the pressure taps are connected to the pressure transducers.

Table 3. Components of experimental setup

S/N	Component	Manufacturer	Model	Description/Specifications
1	Data Acquisition	Agilent	34972A	34972A LXI Data Acquisition/Switch Unit Used with Multifunction Module, DIO/Totalize/DAC and 2x 34901A Multiplexer, Agilent Benchlink Data Logger 3
2	D.C. Source	Agilent	N5761A	LXI Class C, 6V/180A, 1080W
3	Mass flow meter			Micro motion mass flow sensor, Pmax-1812psi at 25°C, process temp. range -240-204°C, ambient -40-60°C. Accuracy = +/0.05%
4	Pump	Leeson Washguard	C6T17WK1J	Variable speed, gear pump, 1/2hp, 1725rpm, 208-230v, 60hz,
5	Pressure transducers	Emerson		MWP: 6092psi at @ 200F, 4000psi @ 400F,, Body/Trim316SS,, PG 10-1100121903
5	Flow measurement transmitter	Emerson	S/N 3207964	Measuring accuracy equals ±0.65% of span
6	Valves	Swagelok		
7	Thermocouple connector	Omega	SMPW-T-MF	Flat pin connectors, color coded for ANSI or IEC
10	Thermocouple	Omega	T-type	
9	Flow guide	Omega		Copper Ferrules
8	Cover Insulation			
11	Insulation			
12	Precision Shunt resistor	DELTEC	MKB C 1210	50 millivolt, 500 ampere
13	Pipe connectors			

Table 3 shows the major components of the experimental system setup and their specifications as necessary.

Liquid Tank: A PVC tank with a holding capacity of 15 liters serves as reservoir, from which fluid is pumped. The tank rests on a flat surface 1m above the center line of pump shaft. See Table 3 for specifications/ratings of pump and other components of the flow system.

Figure 8 Pressure transmitter in-use position

Figure 9 Agilent Data Acquisition unit

The experimental test sections are three C260 hypodermic (ASTM 135) hexagonal tubes of hydraulic diameters (D) 1.67, 2.46 and 3.26 millimeters respectively. They each have a thickness of 0.014inch. Thermocouple pairs are cemented in in a t-joint form to the flats along the axis of each test section at intervals of 1.0 inch, with the first pair of 10 being installed 1.5 inch from the entrance of the test section. The member of each thermocouple pair are separated radially at an angle of 180 degrees. The thermocouples are painstakingly cemented on the surface of the test section using epoxy, and insuring only the welded tip of the thermocouple actually touch the TS surface to minimize conductive from multiple surfaces. C260 Cartridge Brass Alloy is commonly used for electrical/electronic components and other micro cooling applications, and readily available in the configuration of the flow cross section of interest.
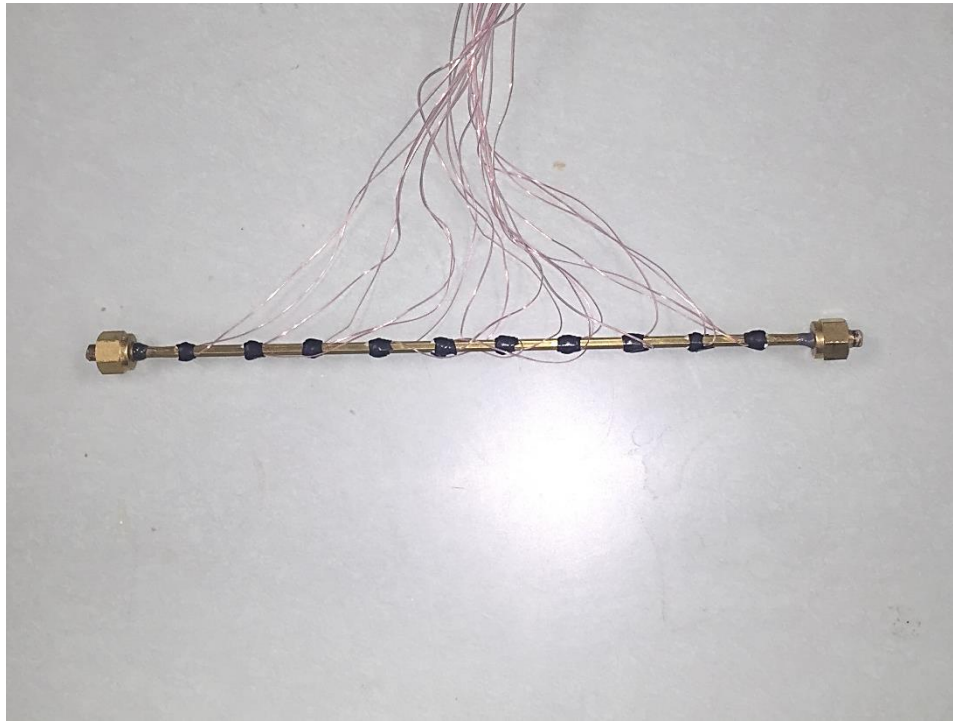
Figure 10. External view of test section with D = 3.26 mm

Location of Thermocouple: The thermocouple locations (see Table 4) on the tests sections are given by the dimensionless distance (x/D) where x is the distance from the entrance of fluid into test section.

Table 4. Location of thermocouple on test section

Test section hydraulic diameter		Location of of thermocouple (X/D)									
[m]	[in]										
0.0017	0.07	22.81	38.02	53.23	68.44	83.65	98.86	114.07	129.28	144.49	159.70
0.0025	0.10	15.46	25.77	36.08	46.39	56.70	67.01	77.32	87.63	97.94	108.25
0.0033	0.13	11.70	19.49	27.29	35.09	42.88	50.68	58.48	66.28	74.07	81.87

Figure 11 Bead welding machine

The thermocouples end were joined by forming a bead junction using the welder shown in Figure 11. The beads were of average diameter of 0.05 mm to prevent or minimize loss of point temperature measuring accuracy

3.3 Temperature and Heat Transfer Considerations

Effects of local boiling were minimized by conducting the experiments at temperatures between 15°C and 65°C. The outer surface local temperatures of the test sections are measured with the aid of the T-type thermocouples. The used attachment of thermocouples to the outer surface of the wall of the test sections was a more feasible approach than drilling through the walls so as to reach the flow surface wall. Contingencies from the latter approach may be too complex to account for without good vision of the thermocouple location. The internal wall temperatures are computed from an appropriate conduction equation. Two T-type thermocouples are installed to measure the bulk fluid temperatures at the inlet and exit of flow. The thermocouples have been calibrated for a measuring accuracy of ±0.1°C.

The inlet and exit temperature probes measure the fluid's bulk mean temperature. It is only practical that boundary layer approximations and steady state assumptions are made to ease the complexity of the resulting analysis. The free stream temperature T_∞ is the temperature of the fluid nearest to or at the axis of symmetry of the flow where the temperature of the fluid is constant in the radial direction away from the way. Precautions were taken during experimentations to insure that these assumptions remain reasonably valid. The bulk mean temperature of the flowing fluid T_b is approximated similar to the mean fluid temperature for constant surface heat flux flow conditions for circular tubes which varies linearly in the flow direction.

$$T_{bx} = T_i + \frac{x}{L}(T_e - T_i) \tag{3.1}$$

The inner wall temperatures are computed with the conduction correlation for fully developed flow through a circular pipe with wall under constant heat flux given by Çengel and Ghajar (2011) as follows:

$$T_{wo} = T_{wi} - \frac{q_s R}{k_w}\left(\frac{3}{4} - \frac{r^2}{R^2} + \frac{r^4}{4R^4}\right)$$

(3.2)

where r = D/2 and R = D/2 +t. Note that t is the thickness of the test section. The inner wall temperatures differed from the outer wall temperature by a maximum of 0.1°C for all local points considered for all the test sections. This no surprise since the walls of the test sections are very the thin with thickness of 0.14 inch.

3.4 Transport Considerations

Specific Heat and Viscosity

The specific heat of the nanofluid have been evaluated by curve-fitting of data from the literature. The equation is given in the calculations section of the thesis. The differential scanning calorimetric method may be used in future work to measure specific heat capacity of the nanofluids. The specific heats of the nanofluids decreased compared to water as was expected.

Sharif (2015) used the rotational Brookfield DV-II+ Pro Extra viscometer in the experiments on the viscosity of the nanofluid in view and water as well. The accuracy of the method was verified by comparing the measured data of water with literature values and was found to be within acceptable margins of error. The data obtained by Sharif (2015) showed that the nanofluid in view was non-Newtonian. Initial estimates of Reynolds number and Prandtl number in this thesis relied on the information from their experiments.

42

Non-Newtonian Fluids

Regardless of how much it is sought, it's almost impossible to definitively describe the rheological relation for this class of fluid suitable for general engineering applications (Dodge and Metzner, 1959). Unlike Newtonian fluids, the viscosities, μ, of non-Newtonian fluids are dependent on the rate of shear, *du/dy*, and so Non-Newtonian fluid properties cannot be adequately described using the Newton's law of viscosity. While countless number of classification may exist for non-Newtonian nanofluids, broadly speaking, they may be categorized as time-dependent or time-independent. The complexity of the non-Newtonian fluid may even be expanded depending on whether it is time-dependent (in which case it's viscosity either decreases or increases with duration of stress).

Although the Metzner and Reed (1955) correlations were developed using pseudoplastic non-Newtonian fluids flowing through circular pipes, the paper suggests the equation can be applied to dilatant fluids to give very practical estimation as well. Further experiments have shown that a vast spectrum of non-Newtonian fluids may be represented over wide ranges of shear rate by a two-constant power law. While a fluid may fall into a category of classification, rheological properties or even assigned values resulting from such classifications appear to be very sensitive to the conditions of experiment under which they are developed. The nanofluids presented have been found to be time-independent from the experiments conducted by Sharif (2015).

Nanofluid viscosity underlie the analysis of both the hydrodynamic and heat transport for nanofluids. The dynamic viscosity of a fluid may best be visualized in a *Couette flow*: this flow type is an idealistic representation of a fluid layer sandwiched by

two horizontal smooth plates (see Figure 12), one of zero velocity the other traveling parallel to the fluid surface at fixed velocity u. Edge effects are neglected since the plates are infinitely wide.
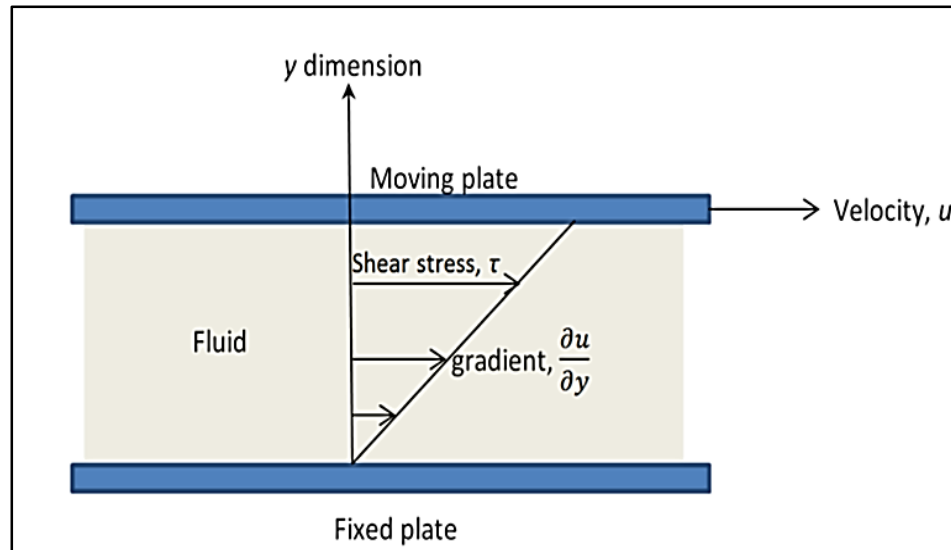

Figure 12. Velocity gradient formed between two parallel plates.

The movement of the top plate is thought of as occurring only due to the application of a parallel force *(F)* on the end opposite the direction of velocity. This movement thus causes a velocity gradient *(∂u/ ∂y)* to develop within bulk the fluid (in other words, layers of different velocities each with the layer adjacent to moving wall having the wall velocity while the layer closest to the stationary wall has a velocity of zero i.e. no slip condition). Layer velocities decrease from top to bottom when viewed as a longitudinal cross section. The flow properties of nanofluids including viscosity, for example, may elude conventional two-phase flow description in the view of the effects posed by factors such as gravity, Brownian motion, fluid/particle and or fluid/fluid frictions, and Brownian diffusion

3.5 Instrument Calibration and Experimental Procedure

Proper calibration of instruments have been carried out to insure high accuracies are achieved for instruments. The thermocouples were calibrated in a thermostat water bath and the accuracy was found to be within 0.1 K. Calibration procedure for transducers are described in the following subheadings.

3.5.1 Pressure Transducer Calibration

Each one of the three transducers is calibrated with the aid of a handheld pneumatic pump of range 0-580psi and an electronic gauge of range 0-300psi. The temperature outputs from transducers are read against applied pressure from the pneumatic pump. The procedure is outlined as follows:

1.   Connect the digital pressure gauge to the hand pump.

2.   Connect the hand pump to the high pressure side of pressure transmitter and apply some pressure

3.   Observe arrangement for pressure loss for about 2minutes, if not proceed to next step

4.   Apply pressure starting from 1psi and record corresponding voltage observed on electronic gauge

5.   Repeat step 4 for stepwise pressure increment of 1psi until upper range of pressure transmitter is achieved

Results obtained for each transducer are plotted into linear graphs. Graphs are curve fits showing the relationship between pressure applied on transducers and voltage drop

across transmitter. The linear equation is programmed into the data unit to read off pressure drops.

3.5.2 Pressure Drop Measurement

1.   Inspect assembly ensuring all fittings are in place with all valves except flow loop bypass valve closed.

2.   Turn on data acquisition unit and open interface program on PC

3.   Start-up pump keeping a relatively low flow rate and allow to self-prime

4.   Open heat exchanger water supply

5.   Open all other valves in the flow loop to allow flow though the main flow loop

6.   Shut bypass valve

7.   Allow flow to stabilize

8.   Adjust pump power to give desired flow rate, fine-tuning with the fine-tune valve

9.   Allow flow to steady at desired flow rate, ensure pressure readings are the same for all transducers unless reading are outside range specified for shorter range transducers

10.   Observe process until a steady state trend

11.   Restart data monitor/collector user interface and collect data

12.   An average of 150 Scans per data set is recommended

13.   Repeat steps 1-12 for other desired flow rates.

14. After runs have been completed, to shut down setup, first open the bypass valve in step 6 and the shut inlet valve, and then gradually turn down pump power until pump stops completely

3.5.3 Heat Transfer Measurements

1. Repeat steps 1-10 as described for pressure drop measurement

2. Turn on DC supply unit

3. Set DC until a maximum temperature no more than 59°C is recorded

4. Ensure steady state is observed, then repeat steps 11-13 as described for pressure drop measurement above

5. For better accuracy, the difference between the fluid exit and inlet temperatures should be not be less than 4°C

6. Insure that the DC power supply is turned off first and then the pump. Turning the pump first might cause excessive temperature in the test section damaging the thermocouples and the test section. For nanofluid, excessive heat can cause dry out and clog up the test section.

3.6 Validation of Experimental Method

Validation of the method of experimentation used in developing the data being analyzed in this thesis work is carried out with the testing of the experimental setup using a well characterized conventional fluid which is distilled water. Because water data are readily available in the literature, it serves the most convenience for the purpose of vetting

the experimental method. Comparison of obtained data with those established in the literature help to validate the experimental approach employed here.

Metzner and Reed (1955) had developed, for conventional friction coefficient and Reynolds number for non-Newtonian fluid flow through pipes, correlations that are theoretically rigorous in the laminar flow region. These correlations were tested with experimental data for 16 different non-Newtonian fluids. The development of the correlation was based on the Raboninowitsch expression for the rate of shear of a fluid and entirely independent of the fluid properties provided the fluids neither experiences time-dependent shear thinning (thixotropic) nor shear thickening (rheopectic). They also observed that the derivative or slope of the log plot of the wall shear stress, DΔP/4L versus shear rate of the fluid, 8V/D, measured for fluid flow through a pipe and the intercept of the plot are constant over a wide range of values of DΔP/4L or 8V/D. And, K' and n' represent the apparent viscosity (of the fluid under the circumstance) and the degree to which the fluid is non-Newtonian respectively. K' is the exponential of the log plot intercept and n' the slope of the graph

Where n' is less than unity, the fluid is pseudoplastic otherwise it is dilatant. A value of unity for n' means the fluid is Newtonian. The following equation from the basis for the development of the power law model used to describe the relationship between the shear stress and the shear rate of many non-Newtonian fluids,

$$\tau_w = K'\left(-\frac{du}{dr}\right)_w \tag{3.3}$$

Tw is he shear stress exerted by flow on the wall and du/dr is the stain exerted on the fluid by the wall, (no slip boundary condition was assumed). Note that the Metzner and Reed (1955) described in the preceding paragraph had been developed off the power law model.

Metzner and Reed (1955) thus developed an equivalent of the Poiseuille relation for the Darcy friction coefficient *f* and a generalized Reynolds number N_{Re} which may occasionally be referred to as the Metzner Reynolds number for the remainder of the report:

$$f = \frac{16\gamma}{D^{n'}V^{2-n'}\rho} \tag{3.4}$$

Where $\gamma = g_c K'8^{n'-1}$, and g_c is a conversion factor since the equation has been developed using Customary units, with a value of ***32.2ft.lb/s²lbf***, and equals unity for *SI* units.

And, the Reynolds number N_{Re} based on the (Metzner, Reed 1955) is given as follows.

$$N_{Re} = \frac{D^{n'}V^{2-n'}\rho}{\gamma} \tag{3.5}$$

The investigated pipe diameters varied from 1/8-12*in*. It must be noted, though, that there had be a testing of their result on thixopectic, rheopectic or dilatant fluids, but, they suggest the extension of the developed correlations would shed more light for both theoretical and practical points of view.

The above Metzner and Reed (1955) equations are robust and correlate the hydrodynamic characteristics of water very closely. The results are given in the next chapter as validation of the methods performance and applicability to the nanofluid.

The following conventional correlations serve as basis for comparing the results from the experiments conducted for distilled water and nanofluid.

Conventional Reynolds number

$$\text{Re} = \frac{\rho V D}{\mu} \tag{3.6}$$

Conventional friction coefficient C_f or the fanning friction factor is one-fourth of the Darcy friction coefficient for circle. Theoretical friction coefficient of laminar flow is calculated by the Poiseuille equation for hexagonal tubes,

$$C_f = \frac{15.05}{N_{\text{Re}}} \tag{3.7}$$

Bhatti and Shah (1987), Colebrook and White (1937) and the Blasius (1913) relations for friction coefficients are renowned for their robustness in predicting turbulence and are given by equations 3.8, 3.9 and 3.10 respectively

$$C_f = (0.00512 + 0.4572 N_{\text{Re}}^{-0.311})/4 \tag{3.8}$$

$$C_f = 0.316 N_{\text{Re}}^{-0.25} \tag{3.9}$$

$$C_f = \frac{\left\{-2 \log_{10}\left[\frac{\varepsilon}{3.7} - \frac{5.07}{Re} \log_{10}\left(\varepsilon - \frac{5.02}{Re} \log_{10}\left(\frac{\varepsilon}{3.7} + \frac{13}{\text{Re}}\right)\right)\right]\right\}^{-2}}{4} \tag{3.10}$$

The generic Colebrook and White (1937) implicit relation (Equation 3.10) was developed by Zigrang and Sylvester (1982) and can be can be extended to predict transition flow. Brkić (2011) reviewed explicit approximations of the Colebrook and White (1937) equation by carrying out statistical analysis of various approximations of the correlation equation. They recommended the Zigrang and Sylvester (1982) correlation because of the high accuracy with which it predicts friction factors for turbulent pipe flows. The equation is developed for Reynolds number ranging between 4000 and 10^8 and $0.00004 < \varepsilon/D <$

0.05. The results obtained from using this equation will shed more light on the smoothness of the pipe inner wall surface.

Lienhard and Lienhard (2013) defines the roughness Reynolds number, Re_ε.

$$Re_\varepsilon = Re_D \frac{\varepsilon}{D} \sqrt{\frac{f}{8}} \tag{3.11}$$

The above relationship is used to determine where flow is hydraulically smooth, transitionally or fully rough. Note that the Blasius (1913) correlation is valid for $4000 < Re < 5 \times 10^5$ and the Bhatti and Shah (1987) is valid for $4000 < Re < 5 \times 10^7$.

The theoretical heat transfers for both fluids are calculated with Lienhard and Lienhard (2013) and Gnielinski (1976) correlations for laminar and turbulent flow respectively. The correlations of Lienhard and Lienhard (2013) valid for $1000 < Re < 3000$ and Gnielinski (1976) valid for $3000 < Re < 5 \times 10^6$ are given by Equations 3.12 and 3.15 respectively

$$Nu = 4.364 + 0.263 \left(\left(\frac{x^+}{2} \right)^{-0.506} \right) \exp \left(-\frac{41x^+}{2} \right) \tag{3.12}$$

where x^+, as described by Lienhard and Lienhard (2013), is the dimensionless axial location or twice the inverse of the Graetz number Gz, an independent variable valid for the solution of the uniform wall temperature and uniform wall heat fluxes.

$$x^+ = 2/Gz \tag{3.13}$$

$$Gz \equiv \frac{Re_D PrD}{x} = \frac{PeD}{2} \tag{3.14}$$

$$Nu_D = \frac{\left(\frac{f}{8}\right)(\text{Re}_D - 1000)Pr}{1 + 12.7\sqrt{\frac{f}{8}}\left(Pr^{\frac{2}{3}} - 1\right)}$$ (3.15).

where *f* is the Darcy friction factor

3.7 Data Processing

The empirical friction coefficient is derived from measured parameters using the following Darcy-Weisbach relation:

$$f = \frac{D\Delta P}{2L\rho V^2}$$ (3.16)

Local heat transfer is expressed in terms of the Nusselt number which has been defined based on the hydraulic diameter of the test section. The Nusselt number,

$$Nu_D = \frac{hD}{k_{nf}}$$ (3.17)

The local heat transfer coefficient, as defined by (Kays, Crawford et al, 2012)

$$h_x = \frac{q_s}{T_{wi} - T_{bx}}$$ (3.18)

The experiment is performed at constant surface heat flux q_s, for each test section

$$q_s = \frac{IV}{A_s}$$ (3.19)

Thermal conductivity of the nanofluid with respect to temperature is obtained using the fitted equation from Sharif (2015) data which had been obtained with a KD2 pro thermal properties analyzer with an accuracy of ±5% for the range: 0.2-2.0 W/mK

$$k_{nf} = 0.0013T_m + 0.056 \tag{3.20}$$

Thermal conductivity of tube wall (or brass), k_w with respect to temperature is obtained by curve fitting data from Kothandaraman (2004)

Specific heats of water as is related to temperature is curved fitted from data available in Haynes (2013) and SiO2 are obtained by curve fitting data from the literature.

The nanofluid mixture's specific heat capacity is given by:

$$C_{nf} = (1 - \varphi_{np})C_{bf} + \varphi_{np}C_{np} \tag{3.21}$$

where C_{bf} and C_{np} are the specific heats of the basefluid and nanoparticles respectively, and φ_{np}, the mass fraction of the nanoparticles.

Prandtl number for liquid is given by:

$$Pr = \frac{\mu C_p}{k} \tag{3.22}$$

For nanofluid, the apparent viscosity which is determined experimentally, represents the dynamic viscosity. For water, viscosity is determined by the fitted curve of data from of (Kestin et al, 1978).

Measuring uncertainties are given as ±0.5°C and ±0.31°C for the T-type and RTD sensors respectively.

CHAPTER IV

EXPERIMENTAL RESULTS

The application of nanofluid to engineering systems is daunted by the lack of consistent data pools. These discrepancies particularly exacerbate the difficulty of estimating the benefits of using nanofluids for heat transfer purposes. Nanofluids have high area to volume ratio and are promising for advanced heat transfer purposes where high effectiveness are required. This Chapter will discuss the results in terms of friction coefficient and Nusselt Number.

Reynolds number is a dimensionless parameter that serves as a measure of scales of fluid flows. It depends on the density, viscosity and travel velocity of the fluid as well as the characteristic length (hydraulic diameter has been used throughout this thesis) of the of the flow channel. For non-Newtonian fluids such as silicon (IV) oxide (9.58% in H_20) colloidal dispersion, which is being investigated in this thesis, determination of Reynolds number values are extremely challenging. This poses a blockade to predicting flow regimes making design decisions more difficult to make. It is for this reason, the thesis uses the well tested Metzner and Reed (1955) correlation for non-Newtonian flow to attempt to predict flow regimes. Because, the method had also been established to work for Newtonians alike, it makes sense to first test it using a well characterized Newtonian fluid. Results of the validity test are presented in the section of the thesis as well.

4.1 WATER RESULTS

The following results are presented for experiments carried out with water. They are set to validate and visualize the adequacy of the methodology used in this work. For simplicity the test sections may be referred to simply by their hydraulic diameters for the remainder of the results and discussion, that is to say that the test section whose hydraulic diameter is 1.67mm will simply be referred to as D = 1.67mm. In the same way the other two sections are D = 2.46mm and D = 3.26mm. Note that the test sections are of equal lengths and thickness (12 inches and 0.14 inches respectively)

4.1.1 Friction coefficient

Here, friction coefficient for all three test sections are presented for all flow regimes. The results obtain clearly point to the suitability of the experimental method to the thesis work objectives. To allow for ample time for fluid flow to re-laminarize, the T-type thermocouples which measure the inlet and exit bulk temperatures of the working fluid had been placed sufficiently far from both ends of the test section. The length covering the test section and both thermocouples are adequately lagged to avoid loss of heat to the ambient and insure boundary conditions are maintained over for the entire duration of the experiments.
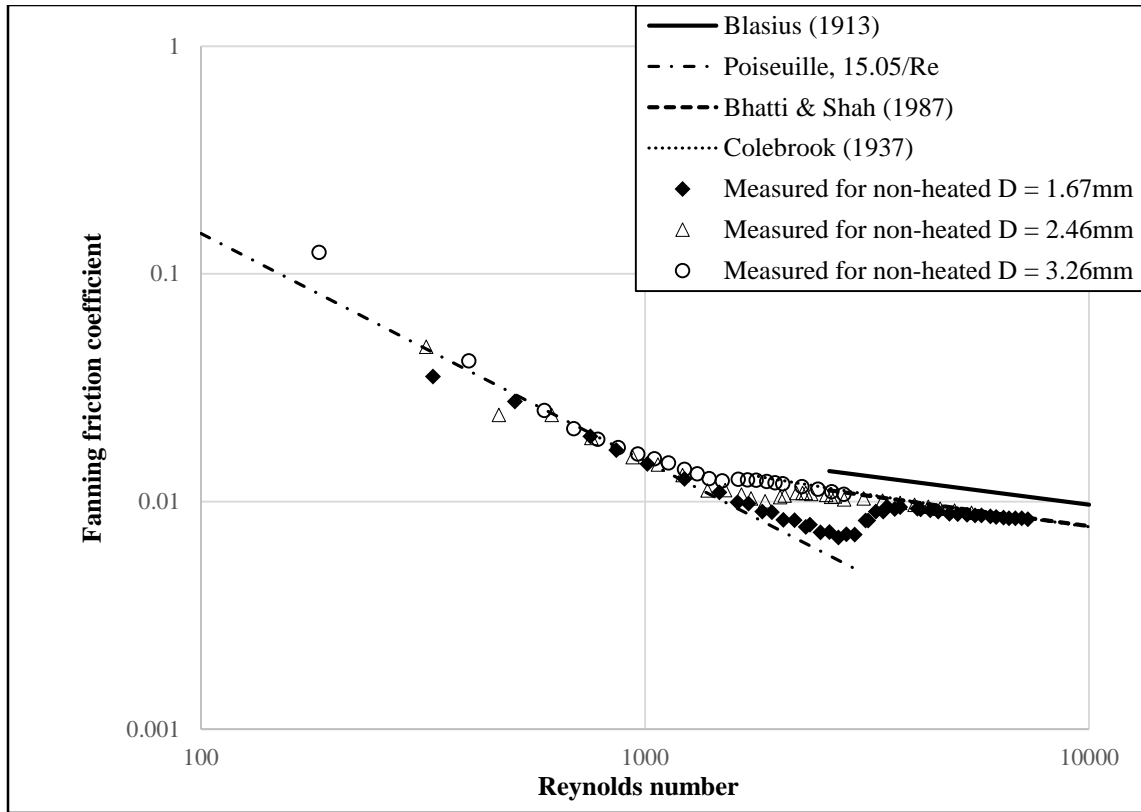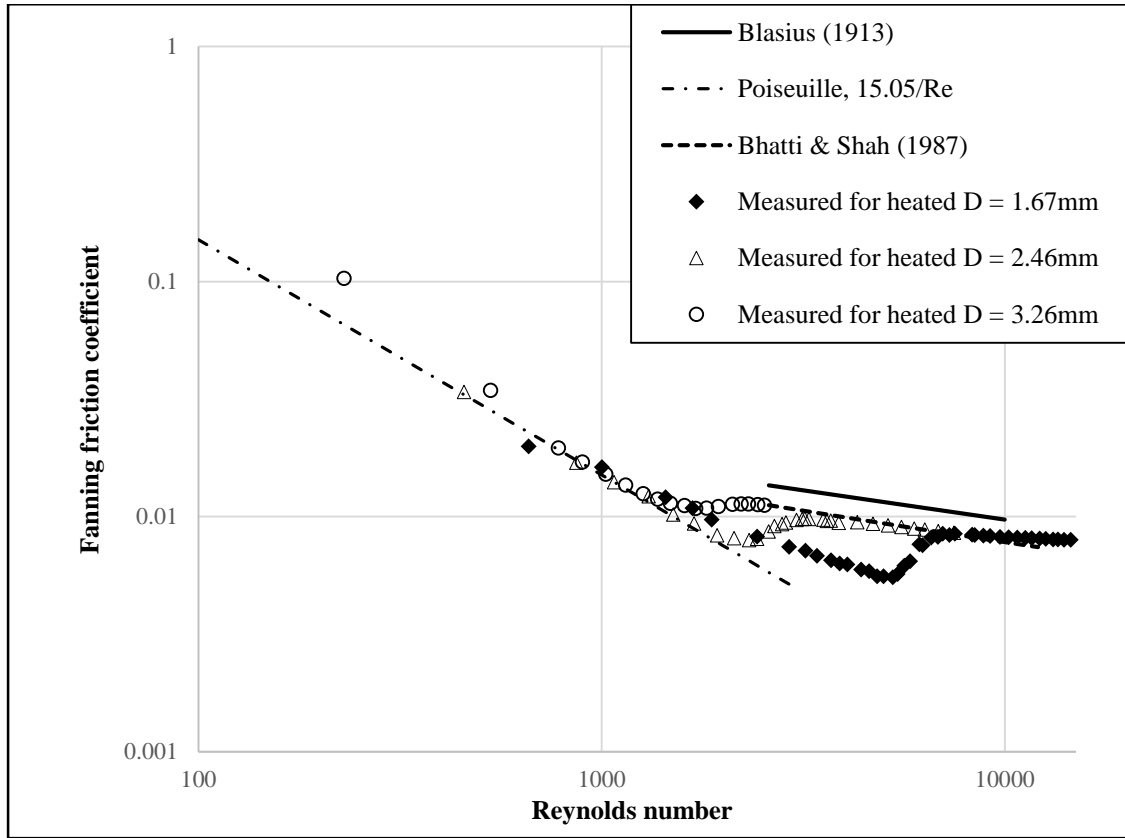
Figure 13. Comparison of friction factor for distilled water flow in unheated test sections D = 1.67 mm, D = 2.46 mm and D = 3.26 mm

In the Figure 13 above, it can be seen that flow regimes generally follow classical theories. At very low Reynolds numbers, for all test sections, the effect of non-smooth entrance (due to connections) are manifested in the apparent deviations or short term turbulence seen initially in the friction factor plots at low Reynolds numbers. The transition regions appear to be less apparent with increasing hydraulic diameter of the test sections. It does appear that transition of flow from laminar to turbulent occurred earlier at a Reynolds number slightly over 2000 for D = 2.46 mm and D= 3.26 mm and seemed protracted. Whereas, for the smallest test section i.e. D = 1.67 mm, transition seemed swift but occurred much later at Re > 3500. The turbulent Blasius correlation over predicts the friction coefficient by 20%, data looks to correlate almost precisely with the Bhatti and

Shah (1987) correlation which seems more robust and able to account for the hexagonal cross-sectional area of the tubes, unlike the Blasius (1913) correlation that had been developed for circular pipes.

Figure 14. Comparison of friction factor for distilled water flow in heated test sections D = 1.67 mm, D = 2.46 mm and D = 3.26 mm

Figure 14 shows plots of friction coefficient versus Reynolds number for each test section with water flowing through it when the test sections are supplied with heat. The trends are not dissimilar to those obtained when no heat has been applied, the friction coefficients, however, appeared to be augmented when no heat is applied to a test section, and the onset of turbulence seemed earlier with heat as well. Figures 15, 16 and 17 show these details.
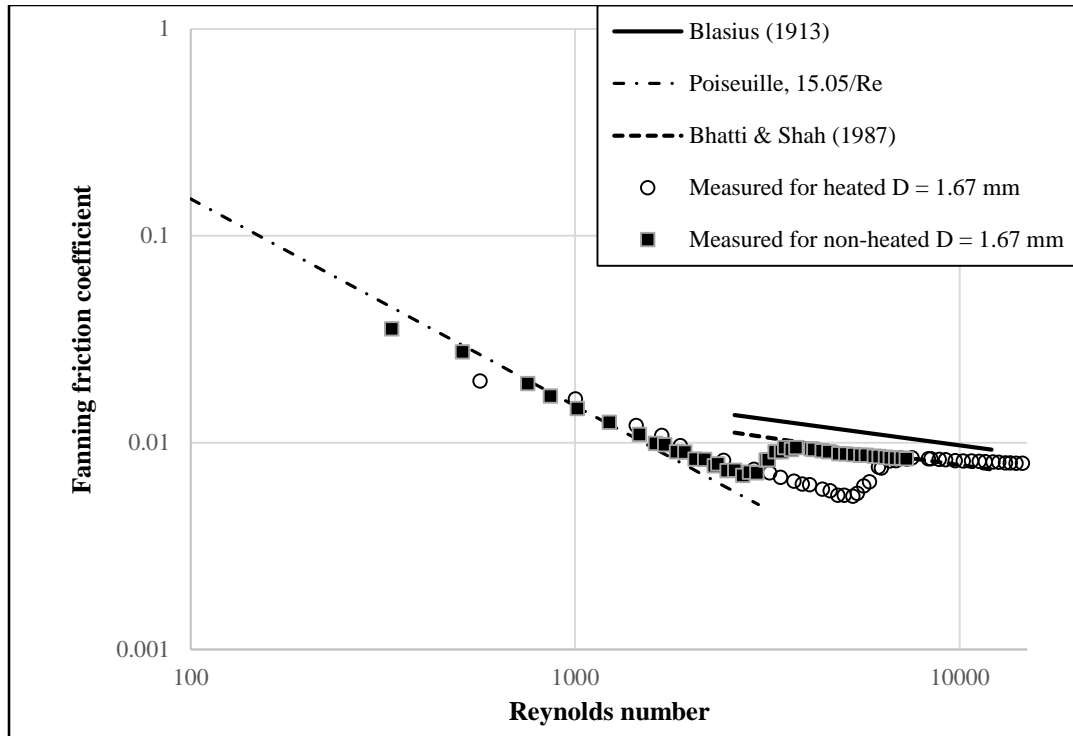
Figure 15. Comparison of friction factor for heated vs unheated flow of distilled water flow in test section D = 1.67 mm
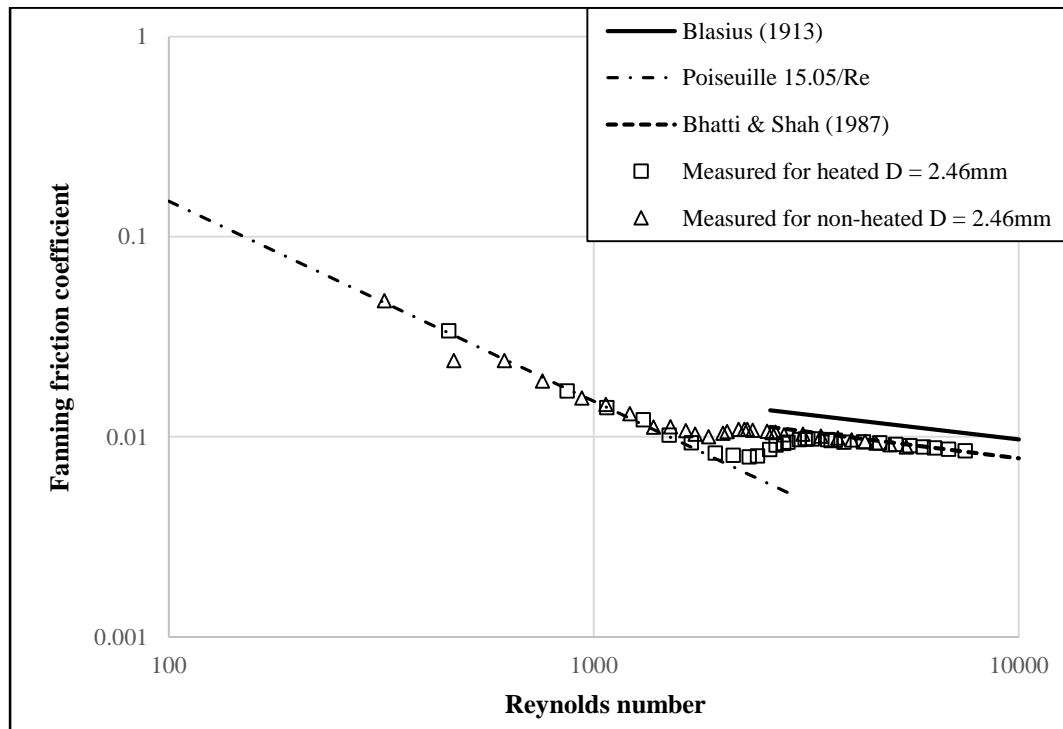
Figure 16. Comparison of friction factor for heated vs unheated flow of distilled water flow in test section D = 2.46 mm
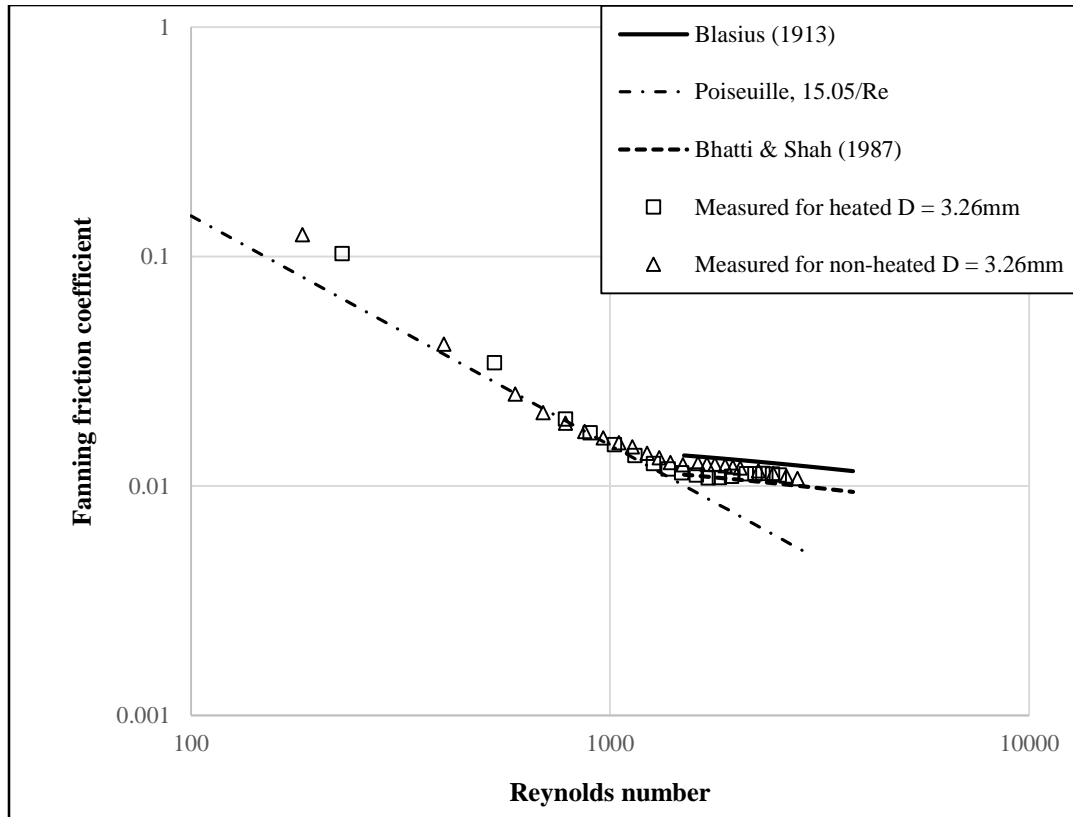
Figure 17. Comparison of friction factor for heated vs unheated flow of distilled water flow in test section D = 3.26 mm

The Colebrook's equation predicts turbulence for all three test sections very closely, thus confirms the validity of the assumption here that the test sections are hydro-dynamically smooth (See Figure 13). For the calculation done in this thesis $\varepsilon/D = 0.0004$ had been used. Note that for a smooth surface $\varepsilon/D < 0.0015$.

The Blasius (1913) equation seems to over-predict the friction factor, this may is because the equation was developed for circular tubes whereas the test sections being considered are of hexagonal flow section and the equation cannot account for the effects of the edges of the hexagonal flow area.

4.1.2. Heat transfer

The average of the local Nusselt number based on hydraulic diameter against Reynolds number is shown in Figure 18 for all three test sections as measured water flowing through each of them. Tests results have been collated for $\Delta T \geq 3°C$, where ΔT represents difference between inlet and exit temperature of fluid flowing through a test section. This is done in order to keep experimental within reasonable limit of error based on the accuracy of experimental apparatuses.
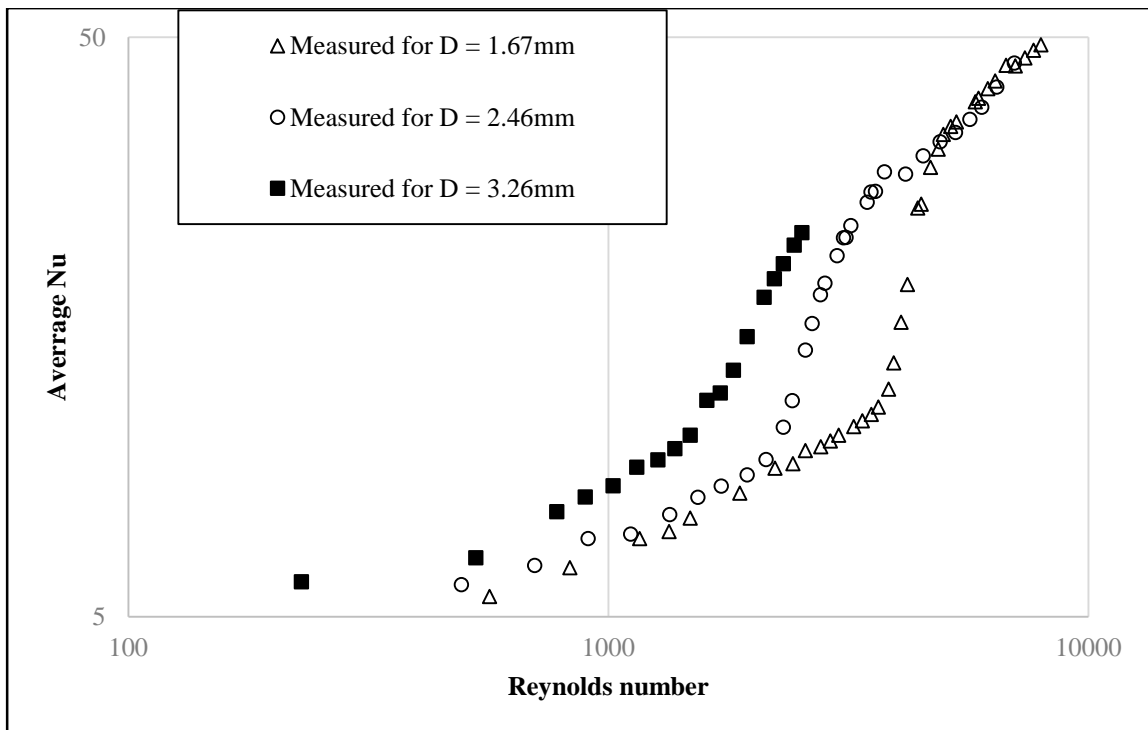

Figure 18. Comparison of measured Nusselt number vs Reynolds number for distilled water flow through heated test sections

The measured Nusselt numbers for the laminar and turbulent flow through each test section is given in the following plots. See Figures 19 and 20, the average Nusselt number for D = 2.46 mm plotted for specific Reynolds number for the laminar and turbulent flow

regimes respectively. The same way, results are presented for D = 1.67 mm and D = 3.26 mm in the following Figures 21 to 24. The measured local Nusselt numbers are compared with the average of the Lienhard and Lienhard (2013) Nusselt number for laminar flow, having been plotted against dimensionless distance x^+. The results obtained show compliance with the Graetz flow problem, where flow velocity profile but not thermal profile develops quickly. A general model was developed by Muzychka and Yovanovich (2004) for predicting heat transfer coefficient in the combined entry region of non-circular ducts.
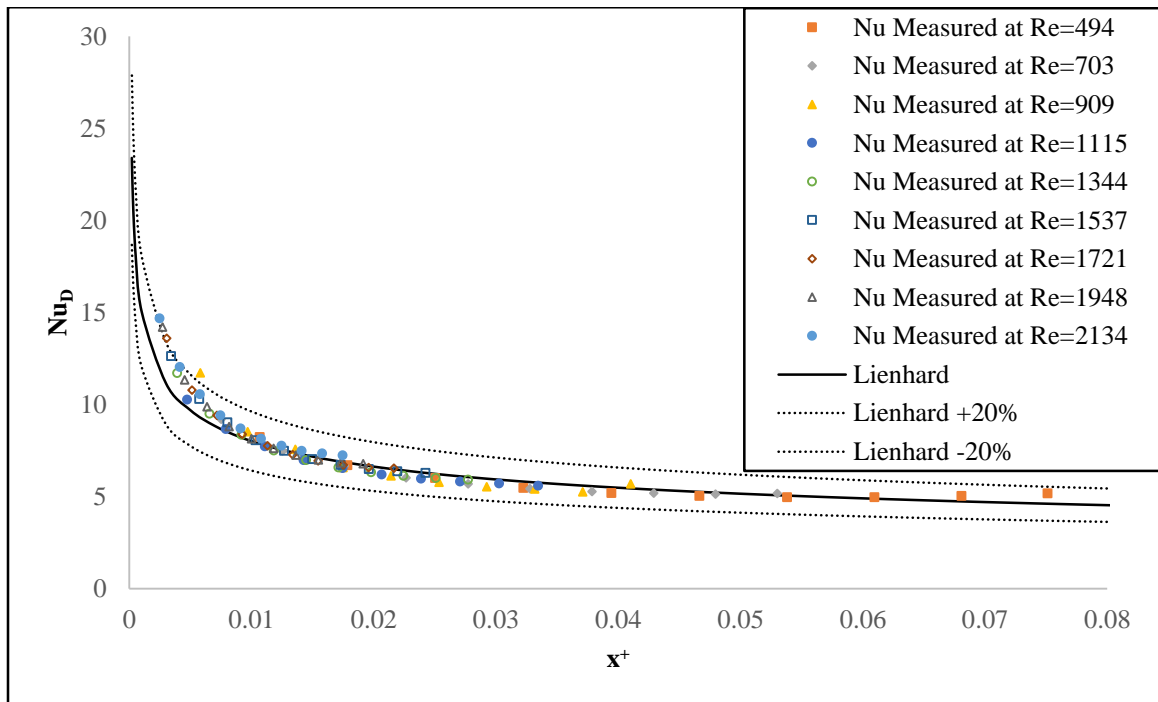
Figure 19. Measured Laminar flow Nusselt number vs x^+ for distilled water flow in heated test section D = 2.46 mm compared with the Lienhard and Lienhard (2013) correlation. Dotted lines represent ±20% error limits.

In Figure 20, the data points indicate the early stages of turbulent fluid flow by crossing the solid line, further down the data points seem to align with the solid. This is indicative of full turbulence.
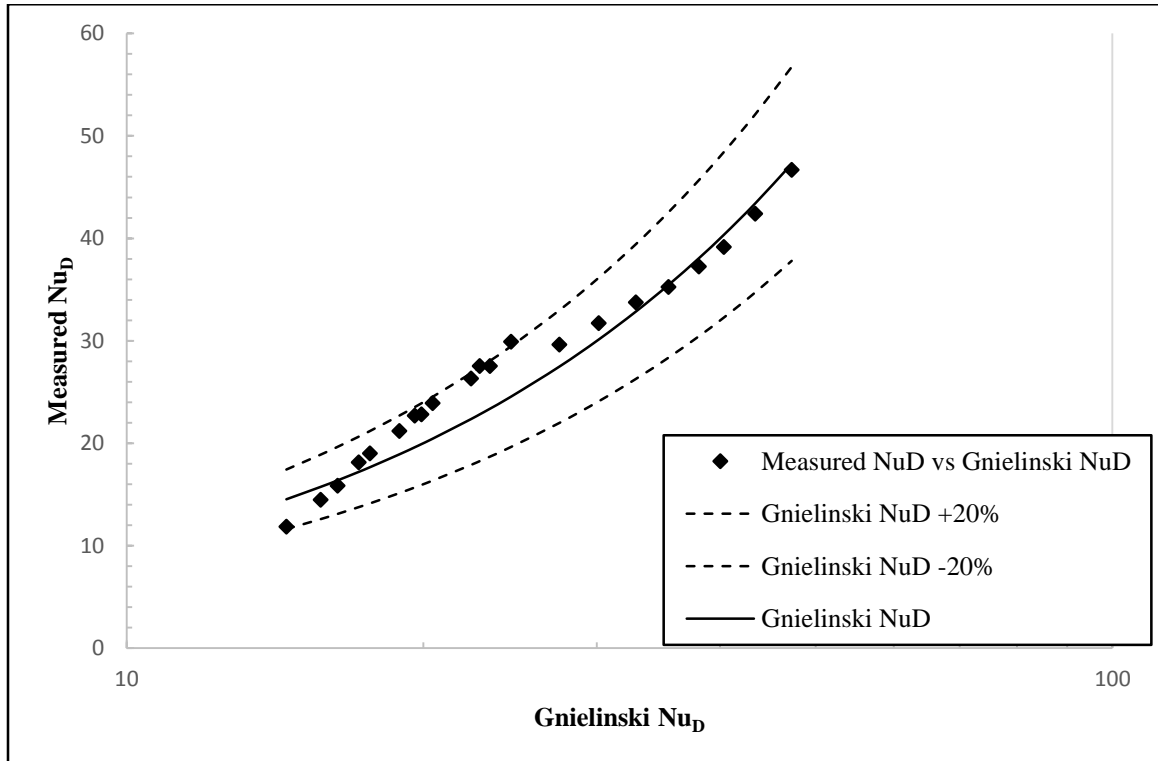

Figure 20. Comparison of Measured Nusselt number vs Gnielinski (1976) for distilled water flow in heated test section D = 2.46 mm. Broken lines represent error limits of ±20%

The results all indicate that the data collected for water correlate well with the Lienhard and Gnielinski correlations for Nusselt number in the laminar and turbulent regimes respectively, and are within an accuracy of 20% at all three flow regimes for all test sections. The results indicate that the flows are not thermally developed for all the cases (i.e tube sizes) considered.
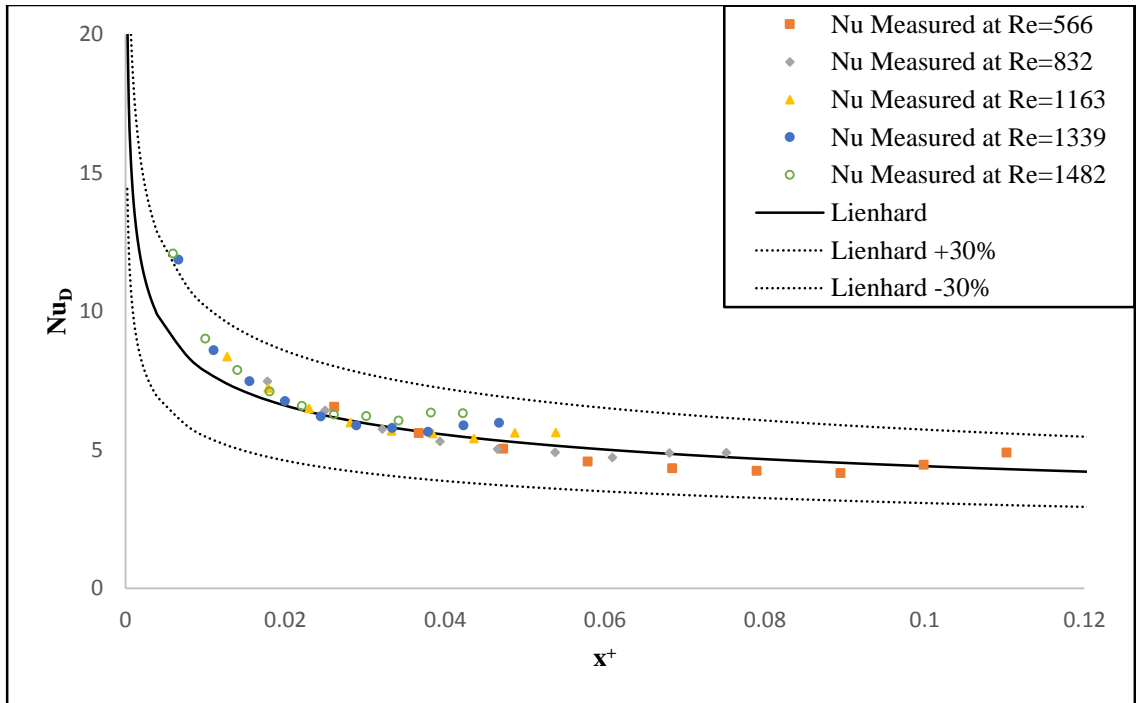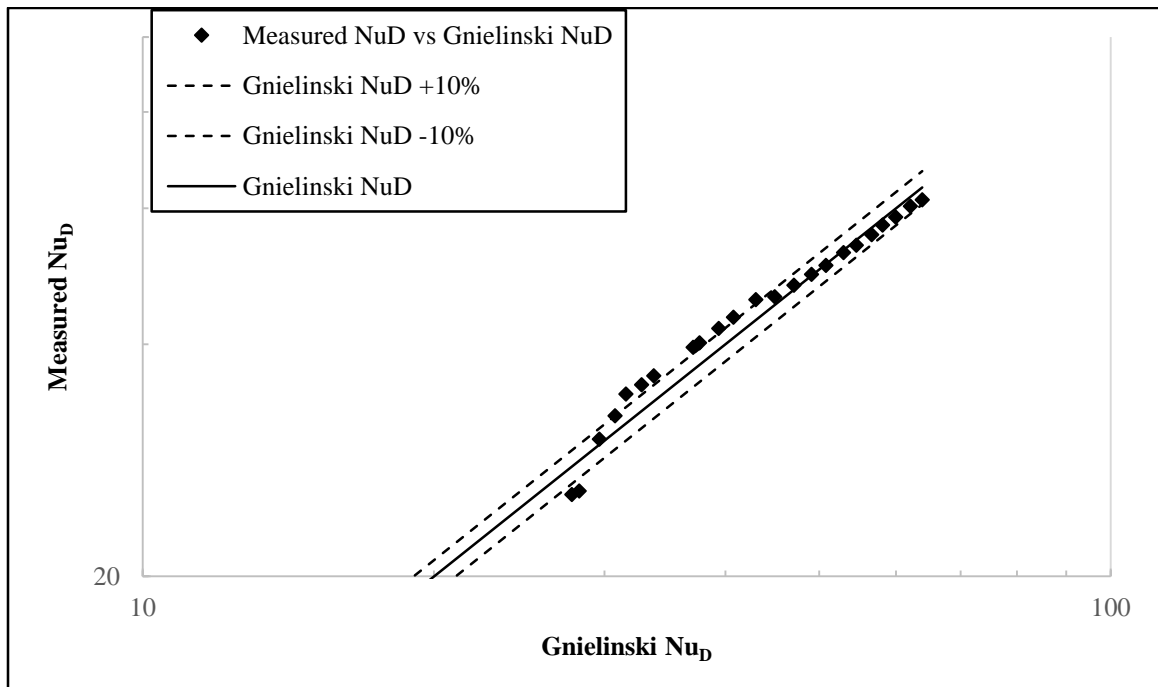
Figure 21. Measured Laminar flow Nusselt number vs x⁺ for distilled water flow in heated test section D = 1.67 mm compared with the Lienhard and Lienhard (2013) correlation. Dotted lines represent error limits of ±30%.

Figure 22. Comparison of Measured Nusselt number vs Gnielinski (1976) for distilled water flow in heated test section D = 1.67 mm. Broken lines represent error limits of ±10%
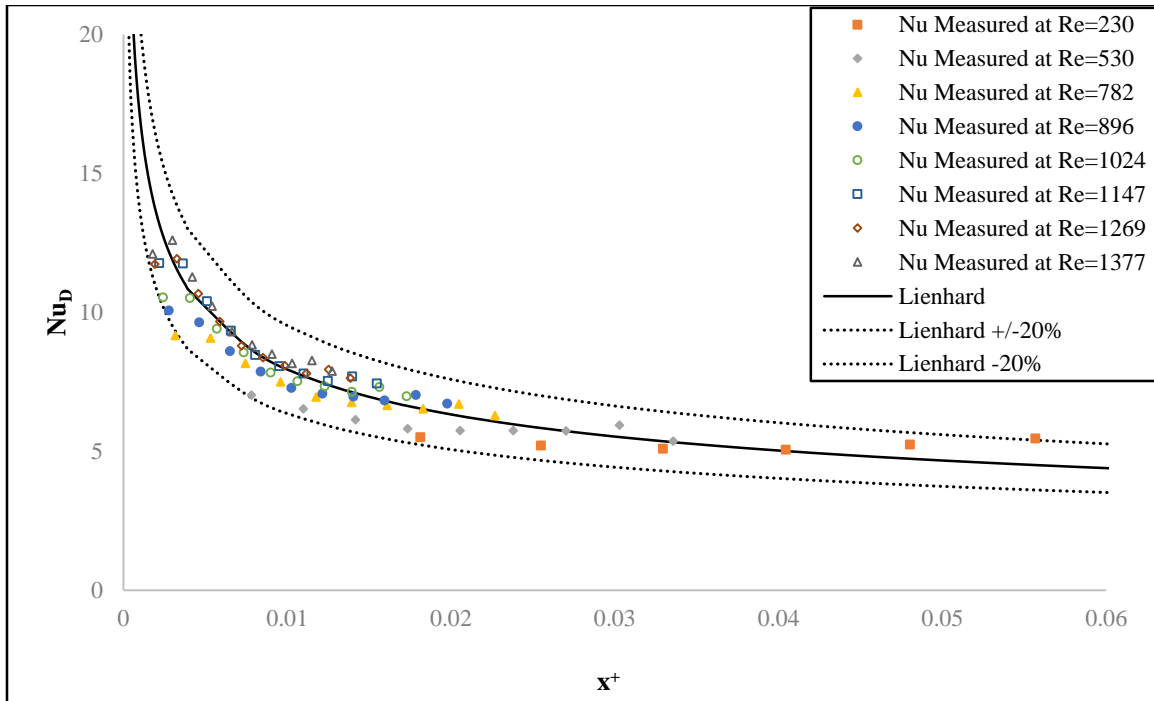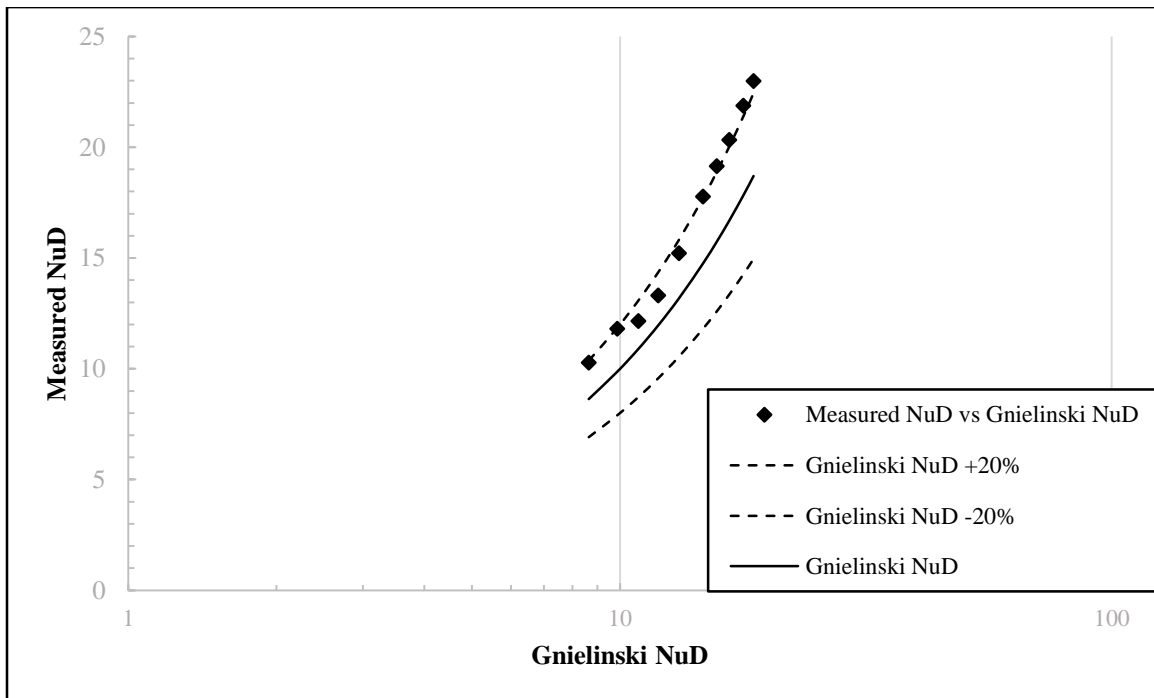
Figure 23. Measured Laminar flow Nusselt number vs x⁺ for distilled water flow in heated test section D = 3.26 mm compared with the Lienhard and Lienhard (2013) correlation. Dotted lines represent error limits of ±20%.

Figure 24. Comparison of Measured Nusselt number vs Gnielinski (1976) for distilled water flow in heated test sections D = 3.26 mm. Broken lines represent error limits of ±20%

64

4.2. Nanofluid (9.8% vol. SiO$_2$-water colloid) Results

4.2.1 Friction coefficient

Results obtained for nanofluid show good resemblance to those of water. The trends are almost identical, although the friction coefficient values for nanofluid appear augmented compared to distilled water. The inflection points seen on the graphs indicate the onset of flow regime change.
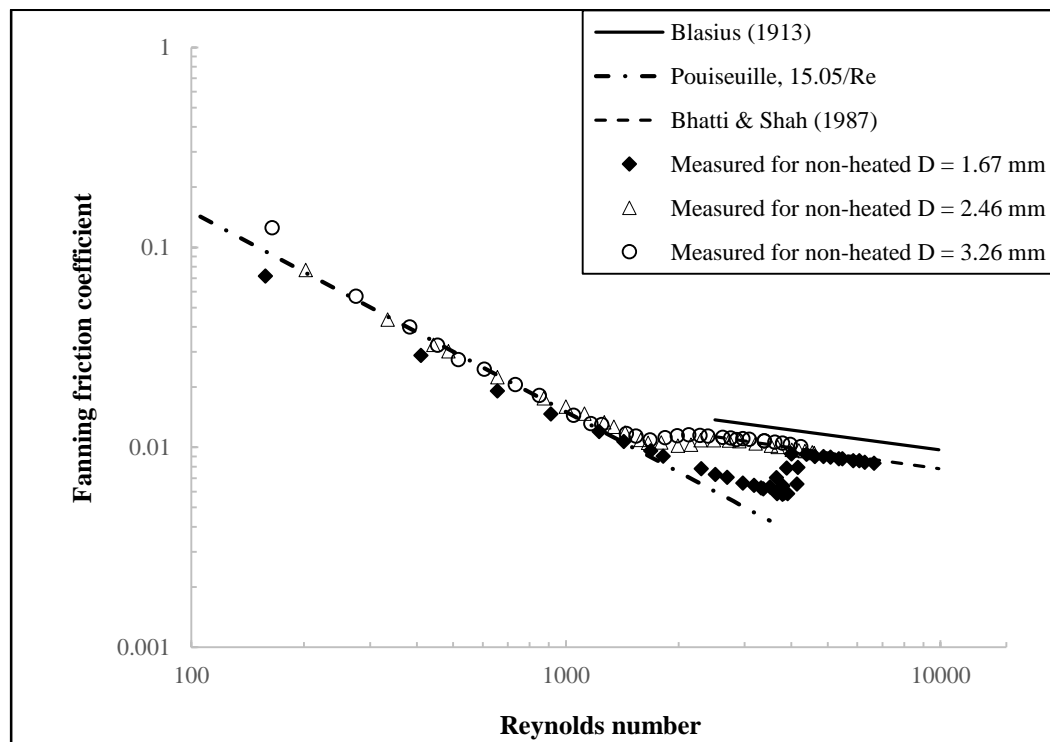

Figure 25 Comparison of friction factor for nanofluid flow in unheated test sections D = 1.67 mm, D = 2.46 mm and D = 3.26 mm

As observed for water, the transitioning of nanofluid flow from laminar to turbulence is more pronounced with decreasing hydraulic diameter, although this happens

relatively quickly as see from the steepness of the slope on the graphs shown in Figure 25. The entrance effects are similar to water, and appear to diminish with increasing Reynolds (See Figures 25 and 26). The outliers seen initially at low Reynolds number soon vanish as flow velocity increasing and the data points beginn to fall in line with the Poiseuille correlations
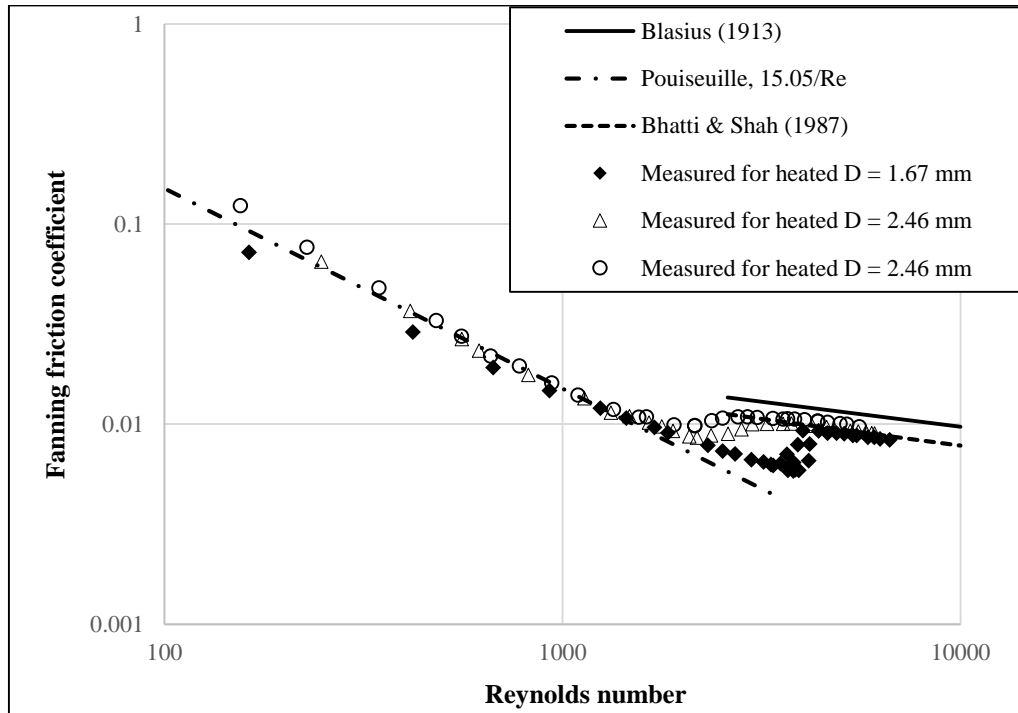

Figure 26. Comparison of friction factor for nanofluid flow in heated test sections D = 1.67 mm, D = 2.46 mm and D = 3.26 mm

For the 9.8% vol. SiO_2-water nanofluid, it does not appear that heating had any significant effect on the friction coefficients, as the friction coefficients were almost the same whether or not the section had been heated. The friction coefficients are compared for the test sections (see Figures 27, 28 and 29) with and without heat. Unlike in water, the onset of transition in nanofluid flow has not been significantly affected by the application of heat. This is probably because for the range of experimental temperatures, the gain in

kinetic energy by particles of the nanofluid are much less compared the convective force

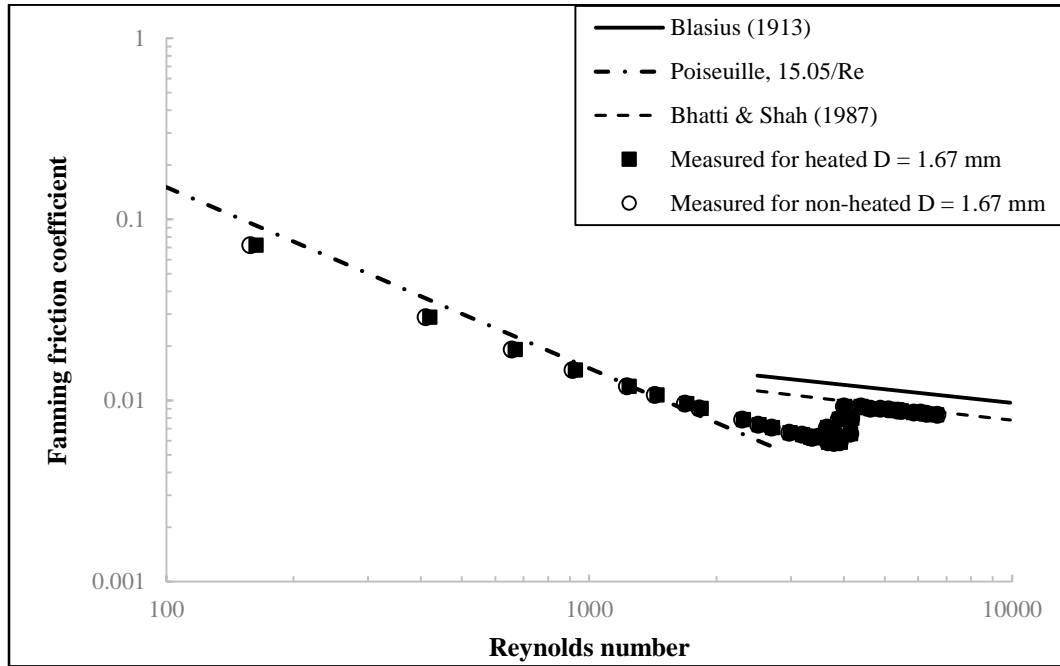due to fluid driver that their effects are overwhelmed.

Figure 27. Comparison of friction factor for heated vs unheated flow of nanofluid flow in test section D = 1.67 mm
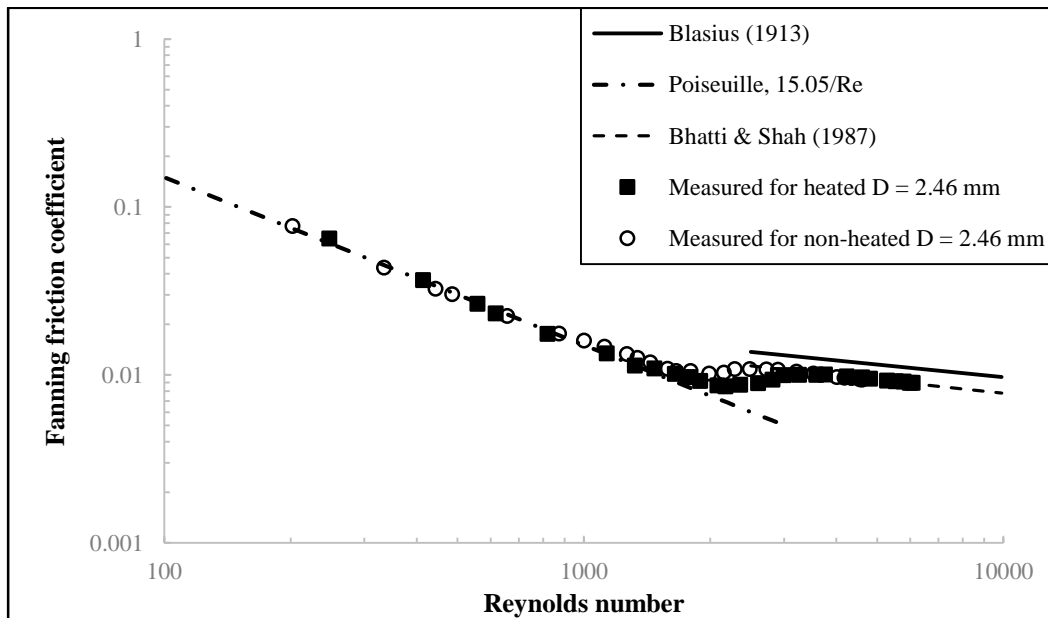

Figure 28. Comparison of friction factor for heated vs unheated flow of nanofluid flow in test section D = 2.46 mm
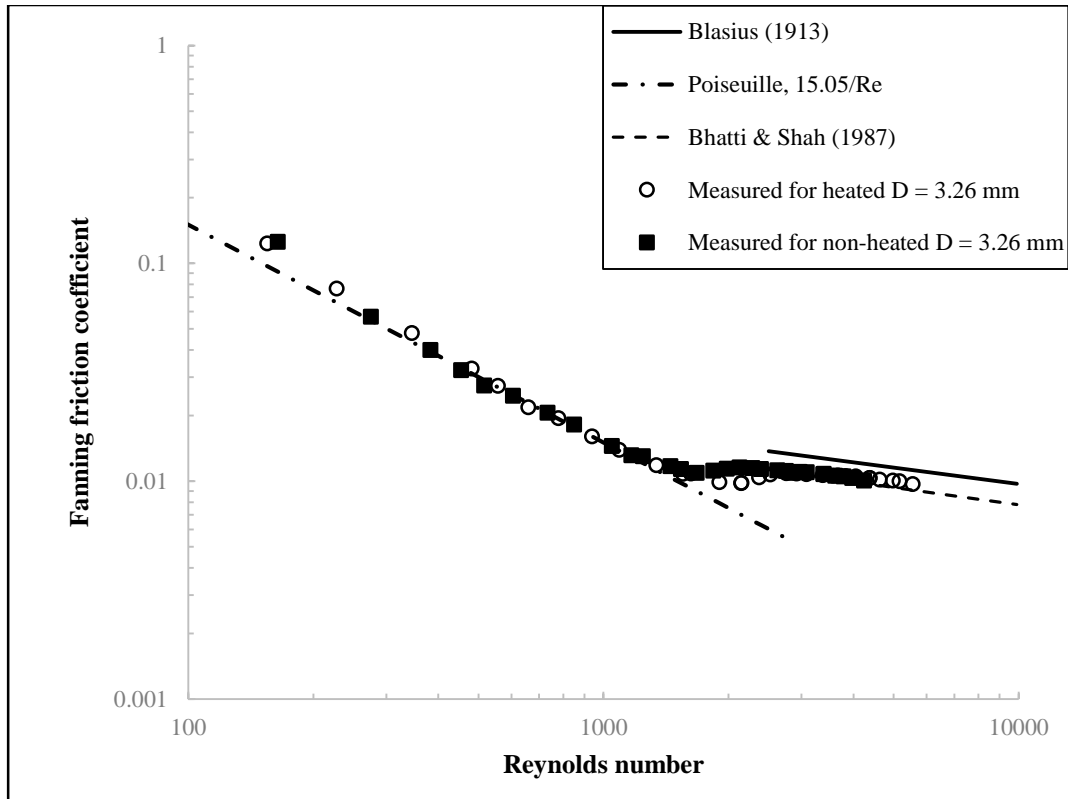
Figure 29 Comparison of friction factor for heated vs unheated flow of nanofluid flow in test section D = 3.26 mm

The effect of heat on the onset of transition is evidently more pronounced for water than nanofluid where it seemed minimal. Property variations (as a result of temperature change) in the boundary layer may have played quite a significant role in these results.

4.2.2. Local surface temperature profile for nanofluid flow

The following graphs clearly show the external surface temperature profile of the nanofluid flow to be consistent with a thermally developing flow. The temperature profile obviously tends to flatten out at high Reynolds number (or turbulence).
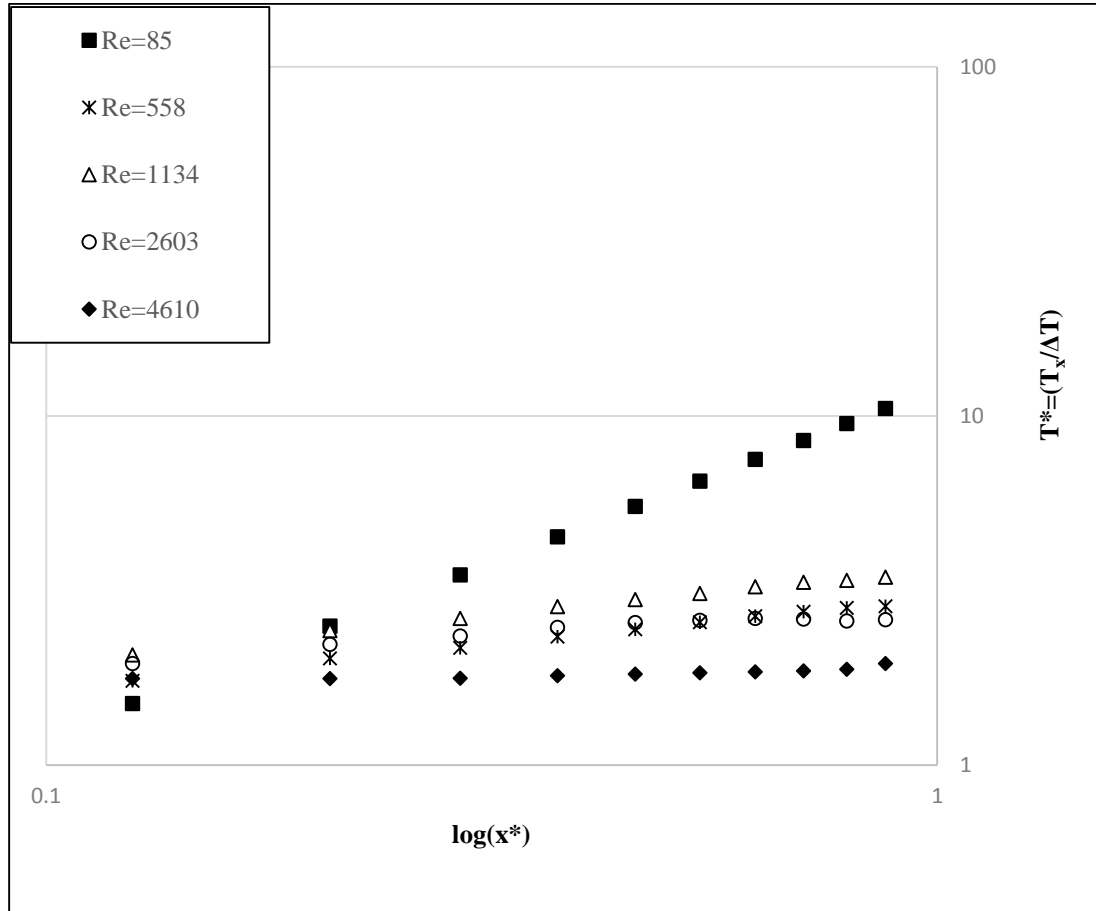

Figure 30. Surface temperature profile for nanofluid flow in test section D = 1.67 mm

The plots of surface temperature profiles for the test sections appear to be consistent with that of mean fluid temperature for flow through a circular tube in the case of constant heat flux. This verifies the earlier assumption (see Equation 3.1) that the nanofluid mean

bulk temperature varies linearly from the inlet to the exit and increases in the direction of the flow.
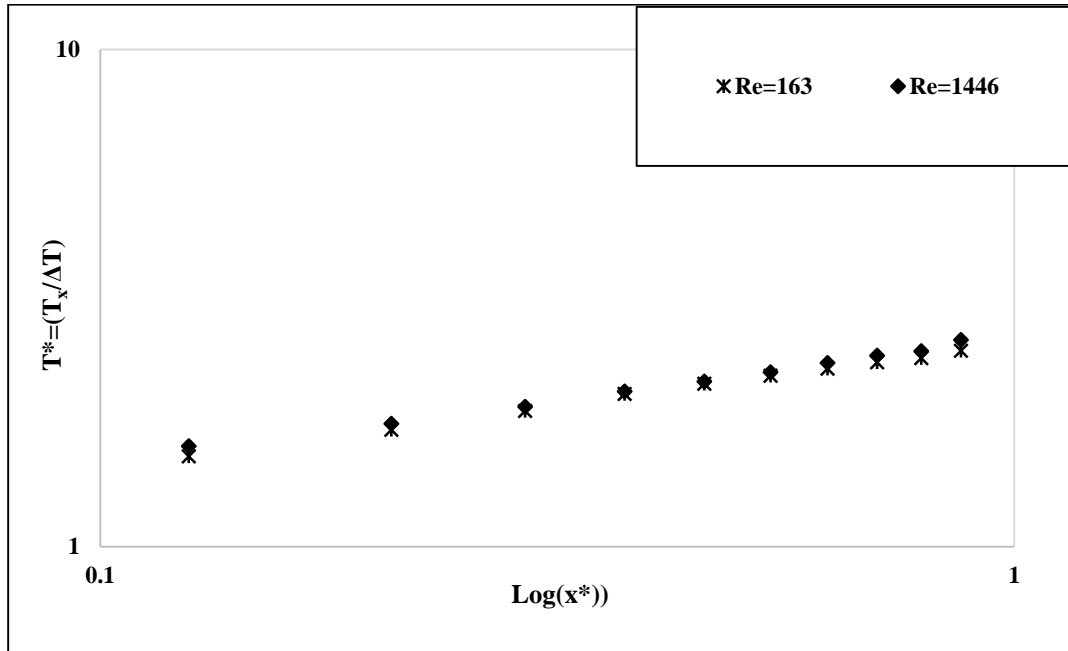

Figure 31. Surface temperature profile for nanofluid flow in test section D = 2.46 mm
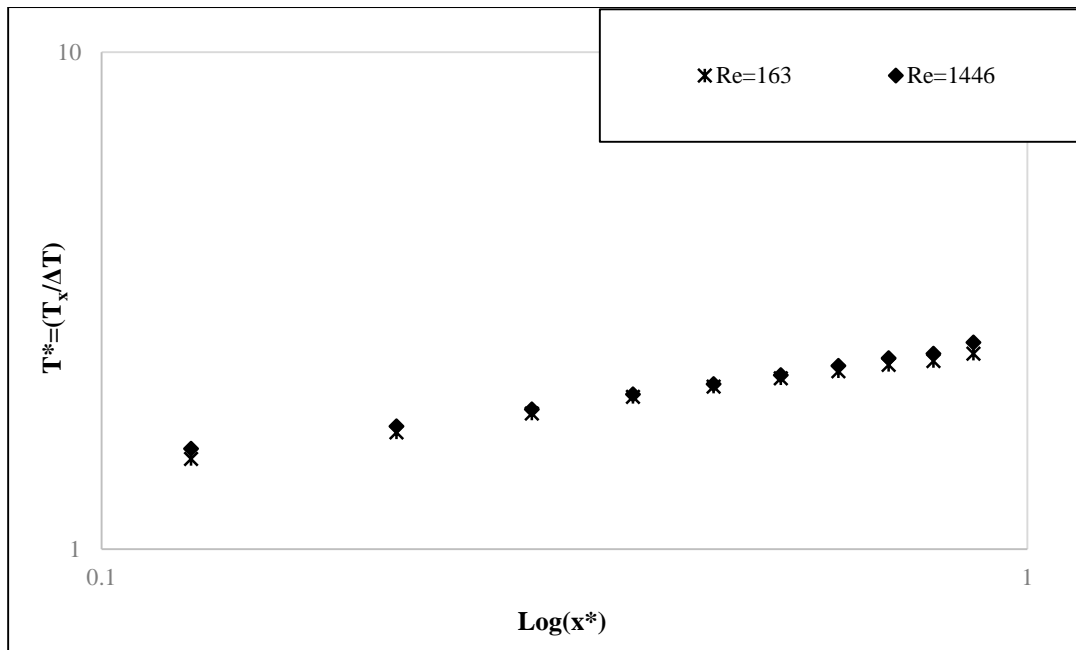

Figure 32. Surface temperature profile for nanofluid flow in test section D = 3.26 mm

4.2.3. Heat transfer

This subsections presents the convective heat transfer for the nanofluid being investigated in this thesis. Figure 33 shows the average of the measured local Nusselt number for all three test sections. It is obvious heat transfer increases with Reynolds number, and appeared to spike during transition from laminar to turbulent flow.

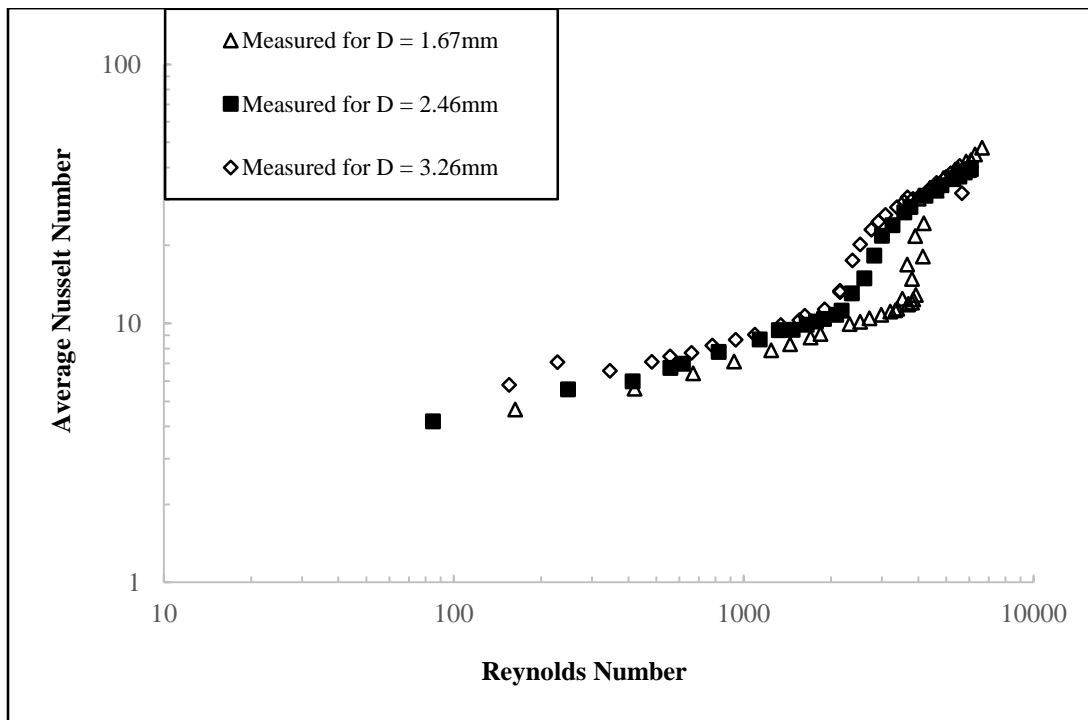**Figure 33. Measured Nusselt vs Reynolds number for nanofluid flow in tubes**

The Nusselt number for the three sections are presented separately for the laminar and turbulent regimes of flow in Figures 34 to 39. The laminar thermal profile for all of the test sections appear to be developing except for very low Reynolds number of about 100 where fully developed profile seemed to be approached.

Figure 34. Measured Laminar flow Nusselt number vs x⁺ for nanofluid flow in heated test section D = 1.67 mm compared with the Lienhard and Lienhard (2013) correlation. Dotted lines represent error limits of ±30%.

Figure 35. Comparison of Measured Nusselt number vs Gnielinski (1976) for nanofluid flow in heated test section D = 1.67 mm. Broken lines represent error limits of ±30%.

72

Figure 36. Measured Laminar flow Nusselt number vs x⁺ for nanofluid flow in heated test section D = 2.46 mm compared with the Lienhard and Lienhard (2013) correlation. Dotted lines represent error limits of ±30%.

Figure 37. Comparison of Measured Nusselt number vs Gnielinski (1976) for nanofluid flow in heated test section D = 2.46 mm. Broken lines represent error limits of ±30%.
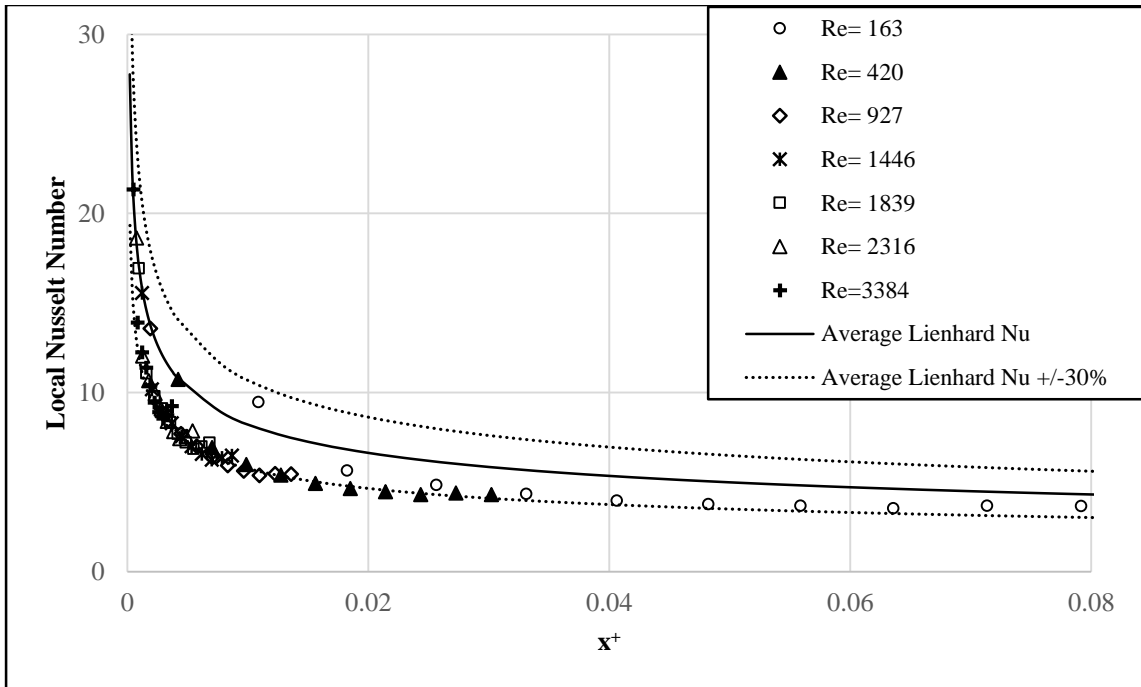
Figure 38. Measured Laminar flow Nusselt number vs x$^+$ for nanofluid flow in heated test section D = 3.26 mm compared with the Lienhard and Lienhard (2013) correlation. Dotted lines represent error limits of ±30%.
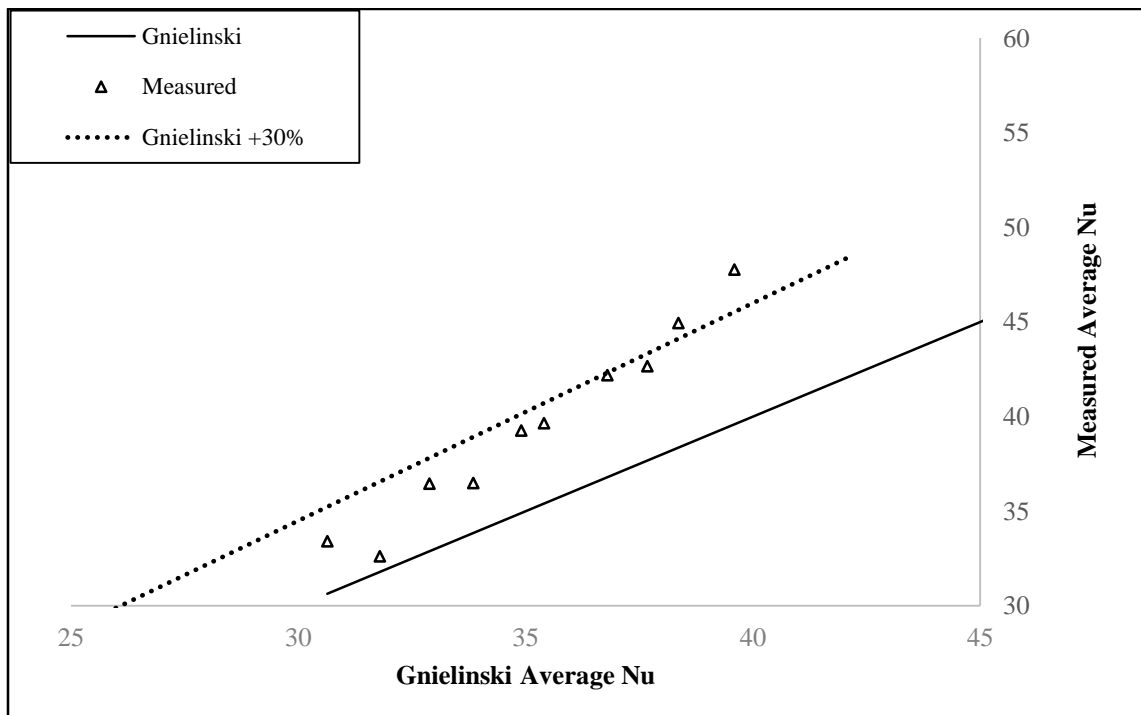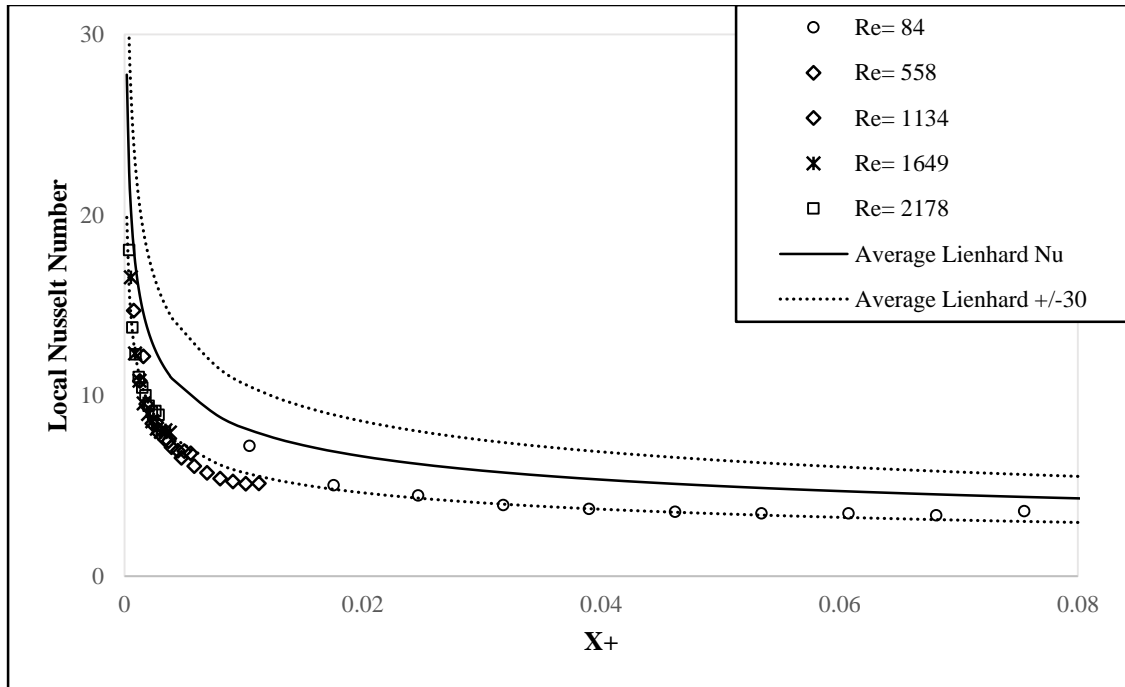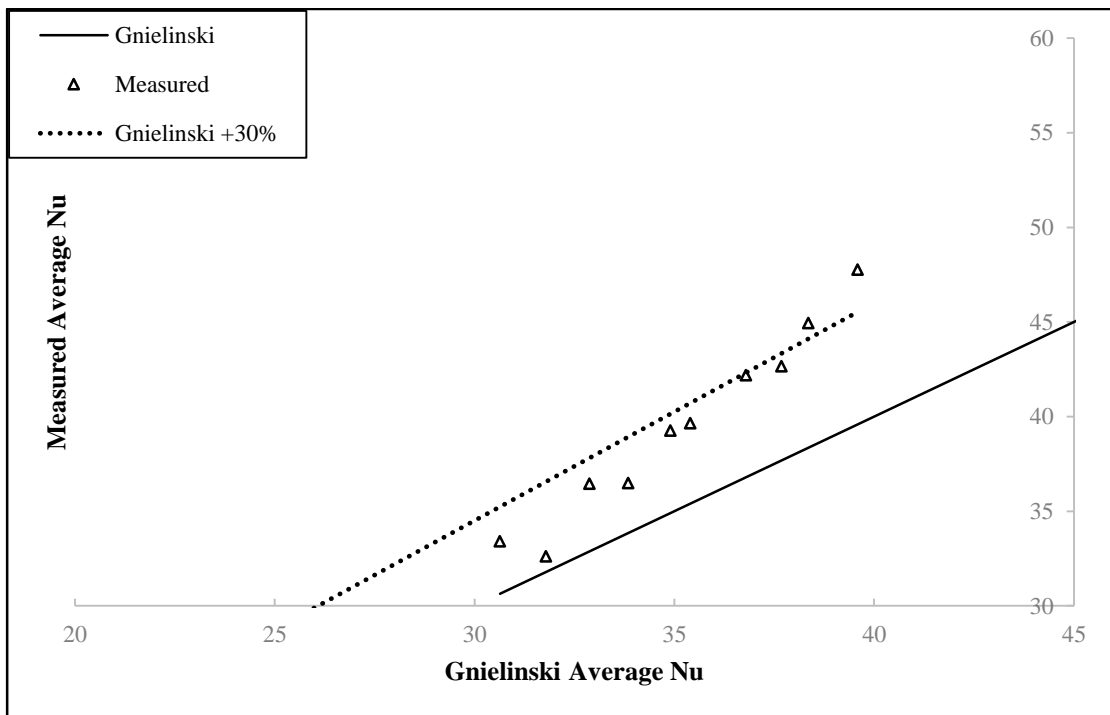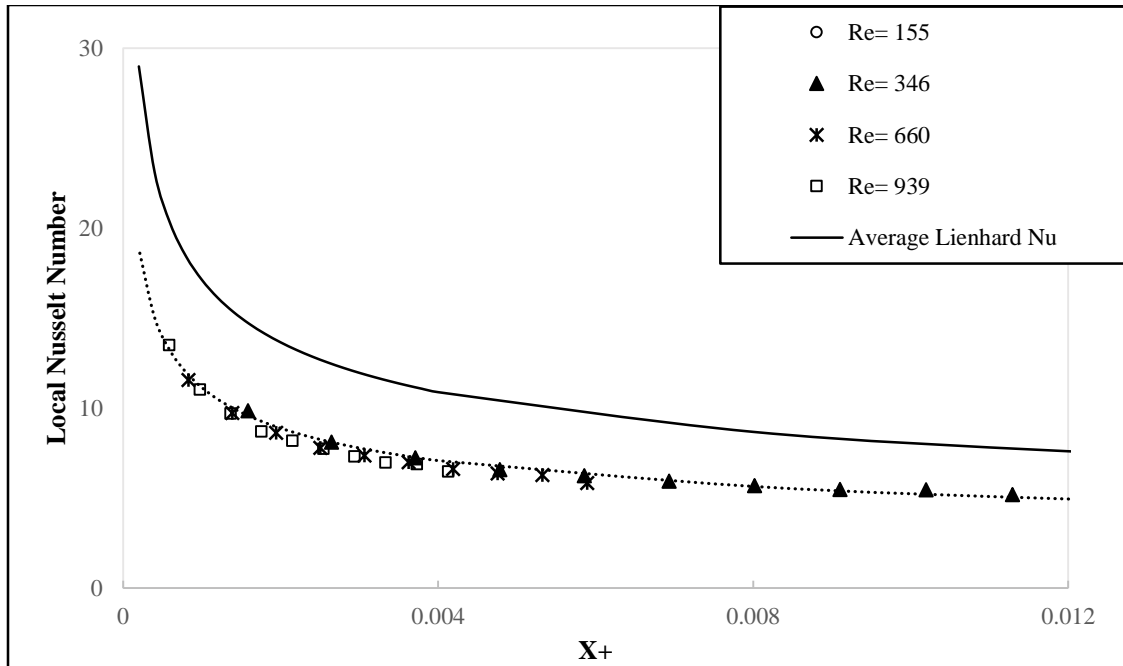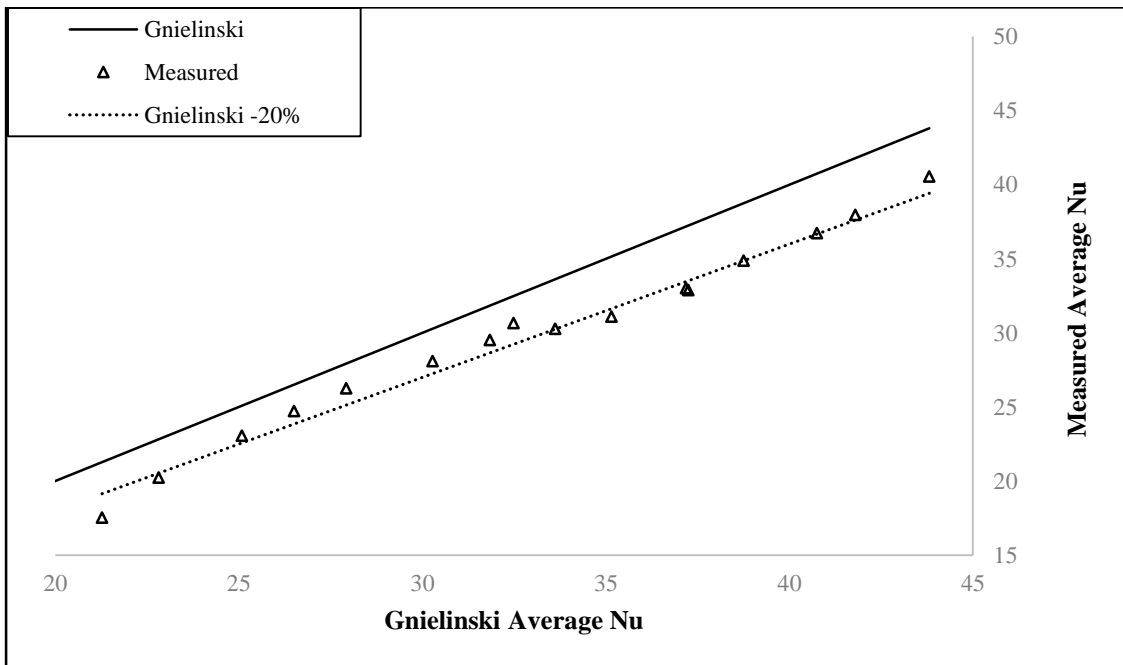

Figure 39. Comparison of Measured Nusselt number vs Gnielinski (1976) for nanofluid flow in heated test section D = 3.26 mm. Broken lines represent error limits of ±20%.

A glance at the local Nusselt number for the test sections quickly conveys to the reader that flow were thermally developing. At the entrance the Nusselt numbers are high, reaching the maximum values, but diminishes rapidly as flow progresses downstream. The flow approaches thermally fully developed flow for low Reynolds number, but do not quite become fully developed. The average Nusselt number for fluids (usually single phase) flow through a circular tube is 4.36 and 3.61 for a square duct. For a fully developed nanofluid flow through a hexagonal, the Nusselt number is expected to lie between those of circular and square duct.

The Lienhard and Lienhard (2013) correlation for Nusselt number for single phase liquid tube flow correlates the experimental data for the laminar flow of the nanofluid. The results are within 31% of the Lienhard correlation for laminar flow for all test sections. In the turbulent regime, though the results fall within 30%, there, however, are significant deviation by the experimental data from the Gnielinski (1976) prediction. This strongly suggests that the nanofluid flow may be a multiphase flow in which slip velocity significantly affects the heat transfer performance and may not be overemphasized.

It is apparent from the Figures 34, 36 and 38 that the measured Nusselt numbers underperform the Lienhard and Lienhard (2013) correlations, but this is not unexpected for the type of geometry of the tubes being used for the experiments. Uncertainties in the estimation of the Reynolds number as well as the Prandtl number could also have contributed the deviations. The Prandtl number depends largely on the thermal conductivity and specific heat capacity of the nanofluids. These thermophysical properties had been estimated from using the mixture concept, which may not be very accurate for the nanofluids, although come within acceptable practical level of accuracy.

Two regression equations have been fitted (using Minitab) for the combined data of heat transfer for the nanofluid laminar and turbulent flows through all three test sections. Equations are valid for the nanofluid type that has specifically been investigated in this report and for the conditions under which the experiments have been carried. Equation 4.1 is fitted for the laminar flow regime.

$$\log Nu_D = 0.945 - 0.598 \log Re + 0.294 \log Re^2 - 0.03229 \log Re^3 \tag{4.1}$$

The turbulent flow Nusselt number regression model is given in the Equation 4.2 below:

$$\log Nu_D = -2403 + 1934 \log Re - 518.8 \log Re^2 + 46.40 \log Re^3 \tag{4.2}$$

The logarithms in Equations 4.1 and 4.2 are written to base ten. These regression models were fitted within confidence and prediction intervals of 95%. The standard error values are 0.0429 and 0.0438 for Equations 4.1 and 4.2 respectively and the residual versus fits plots show good randomness.

4.3. Nanofluid vs Water Friction Coefficient

The following graphs show friction coefficients for nanofluid compared to water for flow in a particular TS with or without heating. Water appear to show higher friction coefficient than nanofluid as flow approached turbulence, irrespective of whether heat is applied or not. It is observed, however, for the smallest test section, D = 1.67 mm that laminar flow is sustained over higher speed for nanofluid than water.

Unheated Test Sections

Figure 40. Friction coefficient compared for unheated water and unheated nanofluid flow in the test section D = 1.67mm

Figure 41. Friction coefficient compared for unheated water and unheated nanofluid flow in the test section D = 2.46 mm

Figure 42. Friction coefficient compared for unheated water and unheated nanofluid flow in the test section D = 3.26 mm

Nanofluid transitions later than water when test section is not heated, this phenomenon appears to be more pronounced with smaller tube hydraulic diameter (see Figure 40). But, it is the exact opposite when heat is applied, as the results show that water sustains laminar flow longer than nanofluid for smaller hydraulic diameter. These observations raise concerns about the effect of nanoparticle movements on the characteristics of the flow.
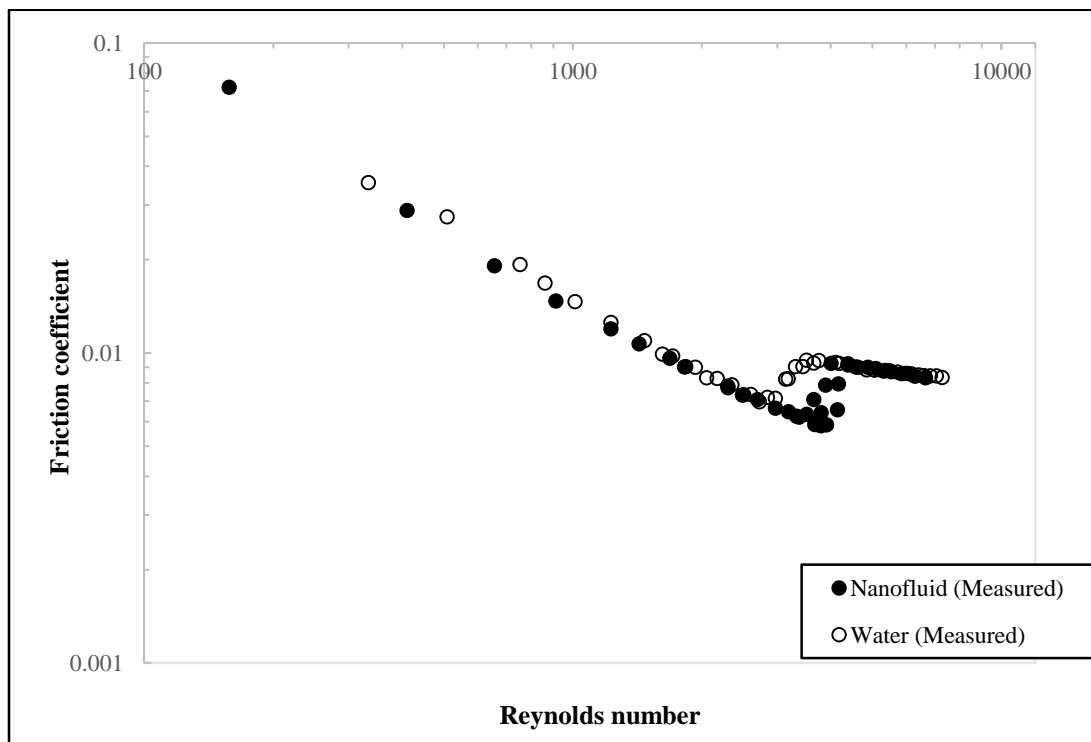
Heated Test Sections
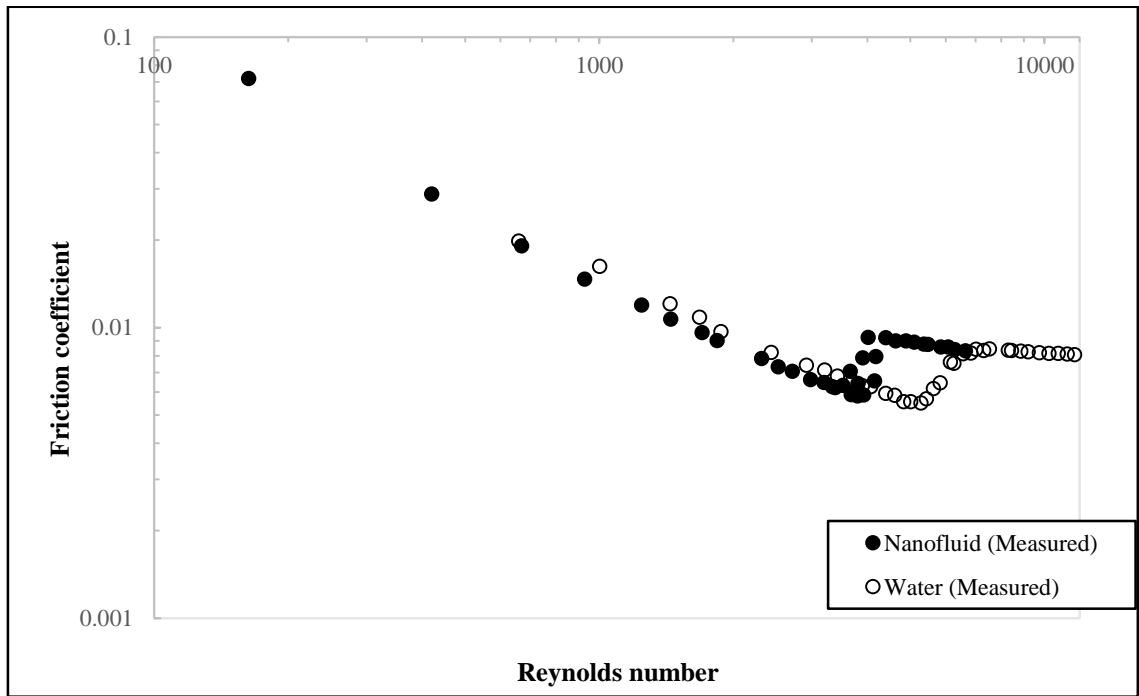
Figure 43. Friction coefficient compared for heated water and heated nanofluid flow in test section D = 1.67 mm
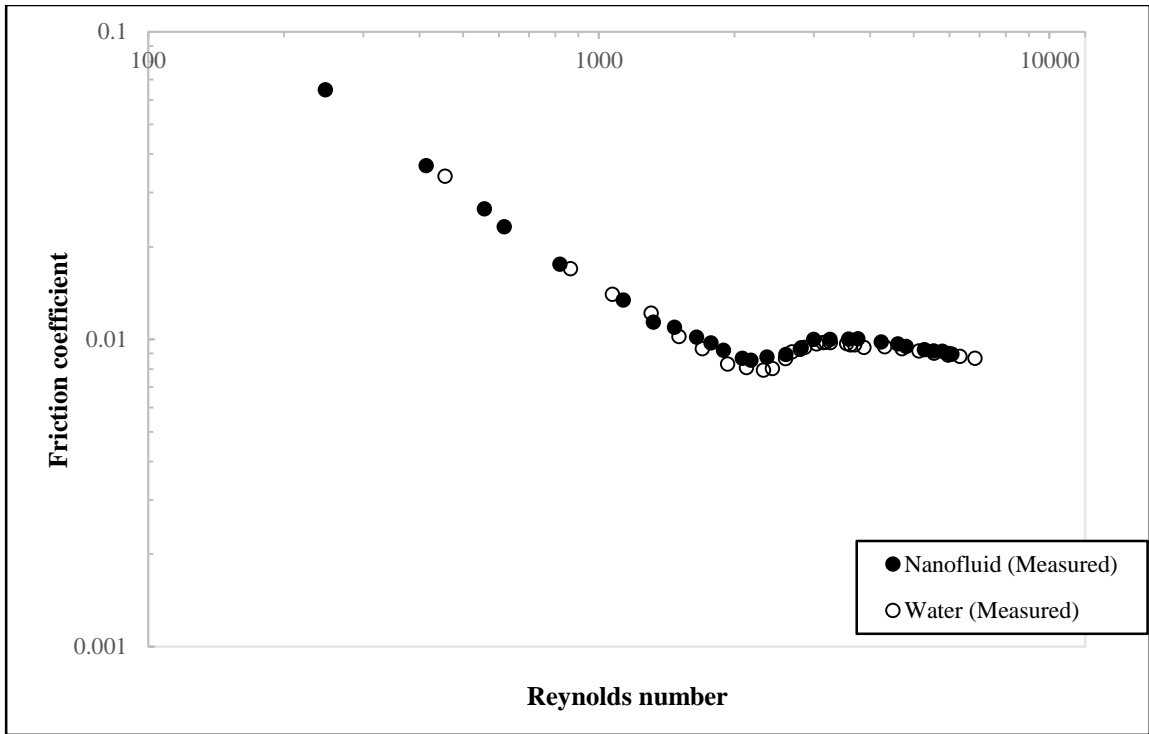
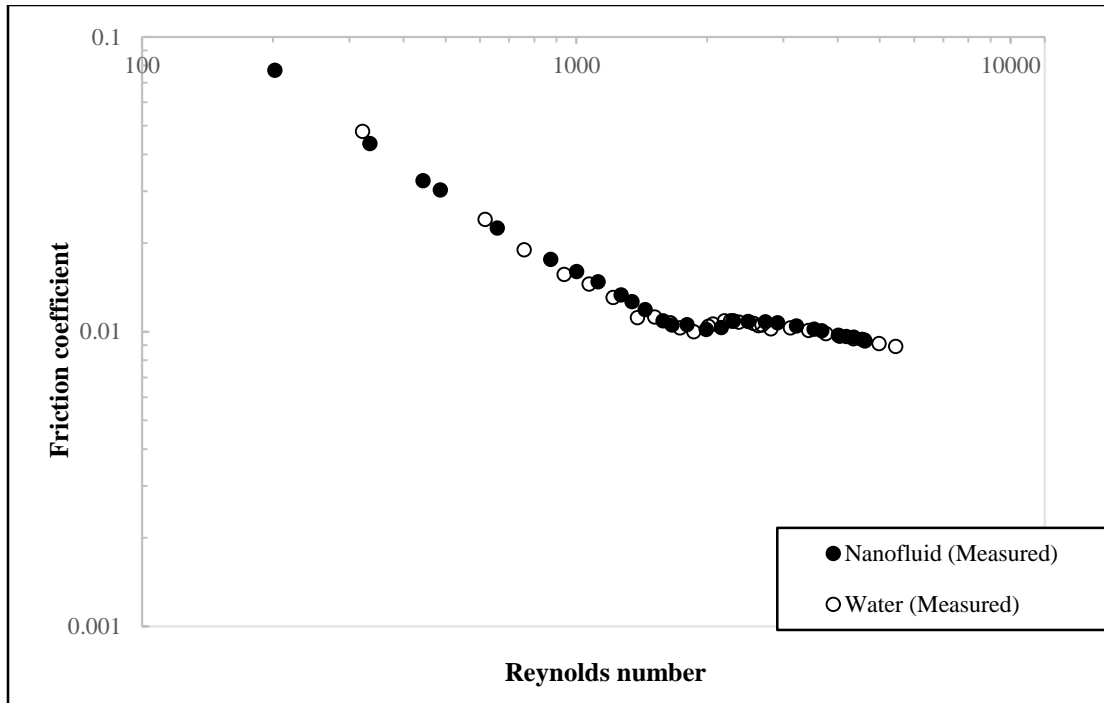**Figure 44. Friction coefficient compared for heated water and heated nanofluid in test section D = 2.46 mm**

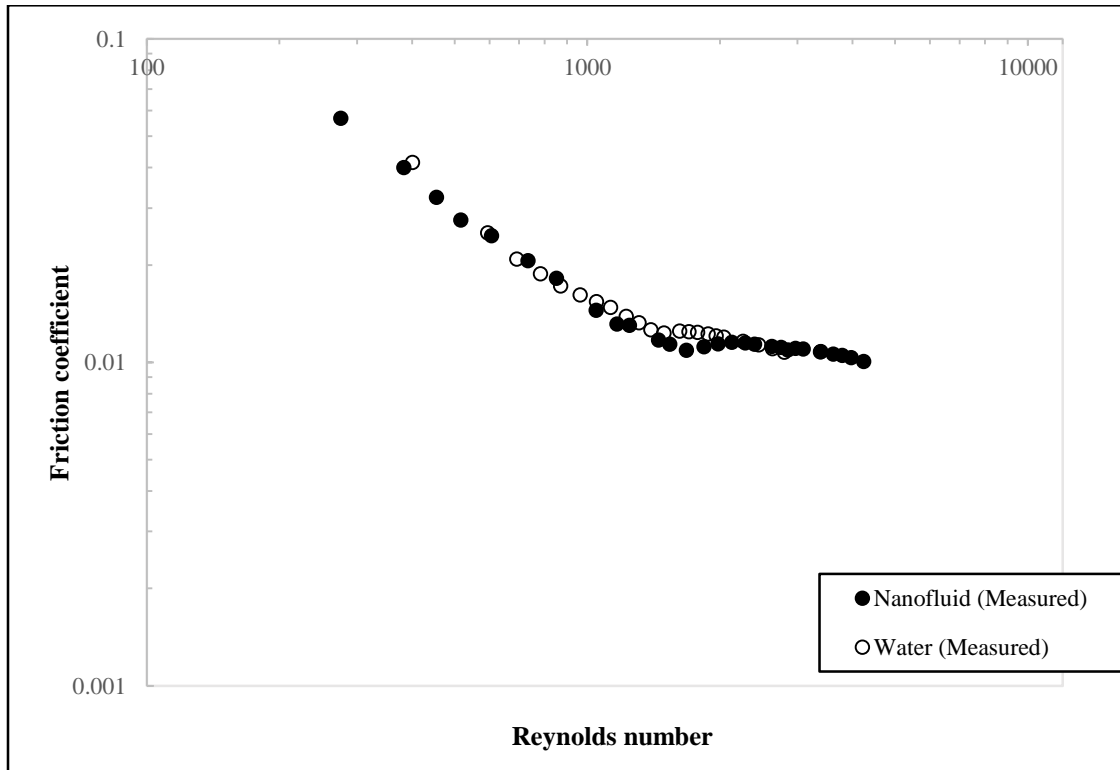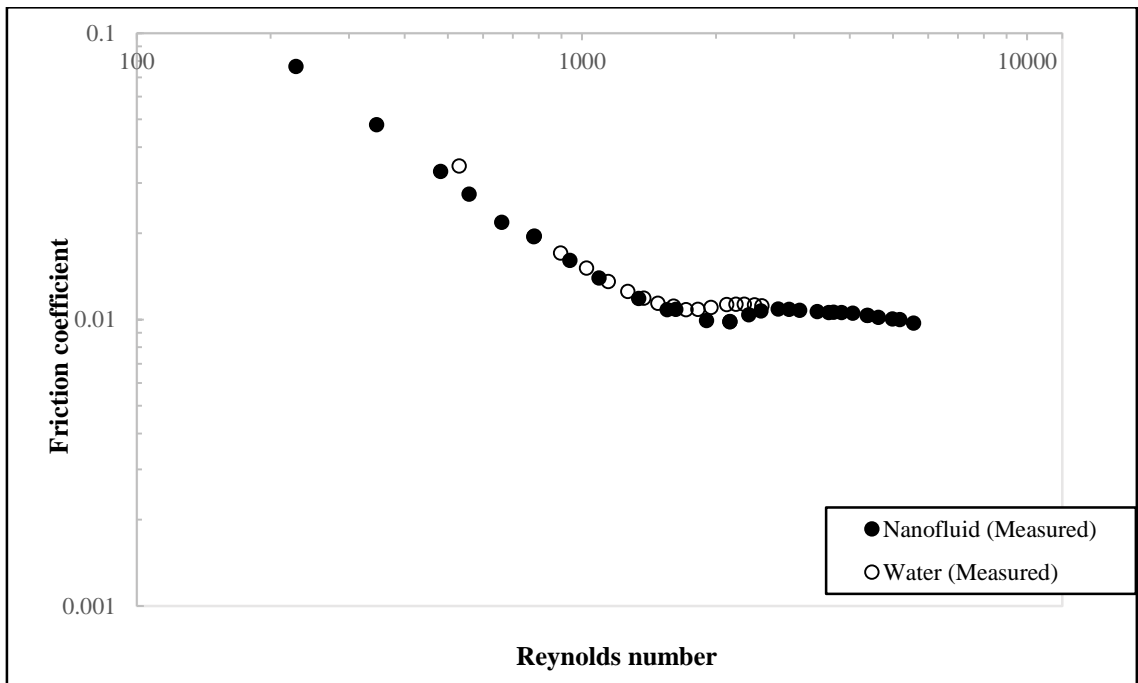**Figure 45. Friction coefficient compared for heated water and heated nanofluid in test section D = 3.26 mm**

4.4. Nanofluid vs water heat transfer

For a clearer sense of how heat transfers for water and nanofluids compare, the following graphs are presented.
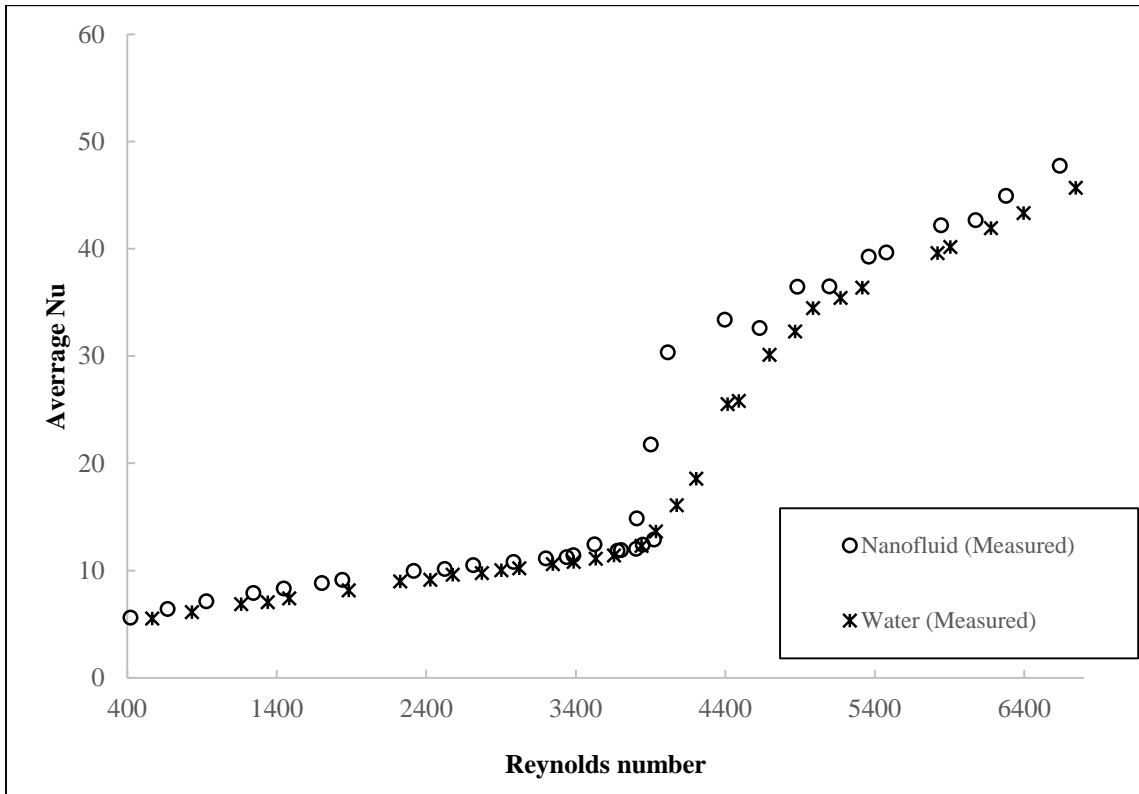
Figure 46. Comparison of nanofluid and water heat transfer for test section D = 1.67 mm

The nanofluid exhibits heat transfer enhancements compared to water in the laminar flow regimes for D = 1.67 mm and 2.46 mm. For D = 3.26 mm, heat transfer results could only be obtained within error limit for the laminar flow regime because of its relatively large hydraulic radius, and like the other test sections, the heat transfer for nanofluids supersedes water by more than 15% in the laminar flow regime and a little over 20 % in the turbulent regime.

81
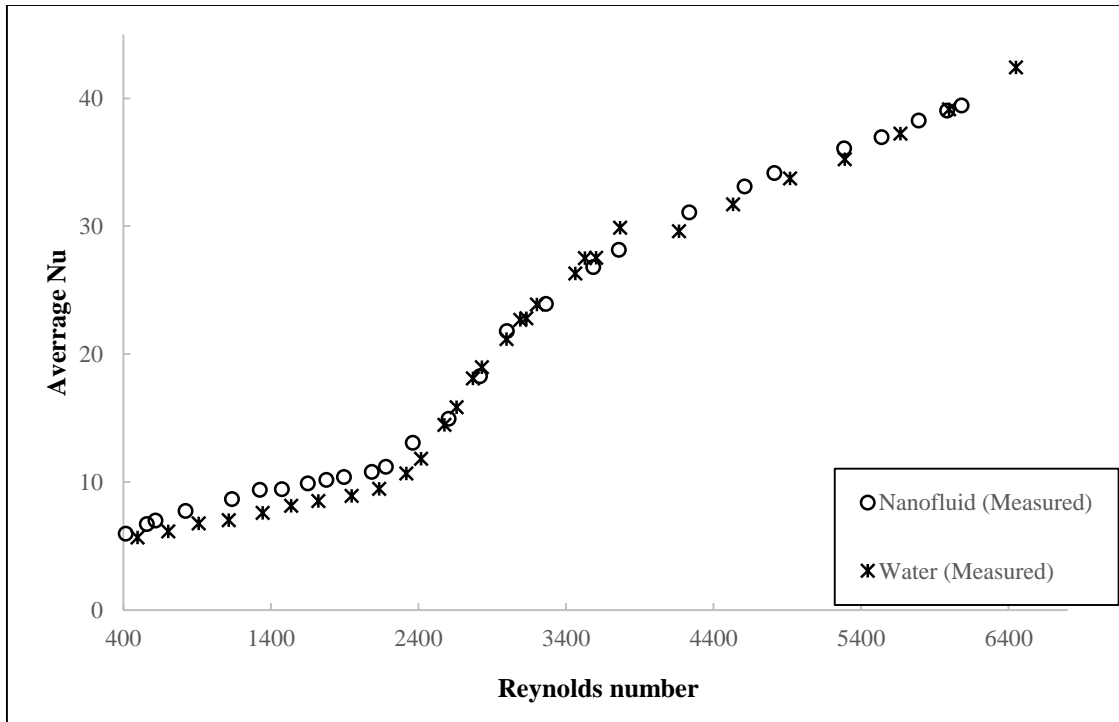
Figure 47. Comparison of nanofluid and water heat transfer for test section D= 2.46 mm
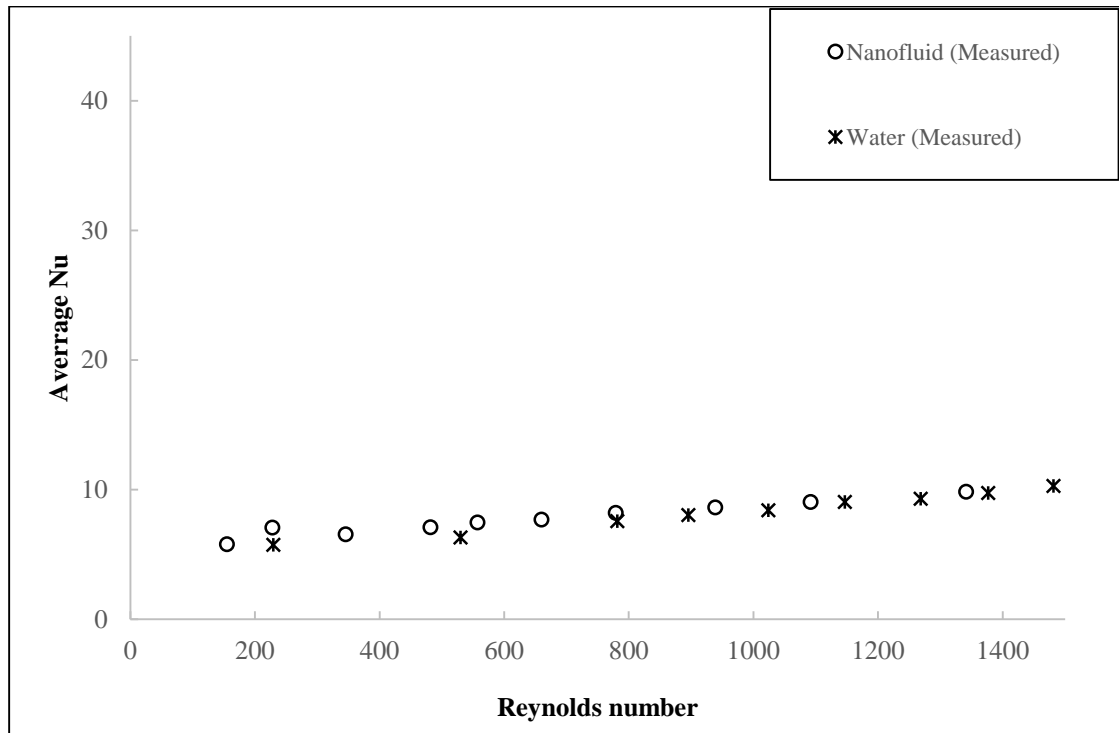
Figure 48. Comparison of nanofluid and water heat transfer for test section D = 3.26 mm

4.5. Pressure drop of Nanofluid Versus Water

A comparison of pressure drop against Reynolds number for water and nanofluid speaks of the potential that nanofluid will create more load compared to water for the pumping system with which they are transported. A pressure drop increase exceeding 100% compared to water is observed for nanofluid fluid in D = 2.46 mm (Figure 46). Similar results have been obtained for flow in the other test sections as well.
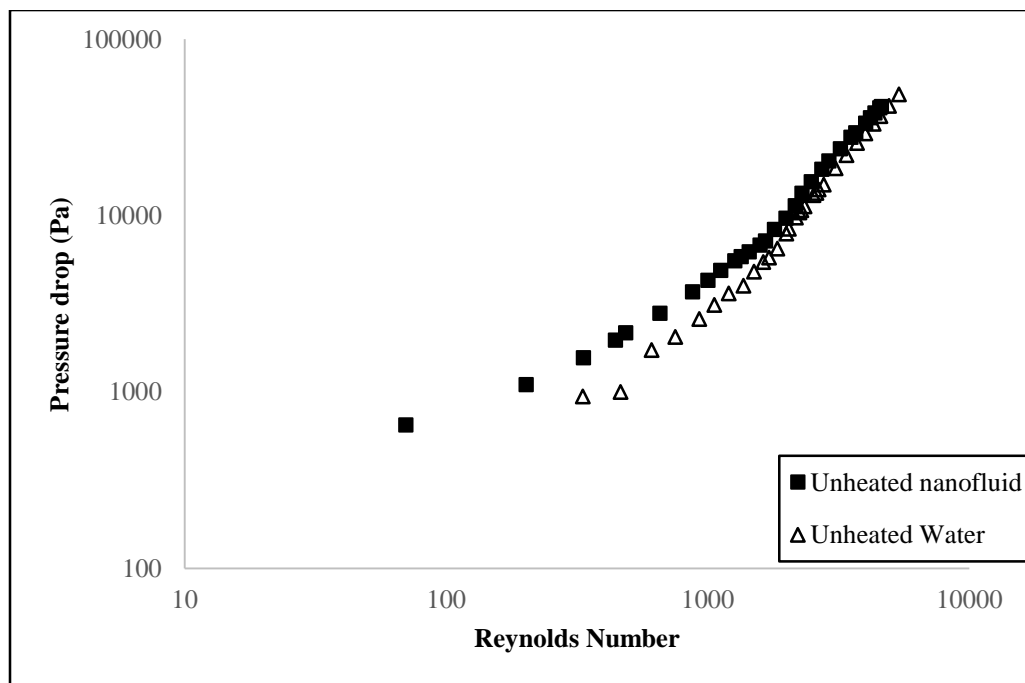
Figure 49. Comparison of pressure drop across test section D = 2.46 mm with respect to Reynolds number
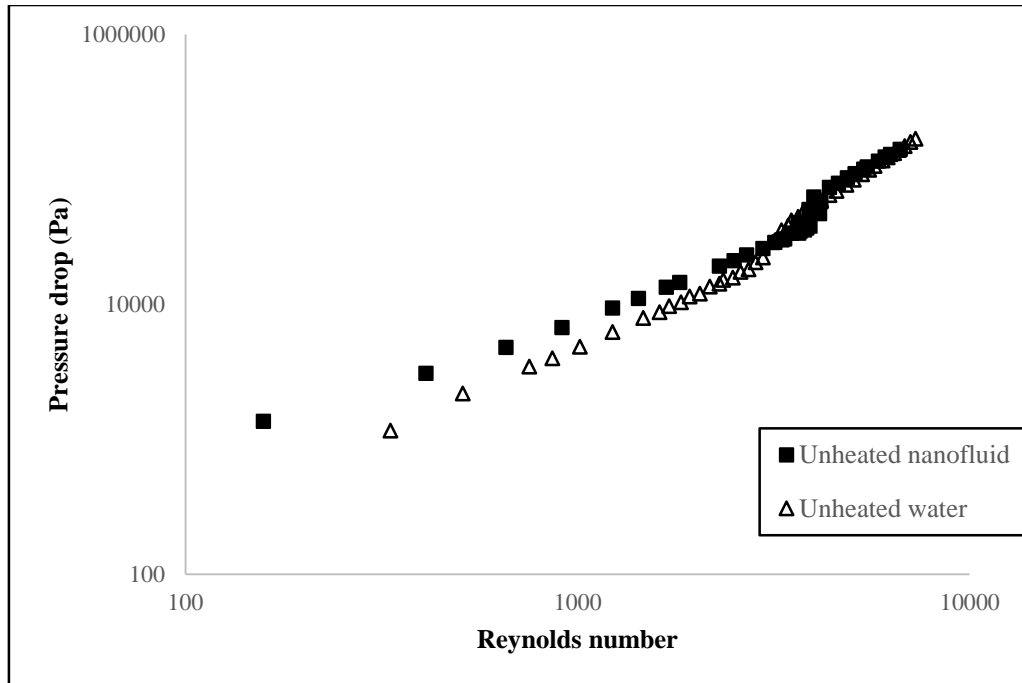
Figure 50 Comparison of pressure drop across test section D = 1.67 mm with respect to Reynolds number
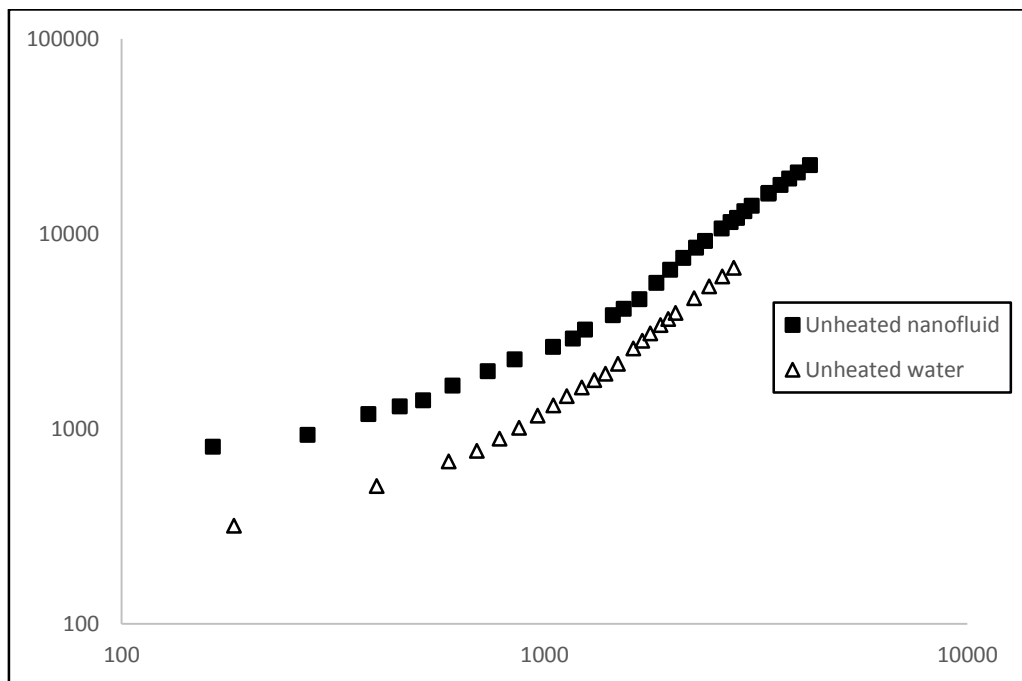
Figure 51. Comparison of pressure drop across test section D = 3.26 mm with respect to Reynolds number

CHAPTER V

CONCLUSIONS AND RECOMMENDATIONS

5.1. Conclusions

The flow and heat transfer characteristics of silicon-dioxide water-based nanofluid in three different sized brass hexagonal tubes have been closely monitored during the experimentations carried out in this thesis. Flows were operated for the range of Reynolds number 400-8000, encompassing the laminar, transitional and turbulent flow regimes. Primarily, pressure drops and tube surface temperatures are the focal parameters through which the fluid characterizations have essentially been drawn or estimated. Reynolds number were controlled by adjusting the rotor speed of the variable speed feed water/nanofluid gear pump.

The Metzner and Reed (1955) correlation proved good for estimating Reynolds number in the laminar flow regime, with a reasonable degree of accuracy in the transition and turbulent flow regimes for water. These experimentations with water are a rigorous method by which the procedures and methods of experiments have been validated in this thesis. It predicts Reynolds number with an accuracy of 90-95% in the laminar regime and between 80 and 85% for the turbulent and the transition regimes.

The pressure drop and heat transfer characteristics of SiO_2-water-based nanofluid flow inside horizontal hexagonal duct brass tubes are investigated for the entrance region. The nanofluid friction coefficients are well correlated by classical single phase fluid correlations suggesting that the nanofluid can very well be treated as single phase fluid rather a mixture.

The nanofluid appears to longer sustain laminar flow (with transition occurring at higher speed or Reynolds number) when fluid is not being heated, while offering superior heat transfer than water. This is a pointer to more prominent shear stress on the wall of smaller test section than the larger ones. On the other hand, upon applying heat to the flow system, water transitioned much later than nanofluid in the smallest tube flow and does exhibit more drag on the wall as indicated by the higher friction coefficient in the laminar flow regime. This is suggestive of a possible net migration of nanoparticles from the wall toward the axis of the flow, it makes one to wonder whether the time of travel of particle from the flow axis to the core might be a contributing factor as well.

The measured results showed high convective heat transfer at high Reynolds numbers, having been compared with the classical correlations, the turbulent heat transfer results were not closely correlated by the classical equations. The observed heat transfer enhancements for high Reynolds number could be due to persistent thermal dispersion which may have been induced by intensified micro-convection and diffusion of nanoparticles at high flow velocities as a result of the effect of temperature gradient on the properties of the nanofluid. As expected, the heat transfers were higher for increasing hydraulic diameters of flow tubes.

Migration of nanofluid particles may be responsible for wearing the viscous boundary layer much faster than for water for which molecules have a higher degree of freedom and much more elastic. The high momentum of nanoparticles at high flow rate may allow them to easily penetrate the laminar boundary layer, and upon heating the particles the gain kinetic energy as well. These inferences are, however, inconclusive without more evidence.

The diminishment in the friction coefficient (probably as a result of depletion of boundary layer as a consequence of particle migration could have led to the fluid losing contact with the flow surface or introducing slip flow resulting in cavitation effect on the surface) can cause localized overheating and cavitation effects on the heat transfer surface. The large pressure drops for nanofluid flow may be attributed to reversal of flow and collision drag. But it is just not the separation of the flow at the wall that should be considered in the study of nanofluid, the interaction of the solid-fluid surface is likely very significant to the heat transfer mechanisms.

Whereas, heat transfer enhancements have been recorded for nanofluid, such enhancements may not be worth the troubles for the corresponding pressure drops (reaching over 60% compared with water) associated with the fluid flows. These high pressure drops leave a dilemma for design of nanofluid heat transfer systems with respect to energy requirements. It is obvious, nanofluid heat exchange systems would require more pumping power to transport the fluid.

5.2. Recommendations and Future Work

More studies need to be conducted to determine what mechanisms are responsible for the flow transitions associated with nanofluids or the heat transfer enhancements for that matter. In the future, more effective method like use of particles size analyzer, electron microscopy (SEM-scanning electron microscope, TEM- transmission electron microscopy will be utilized in the determination of the distribution of nanofluid particle size and aggregates to increase the odds of correctly characterizing the fluid (especially for high concentration of particles). A dispersion model may also be applied in the investigation of the heat transfer mechanisms of nanofluids.

Future work will also include the measurement of pressure drop at multiple locations along the length of the tube. This will be done by fabricating specially shaped pressure tap holes that will enable pressure measurements to be taken without distorting the flow. The use of infrared to measured heat distribution throughout flow domain will also be considered.

The use of peristaltic pump for future work is recommended for more smooth flow. Also, the use of transparent test section and high speed and thermal imaging could prove pivotal in the study of flow and heat transfer mechanisms of the nanofluid.

The approximation of nanofluid as a single phase fluid does have many setbacks especially for high speed flow where compression wave phenomenon for instance would have to be accounted for. Stabilizers or surfactants can effectively change the phase distribution of the nanofluid systems and should be investigated for contribution to the surface tension behavior of the fluid. The overall effect of surfactant concentration on the

thermophysical properties of the nanofluid especially where there may be boiling heat transfer or two phase heat transfer should be investigated as well.

Multiple run of experiments will be done for future experiments to allow for more encompassing and comprehensive investigation of uncertainty to be carried out. Also, there is need to investigate a wider concentrations of the nanofluid to obtain more information on the nanofluid properties and allow for an extended range over which these properties and the dependencies may be more accurately predicted. Working with different concentrations may also help to determine the effect of particle concentration on the length of the region. Carrying experiments for multiple nanoparticle concentrations can be of much help to validating such claims as the effect of particle concentration and mobility on the onset and intensity of turbulence.

Viscosity of Nanofluid (Sharif, 2015)
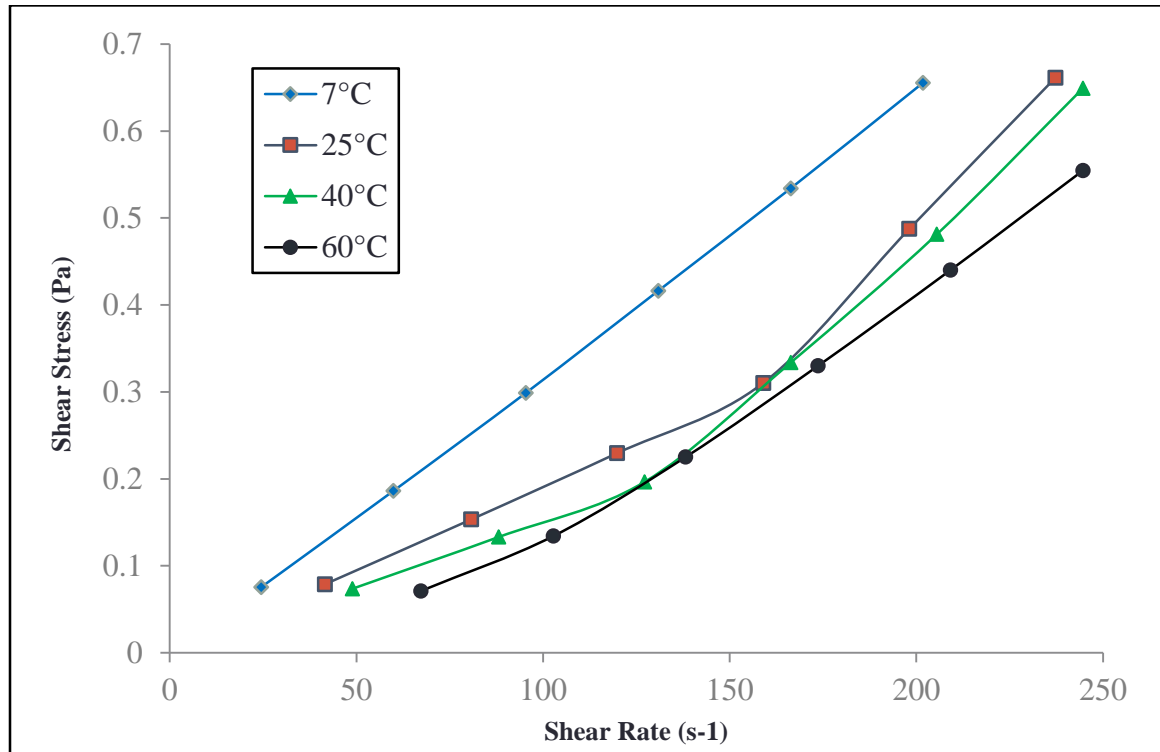
Figure 52 Change of shear stress with shear rate at different temperatures for Silica nanoparticle colloidal suspension (9.58% by volume) Sharif (2015)

Nanofluid at a low temperature of 7°C appeared to behave as a Bingham plastic, however was predominantly dilatant, non-Newtonian in the range of temperature for which it had been tested (see Figure 52). The thermal conductivity of the nanofluid is significantly higher than for water and does appear to increase with temperature. The experiments were performed for temperatures ranging from 5°C to 50°C.

Appendix B

Error Analysis

While the experiments conducted here have be performed with great care, the possibility of errors within the results cannot be overlooked. Errors could be due to inefficiencies in data acquisition procedure, fabrication of system components or human errors. (Note that instrument precision or error of measurement are given in Table 1). Consequently, steps have been taken to minimize these errors. Multiple data points were collected and averaged to minimize bias errors in measurements thus it has been assumed for the directly measured data that fixed errors or biases are negligible and only random (or precision) errors significant in the analysis. Though the root sum square (RSS) method by Moffat (1982) and Moffat (1988) could not be employed to perform further analysis of uncertainty since there were no multiple runs or replicates for the experiment, the analysis however, follows their prescribed method for reporting uncertainty.

Apparent Viscosity, Reynolds Number and Friction Factors Uncertainty

The uncertainty in the Reynolds number comes from the assumption of constant apparent viscosity and density over a wide range of shear stress (see Equations 3.4 and 3.5), however, is a reasonable one from the practical point of view, having been validated by comparing results with data from well-established literature for water. The uncertainty of the density of the nanofluid is estimated at 1.69% by Sharif (2015).

91

The friction factor uncertainty obviously depends on the accuracy of measuring pressure drop, the hydraulic diameter and length of the test section and the fluid's density as well as the mass flow rate. The uncertainty of the pressure drop measurements are given by Tiwari (2012) as ±40.43Pa. The width tolerance for the test sections are specified at ±0.002 inches and that of the thickness at ±0.001 inches by the manufacturer.

Experiments reveal, however, a vast spectrum of non-Newtonian fluids may be represented over wide ranges of shear rate by a two-constant power law. While a fluid may fall into a category of classification, rheological properties or even assigned values resulting from such classifications appear to be very sensitive to the conditions of experiment under which they are developed; without care, such classifications could result in the oversimplification Metzner and Reed (1955). The nanofluids presented have been found to be time-independent in nature from the experiments conducted by Sharif (2015).

REFERENCES

Aladag, B., Halelfadl, S., Doner, N., Maré, T., Duret, S., & Estellé, P. (2012). Experimental investigations of the viscosity of nanofluids at low temperatures. *Applied Energy, 97*, 876-880.

Assael, M., Metaxa, I., Kakosimos, K., & Constantinou, D. (2006). Thermal conductivity of nanofluids–experimental and theoretical. *International Journal of Thermophysics, 27*(4), 999-1017.

Azizian, R., Doroodchi, E., McKrell, T., Buongiorno, J., Hu, L., & Moghtaderi, B. (2014). Effect of magnetic field on laminar convective heat transfer of magnetite nanofluids. *International Journal of Heat and Mass Transfer, 68*, 94-109.

Baby, T. T., & Ramaprabhu, S. (2011). Synthesis and nanofluid application of silver nanoparticles decorated graphene. *Journal of Materials Chemistry, 21*(26), 9702-9709.

Beck, M. P., Yuan, Y., Warrier, P., & Teja, A. S. (2009). The effect of particle size on the thermal conductivity of alumina nanofluids. *Journal of Nanoparticle Research, 11*(5), 1129-1136.

Bhatti, M., & Shah, R. (1987). Turbulent and transition flow convective heat transfer in ducts. *Handbook of Single-Phase Convective Heat Transfer, ,* 4.1-4.166.

Blasius, H. (1913). *Das ähnlichkeitsgesetz bei reibungsvorgängen in flüssigkeiten* Springer.

Brintlinger, T., Qi, Y., Baloch, K. H., Goldhaber-Gordon, D., & Cumings, J. (2008). Electron thermal microscopy. *Nano Letters, 8*(2), 582-585.

Brkić, D. (2011). Review of explicit approximations to the colebrook relation for flow friction. *Journal of Petroleum Science and Engineering, 77*(1), 34-48.

Buongiorno, J. (2006). Convective transport in nanofluids. *Journal of Heat Transfer, 128*(3), 240-250.

Çengel, Y. A., & Ghajar, A. J. (2011). *Heat and mass transfer: Fundamentals & applications* McGraw-Hill.

Choi, S. U. S., & Eastman, J. A. (1995). Enhancing thermal conductivity of fluids with nanoparticles. Paper presented at the *1995 International Mechanical Engineering Congress and Exhibition, San Francisco, CA (United States), 12-17 Nov 1995,* pp. 99-106.

Colebrook, C., & White, C. (1937). Experiments with fluid friction in roughened pipes. *Proceedings of the Royal Society of London.Series a, Mathematical and Physical Sciences, ,* 367-381.

Das, S. K., Putra, N., & Roetzel, W. (2003). Pool boiling characteristics of nano-fluids. *International Journal of Heat and Mass Transfer, 46*(5), 851-862.

Das, S. K., Putra, N., Thiesen, P., & Roetzel, W. (2003). Temperature dependence of thermal conductivity enhancement for nanofluids. *Journal of Heat Transfer, 125*(4), 567-574.

Dodge, D., & Metzner, A. (1959). Turbulent flow of non-Newtonian systems. *AIChE Journal, 5*(2), 189-204.

Duangthongsuk, W., & Wongwises, S. (2010). An experimental study on the heat transfer performance and pressure drop of TiO 2-water nanofluids flowing under a turbulent flow regime. *International Journal of Heat and Mass Transfer, 53*(1), 334-344.

Einstein, A. (1906). A new determination of molecular dimensions. *Ann.Phys, 19*(2), 289-306.

Fakoor-Pakdaman, M., Akhavan-Behabadi, M., & Razi, P. (2013). An empirical study on the pressure drop characteristics of nanofluid flow inside helically coiled tubes. *International Journal of Thermal Sciences, 65*, 206-213.

Fedele, L., Colla, L., Bobbo, S., Barison, S., & Agresti, F. (2011). Experimental stability analysis of different water-based nanofluids. *Nanoscale Research Letters, 6*(1), 1-8.

Fotukian, S., & Esfahany, M. N. (2010). Experimental study of turbulent convective heat transfer and pressure drop of dilute CuO/water nanofluid inside a circular tube. *International Communications in Heat and Mass Transfer, 37*(2), 214-219.

Fotukian, S., & Esfahany, M. N. (2010). Experimental study of turbulent convective heat transfer and pressure drop of dilute CuO/water nanofluid inside a circular tube. *International Communications in Heat and Mass Transfer, 37*(2), 214-219.

Ghadimi, A., Saidur, R., & Metselaar, H. (2011). A review of nanofluid stability properties and characterization in stationary conditions. *International Journal of Heat and Mass Transfer, 54*(17), 4051-4068.

Gnielinski, V. (1976). New equations for heat and mass-transfer in turbulent pipe and channel flow. *International Chemical Engineering, 16*(2), 359-368.

Haynes, W. M. (2013). *CRC handbook of chemistry and physics* CRC press.

Heris, S. Z., Etemad, S. G., & Esfahany, M. N. (2006). Experimental investigation of oxide nanofluids laminar flow convective heat transfer. *International Communications in Heat and Mass Transfer, 33*(4), 529-535.

Howe, K. J., Hand, D. W., Crittenden, J. C., Trussell, R. R., & Tchobanoglous, G. (2012). *Principles of water treatment* John Wiley & Sons.

Hussein, A. M., Sharma, K., Bakar, R., & Kadirgama, K. (2014). A review of forced convection heat transfer enhancement and hydrodynamic characteristics of a nanofluid. *Renewable and Sustainable Energy Reviews, 29*, 734-743.

Jiang, L., Gao, L., & Sun, J. (2003). Production of aqueous colloidal dispersions of carbon nanotubes. *Journal of Colloid and Interface Science, 260*(1), 89-94.

Joshi, M., Bhattacharyya, A., & Ali, S. W. (2008). Characterization techniques for nanotechnology applications in textiles. *Indian Journal of Fibre and Textile Research, 33*(3), 304-317.

Kabelac, S., & Kuhnke, J. (2006). Heat transfer mechanisms in nanofluids--experiments and theory--. Paper presented at the *International Heat Transfer Conference 13,*

Kakaç, S., & Pramuanjaroenkij, A. (2009). Review of convective heat transfer enhancement with nanofluids. *International Journal of Heat and Mass Transfer, 52*(13), 3187-3196.

Kays, W. M., Crawford, M. E., & Weigand, B. (2012). *Convective heat and mass transfer* Tata McGraw-Hill Education.

Keblinski, P., Eastman, J. A., & Cahill, D. G. (2005). Nanofluids for thermal transport. *Materials Today, 8*(6), 36-44.

Kestin, J., Mordechai, S., & William A, W. (1978). Viscosity of liquid water in the range$-$8 C to 150 C. *Journal of Physical and Chemical Reference Data, 7*(3), 941-948.

Kole, M., & Dey, T. (2010). Viscosity of alumina nanoparticles dispersed in car engine coolant. *Experimental Thermal and Fluid Science, 34*(6), 677-683.

Kothandaraman, C. (2004). *Heat and mass transfer data book* New Age International.

Krishnamurthy, S., Bhattacharya, P., Phelan, P., & Prasher, R. (2006). Enhanced mass transport in nanofluids. *Nano Letters, 6*(3), 419-423.

Lee, S., Choi, S., Li, S., and, & Eastman, J. (1999). Measuring thermal conductivity of fluids containing oxide nanoparticles. *Journal of Heat Transfer, 121*(2), 280-289.

Lee, S. W., Park, S. D., Kang, S., Bang, I. C., & Kim, J. H. (2011). Investigation of viscosity and thermal conductivity of SiC nanofluids for heat transfer applications. *International Journal of Heat and Mass Transfer, 54*(1), 433-438.

Li, W., & Wu, Z. (2010). A general criterion for evaporative heat transfer in micro/mini-channels. *International Journal of Heat and Mass Transfer, 53*(9), 1967-1976.

Lienhard, J., & Lienhard, J. (2013). *A heat transfer textbook* Courier Corporation.

Maiga, S. E. B., Palm, S. J., Nguyen, C. T., Roy, G., & Galanis, N. (2005). Heat transfer enhancement by using nanofluids in forced convection flows. *International Journal of Heat and Fluid Flow, 26*(4), 530-546.

Maxwell, J. C., & Thompson, J. J. (1892). *A treatise on electricity and magnetism* Clarendon.

McNab, G., & Meisen, A. (1973). Thermophoresis in liquids. *Journal of Colloid and Interface Science, 44*(2), 339-346.

Metzner, A., & Reed, J. (1955). Flow of non-newtonian fluids—correlation of the laminar, transition, and turbulent-flow regions. *AIChE Journal, 1*(4), 434-440.

Moffat, R. (1982). Contributions to the theory of single-sample uncertainty analysis. *ASME, Transactions, Journal of Fluids Engineering, 104*(2), 250-258.

Moffat, R. J. (1988). Describing the uncertainties in experimental results. *Experimental Thermal and Fluid Science, 1*(1), 3-17.

Muzychka, Y., & Yovanovich, M. (2004). Laminar forced convection heat transfer in the combined entry region of non-circular ducts. *Journal of Heat Transfer, 126*(1), 54-61.

Namburu, P. K., Kulkarni, D. P., Misra, D., & Das, D. K. (2007). Viscosity of copper oxide nanoparticles dispersed in ethylene glycol and water mixture. *Experimental Thermal and Fluid Science, 32*(2), 397-402.

Pak, B. C., & Cho, Y. I. (1998). Hydrodynamic and heat transfer study of dispersed fluids with submicron metallic oxide particles. *Experimental Heat Transfer an International Journal, 11*(2), 151-170.

Phuoc, T. X., & Massoudi, M. (2009). Experimental observations of the effects of shear rates and particle concentration on the viscosity of fe 2 O 3–deionized water nanofluids. *International Journal of Thermal Sciences, 48*(7), 1294-1301.

Sahooli, M., Sabbaghi, S., & Shariaty Niassar, M. (2012). Preparation of CuO/Water nanofluids using polyvinylpyrolidone and a survey on its stability and thermal conductivity. *International Journal of Nanoscience and Nanotechnology, 8*(1), 27-34.

Schwartz, L. M., Garboczi, E. J., & Bentz, D. P. (1995). Interfacial transport in porous media: Application to dc electrical conductivity of mortars. *Journal of Applied Physics, 78*(10), 5898-5908.

Sharrif, T. (2015). Experimental investigation of thermophysical poperties, pressure drop and heat transfer of non-newtonian silica colloid flow in tubes. (Masters, University of North Dakota).

Shaver, R. G., & Merrill, E. W. (1959). Turbulent flow of pseudoplastic polymer solutions in straight cylindrical tubes. *AIChE Journal, 5*(2), 181-188.

Sundar, L. S., & Singh, M. K. (2013). Convective heat transfer and friction factor correlations of nanofluid in a tube and with inserts: A review. *Renewable and Sustainable Energy Reviews, 20*, 23-35.

Timofeeva, E. V., Smith, D. S., Yu, W., France, D. M., Singh, D., & Routbort, J. L. (2010). Particle size and interfacial effects on thermo-physical and heat transfer characteristics of water-based α-SiC nanofluids. *Nanotechnology, 21*(21), 215703.

Tiwari, S. (2012). Evaluation of thermophysical properties, friction factor, and heat transfer of alumina nanofluid flow in tubes. (Masters, University of North Dakota, Grand Forks).

Vajjha, R. S., & Das, D. K. (2009). Specific heat measurement of three nanofluids and development of new correlations. *Journal of Heat Transfer, 131*(7), 071601.

Wang, B., Zhou, L., & Peng, X. (2003). A fractal model for predicting the effective thermal conductivity of liquid with suspension of nanoparticles. *International Journal of Heat and Mass Transfer, 46*(14), 2665-2672.

Wang, X., Xu, X., & S. Choi, S. U. (1999). Thermal conductivity of nanoparticle-fluid mixture. *Journal of Thermophysics and Heat Transfer, 13*(4), 474-480.

Wen, D., & Ding, Y. (2004). Experimental investigation into convective heat transfer of nanofluids at the entrance region under laminar flow conditions. *International Journal of Heat and Mass Transfer, 47*(24), 5181-5188.

Wu, J., & Zhao, J. (2013). A review of nanofluid heat transfer and critical heat flux enhancement—Research gap to engineering application. *Progress in Nuclear Energy, 66*, 13-24.

Xuan, Y., & Roetzel, W. (2000). Conceptions for heat transfer correlation of nanofluids. *International Journal of Heat and Mass Transfer, 43*(19), 3701-3707.

Yu, W., & Choi, S. (2003). The role of interfacial layers in the enhanced thermal conductivity of nanofluids: A renovated maxwell model. *Journal of Nanoparticle Research, 5*(1-2), 167-171.

Yu, W., & Xie, H. (2012). A review on nanofluids: Preparation, stability mechanisms, and applications. *Journal of Nanomaterials, 2012*, 1.

Zhu, H. T., Zhang, C. Y., Tang, Y. M., & Wang, J. X. (2007). Novel synthesis and thermal conductivity of CuO nanofluid. *The Journal of Physical Chemistry C, 111*(4), 1646-1650.

Zigrang, D., & Sylvester, N. (1982). Explicit approximations to the solution of colebrook's friction factor equation. *AIChE Journal, 28*(3), 514-515.